TISSUE INTEGRATION AND ANTIMICROBIAL EFFECTS OF SURFACE-DERIVED NITRIC OXIDE RELEASE

Scott Philip Nichols

A dissertation submitted to the faculty of the University of North Carolina at Chapel Hill in partial fulfillment of the requirements for the degree of Doctor of Philosophy in the Department of Chemistry (Analytical Chemistry)

Chapel Hill
2012

Approved by:

Mark H. Schoenfisch

R. Mark Wightman

J. Michael Ramsey

Bruce M. Klitzman

Dorothy Erie

ABSTRACT

SCOTT PHILIP NICHOLS: Tissue Integration and Antimicrobial Effects of Surface-derived Nitric Oxide Release
(Under the direction of Professor Mark H. Schoenfisch)

The analytical performance of glucose sensors is inhibited by the host's foreign body response (FBR) and risk of bacterial infection. To date, no one strategy has circumvented the physiological reactions to implanted materials. Nitric oxide (NO) is an endogenously produced free radical that acts to initiate events in the FBR and fight bacterial infection. Herein, the potential of NO-releasing surfaces to both mitigate the FBR and bacterial invasion is described.

Evaluation of the performance of NO-releasing surfaces to improve glucose sensor performance in vivo was carried out through imparting NO release to microdialysis probes. Perfusion of saturated NO solutions through implanted probes delivered a constant flux of 162 pmol cm^{-2} s^{-1} delivering 4.6 μmol cm^{-2} NO each day. The NO-releasing probes recovered significantly greater concentrations of glucose after 7 d of implantation versus controls. Histological analysis revealed a thinner collagen capsule and decreased inflammation adjacent to NO-releasing probes.

To investigate the necessary NO-release properties to achieve the observed histological benefits, NO-releasing polyurethane-coated wires were implanted into a porcine model for up to 6 weeks. Polyurethanes were doped with small molecules or nanoparticles to alter the NO release kinetics, fluxes, and total payloads. Materials with a NO-release duration

of 14 d and large NO payload (9.3 μmol cm^{-2}) were most effective at decreasing the collagen encapsulation and inflammation adjacent to the implants. Inflammation was only modulated during active NO release from the implant.

While modulation of the FBR is essential for the development of glucose sensors, infection by bacteria is a constant threat. Biomaterial-associated infections most commonly begin through adhesion to the implanted material. Therefore, evaluation of the anti-adhesive properties of NO-releasing surfaces was undertaken by examining the adhesion of six bacterial strains to a wide range of NO fluxes (0.5–50 pmol cm^{-2} s^{-1}). An average NO flux between 50 pmol cm^{-2} s^{-1} reduced surface coverage of all strains by >80% over 1 h. Further, after incubation of adhered bacteria in bacteriostatic conditions for 24 h, large surface-derived NO payloads (1.7 μmol cm^{-2}) decreased viability of adhered bacteria by ≥85%.

ACKNOWLEDGEMENTS

This work would not be possible without the support I have received. First, I must thank my advisor Prof. Mark Schoenfisch for all of his guidance and support as well as providing a collaborative scientific environment which has allowed me to grow as a researcher and a person.

My in vivo research on the foreign body response has offered me the opportunity to collaborate with Prof. Bruce Klitzman and Nga Le Brown of Duke University. They have both been extremely helpful by providing their surgical skill, knowledge on implantable materials, and analysis of tissue histology. I would also like to thank Daniel Riccio for his help with *S*-nitrosothiol chemistry and synthesis of NO-releasing nanoparticles and xerogels. The work presented herein could not have been completed without the assistance of Ahyeon Koh, Danielle Slomberg, Bin Sun, and Michael Rose all of whom assisted in the development, characterization, and in vivo testing of the NO-releasing polyurethane-coated substrates. I also want to thank my past and present coworkers Alexis Carpenter, BJ Privett, Rebecca Hunter, Katey Reighard, and Wesley Storm for creating an atmosphere conducive to the research I have been able to pursue.

Finally, I must thank my family for their constant support of my endeavors. My mom and dad who allowed me to pursue my dreams (wherever they took me), my brother David who has been a friend and source of support for my (and his) entire life, and my wife Lori for all her help over the past 5 (or so) years. I am so fortunate to have all of you in my life.

TABLE OF CONTENTS

LIST OF TABLES

LIST OF FIGURES

LIST OF EQUATIONS

LIST OF ABBREVIATIONS AND SYMBOLS

~	approximately
°C	degree(s) Celsius
µg	microgram(s)
µL	microliter(s)
µm	micrometer(s)
µM	micromolar
%	percent
λ	wavelength
σ	standard deviation
ε	molar absorptivity
AEAP3	*N*-(2-aminoethyl)-3-aminopropyltrimethoxysilane
AFM	atomic force microscopy
Ag^+	silver ion
$AgNO_3$	silver nitrate
AHAP3	*N*-(6-aminohexyl)aminopropyltrimethoxysilane
AHAP3/NO	*N*-diazeniumdiolate-modified AHAP3
Ar	argon gas
ATCC	American Type Culture Collection
atm	atmosphere(s)
bFGF	basic fibroblast growth factor
BSA	bovine serum albumin
BTMOS	isobutyltrimethoxysilane
C. albicans	*Candida albicans*
Ca^{2+}	calcium ion

$CaCl_2$	calcium chloride
CDI	collagen density index
CFU	colony forming units
cGMP	cyclic guanidine phosphate
cm	centimeter(s)
CO_2	carbon dioxide
CVC	central venous catheter
Cys	L-cysteine
CysNO	*S*-nitrosocysteine
d	day(s)
DBHD	*N*,*N*'-dibutyl-1,6-hexanediamine
DBHD/N2O2	*N*-diazeniumdiolate-modified DBHD
DI	deionized
DNA	deoxyribonucleic acid
DTPA	diethylenetriamine pentaacetic acid
E. coli	*Escherichia coli*
E. faecalis	*Enterococcus faecalis*
e.g.	for example
EDRF	endothelium-derived relaxation factor
EE	extraction efficiency
EE%	extraction efficiency percentage
ELISA	enzyme-linked immunosorbent assay
eNOS	endothelial nitric oxide synthase
et al.	and others
EtOH	ethanol

FBGC	foreign body giant cell
FBR	foreign body response
FBS	fetal bovine serum
FDA	United States Food and Drug Administration
FEP	fluorinated ethylene propylene
Fg	fibrinogen
Fig.	Figure
h	hour(s)
H&E	hematoxylin and eosin
H_2O	water
HA	hyaluronic acid
HCl	hydrochloric acid
HP 93A	Tecophillic HP-93A-100
HPLC	high performance liquid chromatography
HPU	Hydrothane AL 25-80A
Hz	hertz
i.e.	that is
ICP-OES	inductively couple plasma optical emission spectroscopy
IgG	immunoglobulin G
IL-6	interleukin-6
IL-8	interleukin-8
IL-10	interleukin-10
iNOS	inducible nitric oxide synthase
KCl	potassium chloride
k_D	dissociation constant

kDa	kilodalton(s)
kg	kilogram(s)
krpm	kilorevolutions per minute
m	meter(s)
M	molar
MΩ	megaohm(s)
MAHMA	*N*,*N*'-dimethyl-1,6-hexanediamine
MAHMA/NO	*N*-diazeniumdiolate-modified MAHMA
MBC	minimum bactericidal concentration
MCP-1	monocyte chemoattractant protein-1
MeOH	methanol
mg	milligram(s)
MIC	minimum inhibitory concentration
min	minute(s)
mL	milliliter(s)
mm	millimeter(s)
mM	millimolar
mmol	millimole(s)
mol	mole(s)
MPTMS	3-mercaptopropyltrimethoxysilane
MRSA	methicillin-resistant *Staphylococcus aureus*
MTMOS	methyltrimethoxysilane
N	newton
N.A.	numerical aperature
N_2	nitrogen gas

NaCl	sodium chloride
NH_4OH	ammonium hydroxide
nm	nanometer(s)
nmol	nanomole(s)
nNOS	neuronal nitric oxide synthase
NO	nitric oxide
$[NO]_{max}$	maximum NO flux
$[NO]_t$	NO flux at time t
NOA	Nitric Oxide Analyzer
NOS	nitric oxide synthase
NSAID	non-steroidal anti-inflammatory drug
O_2	oxygen gas
$ONOO^-$	peroxynitrite
P. aeruginosa	*Pseudomonas aeruginosa*
P. mirabilis	*Proteus mirabilis*
P. vulgaris	*Proteus vulgaris*
PAES	polyarylethersulfone
PAN	polyacrylonitrile
PBS	phosphate buffered saline, pH 7.4
PC	polycarbonate
PDGF	platelet derived growth factor
PEEK	polyether ether ketone
PES	poly(ether sulfone)
pg	picogram(s)
pH	-log of proton concentration

PLG	poly(lactide-*co*-glycolide)
PLGA	poly(lactide-*co*-glycolic acid)
pM	picomolar
PMMA	poly(methyl methacrylate)
pmol	picomole(s)
ppb	parts per billion
ppm	parts per million
PROLI/NO	*N*-diazeniumdiolate-modified L-proline
PRP	platelet-rich plasma
PU	polyurethane
PVC	poly(vinyl chloride)
Q_d	Flow rate of dialysate
R_{bf}	resistance to mass transfer in biofouling layer
R_d	resistance to mass transfer in dialysate
R_{ec}	resistance to mass transfer in encapsulation layer
R_m	resistance to mass transfer in membrane
R_{tr}	resistance to mass transfer in tissue trauma layer
rev	revolution
s	second(s)
S. auerus	*Staphylococcus aureus*
S. epidermidis	*Staphylococcus epidermidis*
SdrG	Serine-aspartate repeat G
SEM	Scanning electron microscope/microscopy
SiR	silicone rubber
SSD	silver sulfadiazine

t	time
t_{max}	time to max nitric oxide flux
TEOS	tetraethoxysilane
THF	tetrahydrofuran
TMOS	tetramethoxysilane
TP-470	Tecoplast TP-470-000
TPU	Tecoflex SG-80A
TSA	tryptic soy agar
TSB	tryptic soy broth
U	unit(s)
U.S.	United States
UV	ultraviolet
UV-Vis	ultraviolet-visible spectroscopy
v/v	volume/volume
v%	percent by volume
VEGF	vascular endothelial growth factor
wt%	percent by weight
wt/wt	weight/weight

Chapter 1:

Opportunities in Nitric Oxide Release Materials: Towards More Biocompatible Glucose Sensors

1.1. Difficulties with implementation of implantable glucose sensors

Diabetes is a common disease afflicting 25.8 million people in the United States alone.[1] The disease arises from either deficiencies in the production of or response to insulin, a down-regulator of blood glucose. Therefore, diabetic patients must carefully monitor their glucose levels and make suitable adjustments in insulin injections or food intake. Mismanagement of glucose levels can lead to dire consequences including ulcers, amputations, and even death. Currently, long-term self-monitoring of glucose levels is recommended through the finger prick method which consists of piercing a finger with a needle and directly testing the blood.[2] While this method is useful and accurate, there are limitations with patient compliance and the often too little information (snapshot) provided regarding blood glucose levels throughout the day. A single point does not reveal the trend of the blood glucose over time and therefore fosters misinterpretation and subsequent misdiagnosis by the user. Due to these concerns, continuous glucose monitoring (CGM) devices have been sought.[3, 4] Such systems would allow for real-time information on glucose concentrations and presumably improve patient compliance. For example, CGM devices would predict glucose levels and ultimately be connectable to an artificial pancreas to automatically control glucose levels.

Though the benefits of an implantable glucose sensor are quite clear, CGM devices are limited by deficiencies in their biocompatibility. Currently, CGM devices approved by the FDA to work for 5–7 d and are currently intended only to assist a patient in understanding their glucose level trends.[5] These sensors are useful tools, but cannot replace finger-prick methods for extended glucose monitoring and often require frequent calibration (via finger pricks). Implantable glucose sensors are primarily limited by the host's foreign body response (FBR). Significant research has explored methods to increase the biocompatibility of in vivo sensors to extend the analytical functionality and provide reliable and accurate glucose levels.[6]

1.2. Biocompatibility of implanted materials

Many biomedical implants are currently approved for implantation into the human body. While these biomedical materials are routinely implemented, limitations in functionality, safety, and lifetime persist due to the host tissue response, termed the foreign body response (FBR). Even materials considered to be biocompatible elicit a weak FBR, forming a thin, avascular encapsulation which prevents full integration of the implant into the surrounding native tissue. Despite the implementation of aseptic procedures, infection resulting from implanted biomaterials is also commonplace. An implant-associated infection necessitates device removal with large risk for severe complications including amputation or even death. Both isolation of glucose sensors through the FBR and bacterial colonization of the implant site can lead to erratic sensor performance. Thus, significant research has focused on methods to promote the development of native host tissue around an implant.

1.2.1. The foreign body response and sensor performance. As shown in Figure 1.1, the FBR initiates upon the insertion of almost any material into subcutaneous tissue, starting

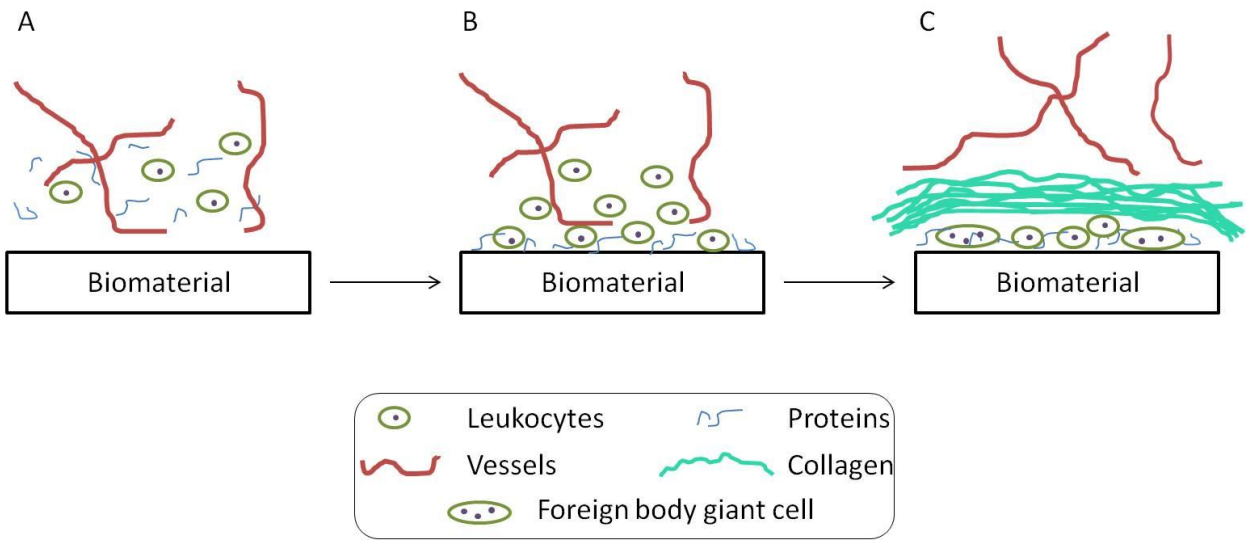

Figure 1.1. The progression of the foreign body response (FBR) with time. (A) Initially, the biomaterial is implanted into injured native tissue composed of blood vessels, proteins and cells. (B) Proteins and cells adhere to the surface and the adhered cells release chemoattractants and cytokines to direct the FBR. (C) At 1–2 weeks, macrophages have fused into foreign body giant cells (FBGCs) and leukocytes have deposited an organized collagen encapsulation sequestering the material from the native tissue and blood vessels.

with the creation of a wound and the wound healing cascade.[7, 8] Instantaneously, proteins adhere to the biomaterial surface in a process referred to as biofouling.[8, 9] The initial protein adsorption is an integral part of the overall FBR as the ensuing interface promotes the adhesion of inflammatory cells that subsequently stimulates blood clotting and the development of a provisional matrix.[9] As part of the FBR, macrophages, monocytes, mast cells, and fibroblasts are recruited to the implant site to initiate clearance of the foreign body by releasing chemokines and cytokines.[7, 8] The concentrations and types of mediators released elicit further cell recruitment and ultimately phagocytosis[10] as the body attempts to digest the implant. This process can result in a local pH's dropping as low as 3.6 and disrupting biosensor performance as the activity of GOx is pH dependent.[11] While preventing all macrophage migration and subsequent phagocytosis at a wound (glucose sensor) is unlikely, the activation state (i.e., M1 or M2) of the macrophage may influence the overall FBR. Indeed, macrophages serve three primary functions in the body: host defense, wound healing, and immune regulation.[12] Since macrophages are vital for the wound-healing process that results from an injury, the phenotype of the cells present at an implant, rather than their concentration, is now believed to be a better indicator of tissue response.[13] As the FBR progresses, frustrated phagocytosis from activated macrophages will lead to the fusion of macrophages into foreign body giant cells (FBGCs) that attempt to further breakdown the implant.[11, 14-16] For example, FBGC formation on polyurethanes has been shown to promote cracking of the underlying biomaterial.[14] After one to two weeks, inflammatory cells deposit a collagen matrix that sequesters the implant from the native tissue. This collagen encapsulation lacks the microvasculature of native tissue.[17] As blood vessels are the primary source of glucose, such encapsulation hinders accurate measurements of blood glucose. The

extent of capsule development is dependent on all other preceding components of the FBR, including protein adhesion, cell activation, and cytokine signaling. The collagen encapsulation will persist for the lifetime of the device, negatively impacting sensor performance with respect to sensitivity and response (e.g., lag times).

While the individual effects of each step in the FBR on glucose sensor performance have been postulated, actual outcomes are more difficult to determine. Researchers have long sought to untangle the complexities that connect various events in the FBR with tissue integration and glucose sensor performance, as this knowledge could lead to the development of materials that address the specific tissue responses that most severely inhibit sensor performance.

The synthesis of antifouling materials has evolved to be a common strategy for improving glucose sensor functionality as the initial adhesion of proteins and cells onto a glucose sensor mitigates sensor performance.[18, 19] Among the earliest reports describing reduced analytical performance, Thomé-Duret et al. implanted polyurethane-coated glucose biosensors to quantify changes in analytical sensitivity.[18] Soon after implantation, the sensors were explanted and tested ex vivo.[18] While the immediately explanted sensors had glucose sensitivities similar to those analyzed in vivo, response to glucose improved after rinsing, albeit not to pre-implantation levels.[18] Nevertheless, this reversibility indicated that the process was passive and likely caused by biofouling on the sensor.[18] Proteomic analysis revealed that the majority of the biofouling proteins on the sensor membrane were fragments <15 kDa.[20, 21] In contrast, Wisniewski et al. evaluated the impact of collagen encapsulation versus biofouling using microdialysis probes and found biofouling effects to actually be minimal.[22] Specifically, the resistance to mass transfer of analyte (i.e., glucose) caused by the

tissue over both short- (3 h) and long-term (8 d) implantation periods were typically 3 to 5 times greater than that caused by biofouling of the probes, regardless of implantation period.[22] The observed biofouling was found to have only relatively small direct effects on the overall resistance and glucose extraction efficiency.[22] It is important to note however that biofouling of proteins and cells at the sensor-tissue interface will also affect the tissue response to a biomaterial as will the composition of the polymers used to fabricate the sensors and dialysis probes.

Following protein adhesion/biofouling, the FBR proceed with inflammatory cells responding to the injury, initiating a more profound immune response to the device. Klueh et al. reported on the effects of mast cells, regulators of inflammation.[23] Both mast cell-sufficient and -deficient mice were implanted with subcutaneous glucose sensors for 28 days. During this period, glucose sensor performance in mast cell-sufficient mice was erratic with temporary response loss occurring within the first 3 weeks. Sensor performance in mast cell-deficient mice was markedly better with reliable sensor function throughout the 28-day period.[23] Histology samples from both experimental groups confirmed that the mast cell-deficient mice exhibited reduced fibrosis and inflammation at the implantation site. To further confirm the effect of mast cells on glucose sensor performance, 10^4–10^5 mast cells were injected at the implant site.[23] While glucose sensor performance recovered soon after injection (~15 min), the sensor response to glucose decreased after 1–2 days, further indicating a link between mast cell action and erratic glucose sensor performance.[23]

The most characteristic outcome of the FBR is collagen encapsulation around the foreign device. Early investigations of capsules formed around sensors focused on the influence of the capsule on glucose diffusion from native tissue. For example, Sharkawy and

coworkers implanted non-porous polyvinyl alcohol (PVA) and stainless steel cages into the subcutaneous tissue of rats.[24] Upon careful explantation of the collagen capsules, the diffusion of sodium fluorescein (376 g/mol) through the capsule was quantified and used to model small analyte transport.[24] Diffusion of the fluorescein through the explanted capsules was ~50% that of normal (i.e., subcutaneous) tissue.[24] Sensor lag times for native tissue was estimated at ~20 min, but tripled when modeled with decreased diffusion due to a capsule.[24] Interestingly, empirical data suggests that lag times range from 10–15 min in vivo, indicating the integral function of angiogenesis in early granulation tissue. In subsequent experiments, Dungel et al. examined the effects of encapsulation on sensitivity by evaluation the response of glucose sensors inserted into polyvinyl alcohol sponges implanted in rats.[25] The glucose sensitivity in vivo peaked at day 7, but then decreased for the duration of the study.[25] Glucose sensitivity correlated well with the collagen encapsulation of the sponges with thicker collagen resulting in greater sensitivity loss.[25] Koschwanez et al. investigated the effects of vascularity on glucose sensor performance in real-time by using an implanted optical window over the sensor, microscopy, and laser Doppler flowmetry.[26] The vessel length and perfusion of the vasculature increased during the implantation period (i.e., 14 d). Despite such increases in vasculature, the sensitivity of the sensor did not increase indicating that angiogenesis is not the only factor in assessing the biocompatibility of CGM sensors.[26]

Mathematical models and simulations of implantable glucose sensors have further helped understand how the processes of the FBR may affect glucose sensor performance. Simulations of glucose concentration oscillations by Jablecki and Gough concluded that increases in mass transfer would increase lag and could potentially decrease the magnitude and differences when fluctuating between high and low glucose sensor signals.[27] While this

conclusion is important for sensor design, the increases to mass transfer were not attributed to any specific part of the FBR and could originate from collagen capsule thickness, blood vessel density, or other unanticipated factors. To consider major tissue reactions individually, Novak and coworkers used a mathematical model to examine FBR effects on glucose sensor performance.[28] Using previous histology data, five parameters (i.e., angiogenesis, cellular glucose consumption, capsule thickness, capsule diffusion coefficient, and capsule porosity) were used to design a mathematical model that mimicked glucose diffusion from capillaries to a glucose sensor in order to simulate the effect on sensor lag time and attenuation.[28] The mathematical model treated vessels as sources of glucose and inflammatory cells as glucose sinks, while the encapsulation properties acted to impede the diffusion of glucose.[28] Changes in cellular glucose uptake and the capsule diffusion coefficient of glucose had little effect on simulated sensor performance.[28] The model was ultimately used to conclude that collagen capsule thickness, a common histological parameter, was the primary source of sensor lag time with little impact on sensor response attenuation.[28] The positive correlation between lag time and capsule thickness supported the models described above.[24, 27, 28] The two greatest factors in reducing sensor attenuation were a low capsule density and high degree of angiogenesis.[28] While these are only mathematical models, the results do identify the histological parameters of key interest when assessing the biocompatibility of materials for glucose sensors.

1.2.2. Bacterial infection. Even when aseptic methods are utilized, incidences of biomaterial-associated infections originating from either endogenous or exogenous bacterial sources remain. Approximately 5% of surgeries result in the development of an infection, regardless of the implantation of a device.[29] The implantation of a device creates a surface on

which bacteria to colonize and proliferate.[30] Current biomaterials do little to prevent implant-associated infections. Furthermore, the administration of systemic antibiotics, the leading treatment for infections, has lead to a dwindling efficacy and the emergence of antibiotic-resistant bacterial strains. The development of an implant-associated infection necessitates the removal of the device and can lead to more serious complications, including death. With the rise in biomedical implant usage and antibiotic-resistant strains of bacteria, the number of implant-associated infections will likely increase.

Implanted biomaterials provide conditions that promote bacterial colonization. Upon implantation, either the native tissue integrates with the implanted material or bacteria adhere to the surface and colonize.[31] Bacteria are most likely to adhere and colonize during the 6 h directly following implantation.[32] This colonization can result in the formation of a persistent biofilm which is difficult to fully eradicate. Killing of bacteria comprising a biofilm versus their planktonic counterparts requires up to 1000x increased doses of antibiotics.[33, 34] Early killing and prevention of adhesion would decrease the susceptibility of implantable materials to bacterial infections. Currently, many clinically approved materials do not sufficiently prevent bacterial adhesion and biofilm formation on their surface.[35]

1.3. Animal models for evaluating biocompatibility

When implanting in vivo, researchers often use rodent models (e.g., mouse[36] or rat[37, 38]) models to assess in vivo biocompatibility and/or glucose sensor functionality, though others (e.g., pigs,[39] dogs,[40] and chimpanzees[41]) are used as well. Such animal models are time and labor intensive while requiring surgical skills. Although an avian chorioallantoic membrane has been proposed as an alternative model for testing biomaterials with obvious expense benefits, long-term studies (i.e., >2 weeks) are not feasible.[42, 43]

Unfortunately, the degree to which animal models accurately predict the FBR and analytical performance of glucose sensors in humans has come under scrutiny. For example, Wisniewski et al. compared the dialysate concentrations of glucose, pyruvate, lactate, glycerol, and urea at a microdialysis probe-tissue interface implanted in the subcutaneous space of both rats and humans to evaluate the validity of the cross-species relationship.[44] The dialysate concentrations were significantly different for all metabolites in rats and humans throughout the first 6 days of the experiment, with the exception of glycerol on day 0.[44] Additionally, the ratio of the glucose concentration in the dialysate to that in blood were significantly different between rats and humans indicating differences in the relative glucose availability in the tissue surrounding an implanted device.[44] Histology samplings from human subcutaneous tissue showed a greater concentration of adipose cells while rat tissue was characterized with larger amounts of collagen.[44] Taken together, these results necessitate careful consideration and caution when extrapolating results from animal models to humans.

In addition to differences between species, one parameter that is not often considered is the differential healing response in diabetic versus healthy (i.e., non-diabetic) patients. Diabetics typically suffer from delayed and diminished wound healing.[45] It is currently not known how such physiology affects the FBR and subsequent sensor performance. In a key study, Gertissen et al. investigated the differences in the FBR between diabetic and non-diabetic rabbits to percutaneous and subcutaneous materials.[46] Histological analysis revealed delayed neovascularization and less matrix production in the diabetic rabbits that clearly could influence glucose sensor performance.[46] Due to such important histological differences, diabetic animals should likely be used to better simulate tissue response and

characteristics of diabetic patients. Of note, many diabetic models are available including both genetic and chemically-induced.[47]

1.4. Nitric oxide

The implantation of a biosensor into a host raises concerns of a lack of biocompatibility (i.e., collagen encapsulation and inflammation) and the potential to promote bacterial colonization and subsequent infection. Thus, a strategy to address these primary concerns has been the release of nitric oxide (NO) from implantable surfaces.

Since NO was identified as the endothelial derived relaxation factor (EDRF) in 1986, there has been extensive research into the many functions of NO in the body.[48] Nitric oxide is an endogenously produced free radical synthesized from L-arginine by one of three isoforms of nitric oxide synthase (NOS): neuronal NOS (nNOS), endothelial NOS (eNOS), and inducible NOS (iNOS).[49] The nNOS isoform is present in many tissues outside the brain including skeletal muscle and islet cells while eNOS is present almost exclusively in the endothelium.[50] These two isoforms create low concentrations (i.e., nM) of NO. Inducible NOS can be expressed in any cell when exposed to certain cytokines or lipopolysaccharide (LPS) and is often expressed by macrophages in response to bacterial infection or inflammation to synthesize μM concentrations of NO.[50]

1.4.1. Roles in the foreign body response. While the mechanisms have not been completely elucidated, NO is known to control many functions of the FBR that may affect implantable glucose sensors. Nitric oxide has been indicated as an angiogenic signaling molecule,[51] and there are several reports of NO up-regulating VEGF production and thereby increasing blood vessel growth.[52] Furthermore, VEGF acts to up-regulate eNOS expression thus inducing vasodilation. The angiogenic behavior exhibited by NO would be helpful for

avoiding the typical avascular encapsulation that plagues successful glucose sensor performance. Additionally, NO is believed to control inflammatory cell recruitment in the early stages of the FBR. Localized NO may cause nitrosation of proteins and down-regulate pro-inflammatory cytokine expression (e.g., macrophage chemoattractant protein-1).[53] Furthermore, NO has been reported to reduce leukocyte adhesion at elevated concentrations and could thereby prevent localization of inflammatory cells at an implanted glucose sensor.[54] The reduction of leukocytes at the implant aids in the reduction of inflammation and subsequent FBR at the wound site.

1.4.2. Antibacterial properties. Macrophages synthesize and release endogenous NO at concentrations >1 μM in response to bacterial infections.[55, 56] Thus, significant research efforts are focused on harnessing the antimicrobial properties of NO. As a free radical, NO is very reactive and can cause damage to cells both directly and indirectly through resulting byproducts (e.g., N_2O_3). At the exterior of a bacterial cell, NO may react with endogenous superoxide to produce peroxynitrite, which is capable of damaging the cell membrane through lipid peroxidation.[57] Observations via atomic force microscopy confirm that NO release compromises the bacteria membrane.[58] Inside the cell, NO can nitrosate proteins and cause strand breaks or base changes in DNA.[59] Unlike many antibiotics, NO acts through multiple killing mechanisms which not only increases the probability of bacterial cell death but also significantly decreases the probability of bacterial resistance evolving.[60]

1.4.3. Controllable delivery of nitric oxide. Given the roles of NO in the immune response, favorable tissue reactions to NO-releasing substrates in vivo are expected, however, due to its gaseous nature, direct delivery of NO in vivo is not trivial. To achieve in vivo release, NO donors have been synthesized as a method to store NO that may be released

upon some trigger.[61, 62] The most commonly studied donors for implant-derived in vivo NO delivery are *N*-diazeniumdiolates and *S*-nitrosothiols (Figure 1.2). *N*-diazeniumdiolates are formed on secondary amines upon exposure to NO in basic conditions.[63] In the presence of a proton source (e.g., water), the *N*-diazeniumdiolate decomposes to release two molecules of NO, regenerating the parent amine in the process.[63] The rate of release from these moieties is therefore dependent on the pH, ionic strength, and surrounding chemical environment.[63, 64] *S*-nitrosothiols are formed on thiols exposed to nitrosating conditions (e.g., acidified nitrite) and degrade when exposed to light, copper (I), or heat, releasing one NO molecule per thiol.[65] Similar to *N*-diazeniumdiolates, the NO release kinetics from *S*-nitrosothiols are dependent on the NO donor chemical structure. The utility of NO donors for improving biocompatibility was initially investigated by incorporating low molecular weight (LMW) NO donors of *N*-diazeniumdiolates (e.g., *N*-diazeniumdiolated L-proline) and *S*-nitrosothiols (e.g., *S*-nitrosoglutathione) into biomaterials to impart NO release capabilities.[66-68] Limitations of LMW NO donors include short release kinetics and cytotoxicity. More recently, there have been efforts to synthesize novel NO donors to both alter NO release kinetics and reduce mammalian cell cytotoxicity. To this end, macromolecular scaffolds have been designed including silica nanoparticles[69-71] and silica xerogels.[72-79] Nanoparticles and xerogels materials can be doped into polymer scaffolds or used as coatings, respectively, permitting NO release from any implanted material. These materials can be used to evaluate the effects of NO release in vivo.

1.5. Evaluating the host response via microdialysis

Microdialysis is a sampling technique in which a fluid is perfused through a probe with a semi-permeable membrane where diffusion between the perfusate and external

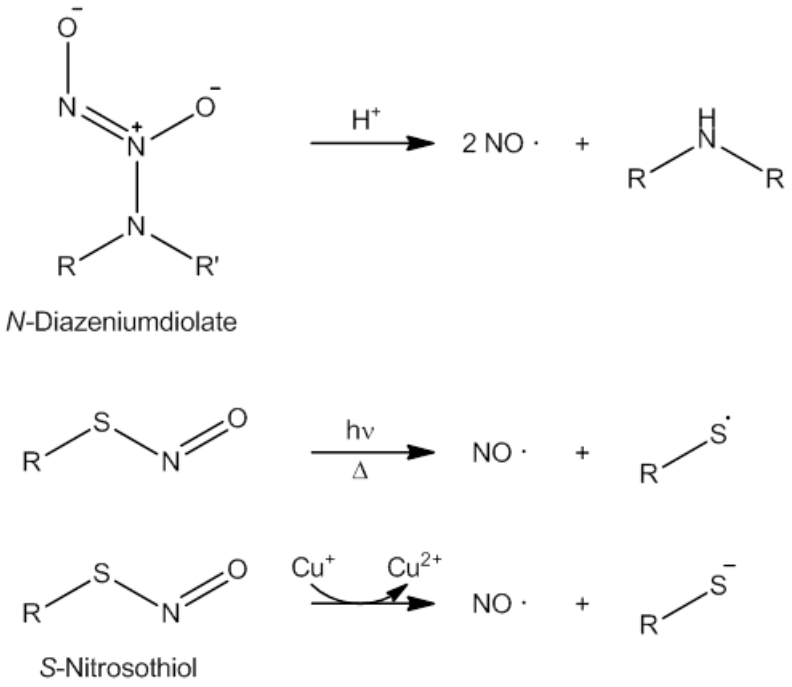

Figure 1.2. Two major nitric oxide donors (i.e., *N*-diazeniumdiolates and *S*-nitrosothiols) and their primary decomposition mechanisms.

medium occurs and is collected as a dialysate. The extraction efficiency (EE) is obtained by comparing the concentrations of a given analyte in the perfusate (C_p), dialysate (C_d), and external medium (C_e) (Equation 1.1). The EE can be further related through the Bungay-Morrison-Dedrick equation to resistances to mass transfer of the dialysate (R_d), membrane (R_m), and external medium (R_e), as well as the flow rate of the perfusate (Q_d) (Equation 1.1).[80, 81] When implemented in vivo, resistances in the external medium may be the result of biofouling or other tissue effects (e.g., collagen encapsulation). Therefore, evaluating the EE over time offers a method to determine the biocompatibility of the probe material. This method is particularly useful for investigating glucose sensors as the resistances to mass transfer also offers insight into the effective lag time of a sensor. While microdialysis allows for simple temporal testing of materials, the materials tested are limited to semi-permeable membranes.

Similar to implantable biosensors, microdialysis probes suffer from diminished analyte recovery over time. This reduction in analyte recovery is associated with increased resistances to mass transfer. Wisniewski et al. examined the effect of microdialysis membrane composition on the EE of glucose in rat subcutaneous tissue.[22] Poly(ether sulfone) (PES), polycarbonate (PC), and polyacyrlonitrile (PAN) microdialysis probe membrane compositions were investigated and glucose recovery was measured at 0, 2, 5, and 8 d post-implantation. The PES membranes exhibited a significant reduction in glucose recovery at 2 d post-implant. All probe compositions experienced diminished glucose recovery after 8 d of implantation. Later investigation by Mou et al. examined recovery of multiple analytes over time in rat subcutaneous tissue using PES and PC microdialysis probes.[82] No significant differences were observed in glucose recovery in vivo between PES and PC membranes. The

$$\mathrm{EE}=\frac{C_d - C_p}{C_e - C_p} = 1 - \exp\left(\frac{-1}{Q_d(R_m + R_d + R_e)}\right)$$

Equation 1.1. The Bungay-Morrison-Dedrick equation relating extraction efficiency (EE) to flow rate (Q_d) and resistances to mass transfer (R).

EE of perfused vitamin B_{12} and recovered glucose by the microdialysis probes after 12 d were reduced by 71.4 and 71.1%, respectively.

Researchers have attempted to improve glucose recovery of microdialysis probes by implementing more biocompatible materials and releasing anti-inflammatory molecules. Norton et al. investigated the EE of glucose in rat subcutaneous tissue using both bare microdialysis probes and those with an overlaying hydrogel interface.[83] The additional diffusion of glucose through the hydrogels resulted in an increase in resistance to mass transfer in vitro. When tested in vivo, the improved biocompatibility provided by the hydrogel caused only non-significant improvements in tissue integration (reduction in resistance to mass transfer of glucose) during the 8 d implantation. Later studies from Mou et al. investigated the effect of actively releasing monocyte chemoattractant protein-1 (MCP-1; a pro-inflammatory drug) and dexamethasone (DX; an anti-inflammatory drug) on the recovery of glucose in rat subcutaneous tissue.[84] The delivery of MCP-1 resulted in a collagen capsule that was 2x the thickness of control probes after 10 d. In contrast, the DX-releasing probes had very fragile collagen capsules due to the low degree of fibrosis in the adjacent tissue and could not be processed for histological analysis. The increased FBR to the MCP-1-releasing probes caused a significant decrease in glucose recovery versus controls 7 d post-implant. However, even with the observed fragile collagen capsules adjacent to DX-releasing probes, no significant differences in glucose recovery were observed over versus controls over the 10 d experiment. However, the DX-releasing probes were functional 2 d longer than control probes, indicating a potential benefit to the anti-inflammatory molecule.

Despite the slight non-significant advantages, the previous studies found that surface modifications with hydrogels and release of anti-inflammatory molecules were incapable of

improving the recovery of glucose in vivo. As NO release has been observed to improve angiogenesis while decreasing collagen encapsulation and inflammation, delivery of the molecule may be able to minimize the in vivo resistances to mass transfer of glucose caused by the FBR.

1.6. Histological analysis of NO-releasing materials

Macromolecular NO donors have been implemented to investigate the potentially positive tissue reactions to NO-releasing materials. Hetrick et al. coated 40% *N*-(6-aminohexyl)aminopropyltrimethoxysilane (AHAP3) balance isobutyltrimethoxysilane (BTMOS) xerogels onto square silicon rubber implants and chemically modified them with *N*-diazeniumdiolates.[85] The substrates were capable of delivering a NO payload of 1.3 μmol cm^{-2} over 3 d.[85] The materials were then implanted into rat subcutaneous tissue for 1, 3, or 6 weeks and histology of the surrounding tissue was examined.[85] The chronic collagen encapsulation was reduced at 3 and 6 weeks by ~20–25% compared to non-NO-releasing xerogels.[85] In addition to the reduced capsule thickness, the chronic immune response (i.e., 3 and 6 weeks) was reduced while angiogenesis was enhanced at 1 and 3 weeks.[85] Indeed, these results indicate a possible long-term benefit for NO-releasing glucose sensors. A mitigated immune response could result in reductions in local glucose consumption and reactive oxygen species, while angiogenesis observed could significantly impact the observed sensitivity of a glucose sensor and decrease lag time by reducing the distance from glucose source to implant surface.

To investigate short-term effects of NO release from implants on the FBR, Gifford et al. doped (Z)-1-[N-methyl-N-[6-(N-butylammoniohexyl)amino]]-diazen-1-ium-1,2-diolate (DBHD/NO) into a polyurethane and polydimethylsiloxane coating which was capable of

releasing NO for 18 h.[21] The materials were implanted percutaneously into rats for 3 d.[21] Subsequent histological analysis of the tissue revealed a decrease in inflammation at 24 h, but not 48 h.[21] The anti-inflammatory benefits correlated well with the NO release duration indicating that the observed benefits may only persist for the duration of NO release, in contrast to observations by Hetrick et al. which observed long-term reductions in inflammation.[21, 85] Such results demonstrate the potential of NO as a mediator of the FBR for glucose sensors.

These studies each focused only on a single NO-releasing material for evaluating the effect on the FBR. Therefore, the differences observed may not be optimal and the proper release of NO from an implantable biomaterial could further enhance tissue integration. Nitric oxide release properties (e.g., maximum NO flux, NO release duration, total NO release) likely have a significant impact, but the role of each parameters is largely unknown. Furthermore, these studies have concentrated on rodent models of the FBR, which while useful, are not the best model of humans. Porcine models may better mimic the response in a human and provide insight into the necessary NO release properties to improve tissue integration.[86]

1.7. Effects of exogenous NO on bacterial adhesion and viability

In addition to NO's role as an antibacterial agent, it reduces bacterial adhesion which can subsequently inhibit bacterial colonization.[76, 78, 87] Inhibiting initial adhesion of bacteria is critical for preventing implant associated infections.[88] Early experiments by Nablo et al. revealed that under static conditions, NO-releasing xerogels provided a flux-dependent reduction in *P. aeruginosa* adhesion. An initial NO flux of 5 pmol cm^{-2} s^{-1} reduced adhesion by 25%, while the largest NO flux investigated (~32 pmol cm^{-2} s^{-1}) inhibited adhesion by

85%. Interestingly, *P. mirabilis* adhesion was also reduced by NO release, but not in a NO flux-dependent manner. Indeed, all NO fluxes examined (ranging from ~10–32 pmol cm^{-2} s^{-1}) reduced adhesion of *P. mirabilis* by ~50% to PVC-coated xerogels.[89] Charville et al. examined the effects of NO release with fibrinogen biofouling to more closely mimic in vivo conditions. Specifically, *S. aureus* was found to adhere ~5.3x more to poly(vinyl chloride) (PVC) surfaces with adsorbed fibrinogen than PVC alone while *E. coli* and *S. epidermidis* exhibited modest enhancements (1.2–1.8x). Even while bacterial adhesion was promoted by fibrinogen adsorption to the surface, NO release reduced bacterial adhesion of *S. aureus* and *E. coli* by 96 and 88%, respectively.[90] NO-releasing xerogels exhibited a flux-dependent reduction in bacterial adhesion. Interestingly, *S. epidermidis* was found to have greater surface coverage even with relatively large NO fluxes (48% reduction at 30 pmol cm^{-2} s^{-1}) and overall was less susceptible to NO-induced reductions in adhesion.

Under flow conditions, substrates that release ~21 pmol cm^{-2} s^{-1} have been shown to reduce adhesion of *P. aeruginosa* by 65% relative to controls.[73] In the same study, Hetrick and Schoenfisch examined the viability of adhered *P. aeruginosa* to varying payloads of NO in static conditions (i.e., phosphate buffered saline). After 16 h of incubation, a NO payload of 750 nmol cm^{-2} reduced viability of *P. aeruginosa* by 96% compared to substrates that released only 25 nmol cm^{-2}, though the viability was not compared to substrates lacking NO release. These results exemplified both the ability for NO to decrease bacterial adhesion and a NO payload-dependent killing of bacteria.

Seabra et al. examined the potential of NO-releasing catheters to reduce bacterial adhesion by mixing poly(sulfhydrylated polyester)s (PSPEs) with polymethylmethacrylate (PMMA) to create a solid polymer. The polymers were nitrosated and upon exposure to 10^5

CFU of either *S. aureus* and *P. aeruginosa* in 1.0 mL to a 1.8 cm^2 surface area, the NO-releasing films achieved close to complete killing after 12 h of exposure, corresponding to a NO payload of ~40 nmol cm^{-2}. Recent work by Cai et al. examined the antibacterial and anti-adhesive properties of a poly(lactic-co-glycolic acid) (PLGA) coating doped with the small molecule NO donor DBHD/NO.[91] A composition of 20% DBHD/NO was capable of releasing NO for 15 d with NO fluxes from 0.6–3 pmol cm^{-2} s^{-1} at 7 d. The materials were exposed to *S. aureus* or *E. coli* for 7 d to allow adhesion and growth of a biofilm onto the surface. Confocal microscopy revealed that NO-releasing materials reduced adhesion of both strains while also causing cell death of those that did adhere. The NO-releasing materials were capable of reducing biomass of *S. aureus* and *E. coli* adhered to the substrates by 3-orders of magnitude.

The in vitro evidence for the action of NO as an antimicrobial agent and in preventing bacterial colonization has led to in vivo investigations. Nablo et al. investigated the anti-infective properties of NO-releasing xerogels when implanted into rats and exposed to 10 μL of 10^8 CFU/mL of *S. aureus*.[92] After 8 d, NO release from the implants caused an 86% decrease in the incidence of infection.[92] Continuing on this research, external titanium fixation screws coated with NO-releasing xerogels were implanted into rat tail vertebrae.[93] The release of NO resulted in diminished colonization of the fixation site at 48 h and presentation of fewer clinical signs of infection versus control screws.[93] However, the success of NO-releasing coatings to inhibit infection is concentration dependent. For example, Englesman et al. did not observe antibacterial properties in vivo to a *C*-diazeniumdiolate implant even though decreased adhesion of several bacteria strains was observed in vitro.[94] This lack of efficacy was likely due insufficient NO levels as the

maximum NO flux reported was ~1 pmol cm^{-2} s^{-1}. Studies reported by Holt et al.[93] and Nablo et al.[92] proved successful inhibition of infection can be achieved with maximum NO fluxes of 20 and 295 pmol cm^{-2} s^{-1}, respectively.

While the works presented have exemplified NO as an active-releasing molecule to reduce adhesion in vitro and subsequently infection in vivo, the amounts necessary are poorly understood. The use of various materials, bacterial strains, and experimental conditions prevents comparisons between the studies and convolutes the data. Additionally, only a few studies have examined the viability of bacteria that adhere to NO-releasing surfaces.

1.8. Summary of dissertation research

My dissertation research has focused on the evaluation of the effects of surface-derived nitric oxide release on the processes involved with the implantation of materials (i.e., mitigation of the FBR and inhibition of bacterial adhesion and viability) and the implications of such effects, specifically related to implantable glucose sensors. My specific aims included:

1) Quantifying the effect of nitric oxide delivery from microdialysis probes in rat subcutaneous tissue on the in vivo resistances to mass transfer of glucose.

2) Evaluating the influence of both nitric oxide release kinetics and payloads on the acute and chronic foreign body response in a porcine subcutaneous model as quantified through collagen encapsulation and the inflammatory response.

3) Determining the necessary nitric oxide surface fluxes and payloads to reduce bacterial adhesion and to induce cell death of adhered bacteria of a range of bacterial strains.

The goal of this introduction chapter was to provide the current statuses of using microdialysis to evaluate the FBR, the effects of NO on the FBR, and the antibacterial

properties of NO-releasing materials. In Chapter 2, the quantification of in vivo resistances to mass transfer of glucose to NO-releasing microdialysis probes to evaluate the FBR over time will be discussed. Chapter 3 details the NO flux-dependent FBR in a porcine model through the evaluation of tissue histology. In Chapter 4, the NO flux- and NO payload-dependent effects on bacterial adhesion and viability, respectively, are examined. Finally, Chapter 5 summarizes the research and provides future directions needed to expand on the work completed.

1.9 References

(1) Inzucchi, S. E., "Diagnosis of Diabetes." *N. Engl. J. Med.* **2012,** *367*, 542-550.

(2) Newman, J. D., Turner, A. P. F., "Home blood glucose biosensors: a commercial perspective." *Biosens. Bioelectron.* **2005,** *20*, 2435-2453.

(3) Heller, A., "Implanted Electrochemical Glucose Sensors for the Management of Diabetes." *Annu. Rev. Biomed. Eng.* **1999,** *1*, 153-175.

(4) Wilson, G. S., Hu, Y. B., "Enzyme based biosensors for in vivo measurements." *Chem. Rev.* **2000,** *100*, 2693-2704.

(5) Buckingham, B., Caswell, K., Wilson, D. M., "Real-time continuous glucose monitoring." *Curr. Opin. Endocrinol. Diabetes Obes.* **2007,** *14*, 288-295.

(6) Koh, A., Nichols, S. P., Schoenfisch, M. H., "Glucose sensor membranes for mitigating the foreign body response." *J. Diabetes Sci. Technol.* **2011,** *5*, 1052-9.

(7) Anderson, J. M., "Biological responses to materials." *Ann. Rev. Mater. Res.* **2001,** *31*, 81-110.

(8) Anderson, J. M., Rodriguez, A., Chang, D. T., "Foreign body reaction to biomaterials." *Semin. Immunol.* **2008,** *20*, 86-100.

(9) Wilson, C. J., Clegg, R. E., Leavesley, D. I., Pearcy, M. J., "Mediation of biomaterial-cell interactions by adsorbed proteins: A review." *Tissue Eng.* **2005,** *11*, 1-18.

(10) Luttikhuizen, D. T., Harmsen, M. C., Van Luyn, M. J. A., "Cellular and molecular dynamics in the foreign body reaction." *Tissue Eng.* **2006,** *12*, 1955-1970.

(11) Zhao, Q. H., McNally, A. K., Rubin, K. R., Renier, M., Wu, Y., Rosecaprara, V., Anderson, J. M., Hiltner, A., Urbanski, P., Stokes, K., "Human plasma alpha-2-macroglobulin promotes in vitro oxidative stress cracking of pellethane-2363-80A - In vivo and in vitro correlations." *J. Biomed. Mater. Res.* **1993,** *27*, 379-389.

(12) Mosser, D. M., Edwards, J. P., "Exploring the full spectrum of macrophage activation." *Nat. Rev. Immunol.* **2008,** *8*, 958-969.

(13) Jones, J. A., Chang, D. T., Meyerson, H., Colton, E., Kwon, I. K., Matsuda, T., Anderson, J. M., "Proteomic analysis and quantification of cytokines and chemokines from biomaterial

surface-adherent macrophages and foreign body giant cells." *J. Biomed. Mater. Res. Part A* **2007,** *83A*, 585-596.

(14) Zhao, Q., Topham, N., Anderson, J. M., Hiltner, A., Lodoen, G., Payet, C. R., "Foreign-body giant cells and polyurethane biostability: In vivo correlation of cell adhesion and surface cracking." *J. Biomed. Mater. Res.* **1991,** *25*, 177-183.

(15) Anderson, J. M., Defife, K., McNally, A., Collier, T., Jenney, C., "Monocyte, macrophage and foreign body giant cell interactions with molecularly engineered surfaces." *J. Mater. Sci.-Mater. Med.* **1999,** *10*, 579-588.

(16) Kao, W. Y. J., Zhao, Q. H., Hiltner, A., Anderson, J. M., "Theoretical analysis of in vivo macrophage adhesion and foreign body giant cell formation on polydimethylsiloxane, low density polyethylene, and polyetherurethanes." *J. Biomed. Mater. Res.* **1994,** *28*, 73-79.

(17) Sieminski, A. L., Gooch, K. J., "Biomaterial-microvasculature interactions." *Biomaterials* **2000,** *21*, 2233-2241.

(18) Thomé-Duret, V., Gangnerau, M. N., Zhang, Y., Wilson, G. S., Reach, G., "Modification of the sensitivity of glucose sensor implanted into subcutaneous tissue." *Diabetes Metab.* **1996,** *22*, 174-178.

(19) Gerritsen, M., Jansen, J. A., Kros, A., Vriezema, D. M., Sommerdijk, N., Nolte, R. J. M., Lutterman, J. A., Van Hovell, S., Van der Gaag, A., "Influence of inflammatory cells and serum on the performance of implantable glucose sensors." *J. Biomed. Mater. Res.* **2001,** *54*, 69-75.

(20) Gifford, R., Kehoe, J. J., Barnes, S. L., Kornilayev, B. A., Alterman, M. A., Wilson, G. S., "Protein interactions with subcutaneously implanted biosensors." *Biomaterials* **2006,** *27*, 2587-2598.

(21) Gifford, R., Batchelor, M. M., Lee, Y., Gokulrangan, G., Meyerhoff, M. E., Wilson, G. S., "Mediation of in vivo glucose sensor inflammatory response via nitric oxide release." *J. Biomed. Mater. Res. Part A* **2005,** *75A*, 755-766.

(22) Wisniewski, N., Klitzman, B., Miller, B., Reichert, W. M., "Decreased analyte transport through implanted membranes: Differentiation of biofouling from tissue effects." *J. Biomed. Mater. Res.* **2001,** *57*, 513-521.

(23) Klueh, U., Kaur, M., Qiao, Y., Kreutzer, D. L., "Critical role of tissue mast cells in controlling long-term glucose sensor function in vivo." *Biomaterials* **2010,** *31*, 4540-4551.

(24) Sharkawy, A. A., Klitzman, B., Truskey, G. A., Reichert, W. M., "Engineering the tissue which encapsulates subcutaneous implants. I. Diffusion properties." *J. Biomed. Mater. Res.* **1997,** *37*, 401-412.

(25) Dungel, P., Long, N., Yu, B., Moussy, Y., Moussy, F., "Study of the effects of tissue reactions on the function of implanted glucose sensors." *J. Biomed. Mater. Res. Part A* **2008,** *85A*, 699-706.

(26) Koschwanez, H. E., Reichert, W. M., Klitzman, B., "Intravital microscopy evaluation of angiogenesis and its effects on glucose sensor performance." *J. Biomed. Mater. Res. Part A* **2010,** *93A*, 1348-1357.

(27) Jablecki, M., Gough, D. A., "Simulations of the frequency response of implantable glucose sensors." *Anal. Chem.* **2000,** *72*, 1853-1859.

(28) Novak, M. T., Yuan, F., Reichert, W. M., "Modeling the relative impact of capsular tissue effects on implanted glucose sensor time lag and signal attenuation." *Anal. Bioanal. Chem.* **2010,** *398*, 1695-1705.

(29) Leaper, D., "Healthcare associated infection: novel strategies and antimicrobial implants to prevent surgical site infection." *Ann. R. Coll. Surg. Engl.* **2010,** *92*, 453-458.

(30) Hetrick, E. M., Schoenfisch, M. H., "Reducing implant-related infections: active release strategies." *Chem. Soc. Rev.* **2006,** *35*, 780-789.

(31) Gristina, A. G., "Biomaterial-centered infection - Microbial adhesion versus tissue integration." *Science* **1987,** *237*, 1588-1595.

(32) Emmerson, M., "A microbiologist's view of factors contributing to infection." *New Horiz.-Sci. Pract. Acute Med.* **1998,** *6*, S3-S10.

(33) Ceri, H., Olson, M. E., Stremick, C., Read, R. R., Morck, D., Buret, A., "The Calgary Biofilm Device: New technology for rapid determination of antibiotic susceptibilities of bacterial biofilms." *J. Clin. Microbiol.* **1999,** *37*, 1771-1776.

(34) Williams, I., Venables, W. A., Lloyd, D., Paul, F., Critchley, I., "The effects of adherence to silicone surfaces on antibiotic susceptibility in Staphylococcus aureus." *Microbiology-(UK)* **1997,** *143*, 2407-2413.

(35) Estivill, D., Arias, A., Torres-Lana, A., Carrillo-Munoz, A. J., Arevalo, M. P., "Biofilm formation by five species of Candida on three clinical materials." *J. Microbiol. Methods* **2011,** *86*, 238-242.

(36) Klueh, U., Kreutzer, D. L., "Murine Model of Implantable Glucose Sensors: A Novel Model for Glucose Sensor Development." *Diabetes Technol. Ther.* **2005,** *7*, 727-737.

(37) Mang, A., Pill, J., Gretz, N., Kränzlin, B., Buck, H., Schoemaker, M., Petrich, W., "Biocompatibility of an Electrochemical Sensor for Continuous Glucose Monitoring in Subcutaneous Tissue." *Diabetes Technol. Ther.* **2005,** *7*, 163-173.

(38) Koschwanez, H. E., Yap, F. Y., Klitzman, B., Reichert, W. M., "In vitro and in vivo characterization of porous poly-L-lactic acid coatings for subcutaneously implanted glucose sensors." *J. Biomed. Mater. Res. Part A* **2008,** *87A*, 792-807.

(39) Gough, D. A., Kumosa, L. S., Routh, T. L., Lin, J. T., Lucisano, J. Y., "Function of an Implanted Tissue Glucose Sensor for More than 1 Year in Animals." *Sci. Transl. Med.* **2010,** *2*.

(40) Moussy, F., Harrison, D. J., Rajotte, R. V., "A miniaturized Nafion-based glucose sensor - In vitro and in vivo evaluations in dogs." *Int. J. Artif. Organs* **1994,** *17*, 88-94.

(41) Wagner, J. G., Schmidtke, D. W., Quinn, C. P., Fleming, T. F., Bernacky, B., Heller, A., "Continuous amperometric monitoring of glucose in a brittle diabetic chimpanzee with a miniature subcutaneous electrode." *Proc. Natl. Acad. Sci. U. S. A.* **1998,** *95*, 6379-6382.

(42) Valdes, T. I., Klueh, U., Kreutzer, D., Moussy, F., "Ex ova chick chorioallantoic membrane as a novel in vivo model for testing biosensors." *J. Biomed. Mater. Res. Part A* **2003,** *67A*, 215-223.

(43) Valdes, T. I., Kreutzer, D., Moussy, F., "The chick chorioallantoic membrane as a novel in vivo model for the testing of biomaterials." *J. Biomed. Mater. Res.* **2002,** *62*, 273-282.

(44) Wisniewski, N., Rajamand, N., Adamsson, U., Lins, P. E., Reichert, W. M., Klitzman, B., Ungerstedt, U., "Analyte flux through chronically implanted subcutaneous polyamide membranes differs in humans and rats." *Am. J. Physiol.-Endocrinol. Metab.* **2002,** *282*, E1316-E1323.

(45) Blakytny, R., Jude, E., "The molecular biology of chronic wounds and delayed healing in diabetes." *Diabetic Med.* **2006,** *23*, 594-608.

(46) Gerritsen, H., Lutterman, J. A., Jansen, J. A., "The influence of impaired wound healing on the tissue reaction to percutaneous devices using titanium fiber mesh anchorage." *J. Biomed. Mater. Res.* **2000,** *52*, 135-141.

(47) Le, N. N., Rose, M. B., Levinson, H., Klitzman, B., "Implant healing in experimental animal models of diabetes." *J. Diabetes Sci. Technol.* **2011,** *5*, 605-618.

(48) Ignarro, L. J., "Nitric oxide: A unique endogenous signaling molecule in vascular biology (Nobel lecture)." *Angew. Chem.-Int. Edit.* **1999,** *38*, 1882-1892.

(49) Walford, G., Loscalzo, J., "Nitric oxide in vascular biology." *J. Thromb. Haemost.* **2003,** *1*, 2112-2118.

(50) Griffith, O. W., Stuehr, D. J., "Nitric oxide synthases: Properties and catalytic mechanism." *Annu. Rev. Physiol.* **1995,** *57*, 707-736.

(51) Cooke, J. P., "NO and angiogenesis." *Atheroscler. Suppl.* **2003,** *4*, 53-60.

(52) Dulak, J., Jozkowicz, A., "Regulation of vascular endothelial growth factor synthesis by nitric oxide: Facts and controversies." *Antioxid. Redox Signal.* **2003,** *5*, 123-132.

(53) Schwentker, A., Vodovotz, Y., Weller, R., Billiar, T. R., "Nitric oxide and wound repair: role of cytokines?" *Nitric Oxide-Biol. Chem.* **2002,** *7*, 1-10.

(54) Carreau, A., Kieda, C., Grillon, C., "Nitric oxide modulates the expression of endothelial cell adhesion molecules involved in angiogenesis and leukocyte recruitment." *Exp. Cell Res.* **2011,** *317*, 29-41.

(55) Wink, D. A., Mitchell, J. B., "Chemical biology of nitric oxide: Insights into regulatory, cytotoxic, and cytoprotective mechanisms of nitric oxide." *Free Radic. Biol. Med.* **1998,** *25*, 434-456.

(56) Mannick, J. B., "Immunoregulatory and antimicrobial effects of nitrogen oxides." *Proc. Am. Thorac. Soc.* **2006,** *3*, 161-165.

(57) Rubbo, H., Radi, R., Trujillo, M., Telleri, R., Kalyanaraman, B., Barnes, S., Kirk, M., Freeman, B. A., "Nitric oxide regulation of superoxide and peroxynitrite-dependent lipid peroxidation. Formation of novel nitrogen-containing oxidized lipid derivatives." *J. Biol. Chem.* **1994,** *269*, 26066-26075.

(58) Deupree, S. M., Schoenfisch, M. H., "Morphological analysis of the antimicrobial action of nitric oxide on Gram-negative pathogens using atomic force microscopy." *Acta Biomater.* **2009,** *5*, 1405-1415.

(59) Miranda, K. M., Espey, M. G., Jourd'heuil, D., Grisham, M. B., Fukuto, J., Freelisch, M., Wink, D. A., Nitric oxide: Biology and pathobiology, in: Ignarro LJ (Eds.), Academic Press, New York, 2000, pp. 41-55.

(60) Stratton, C. W., "Dead bugs don't mutate: Susceptibility issues in the emergence of bacterial resistance." *Emerg. Infect. Dis* **2003,** *9*, 10-16.

(61) Wang, P. G., Xian, M., Tang, X. P., Wu, X. J., Wen, Z., Cai, T. W., Janczuk, A. J., "Nitric oxide donors: Chemical activities and biological applications." *Chem. Rev.* **2002,** *102*, 1091-1134.

(62) Jen, M. C., Serrano, M. C., van Lith, R., Ameer, G. A., "Polymer-based nitric oxide therapies: recent insights for biomedical applications." *Adv. Funct. Mater.* **2012,** *22*, 239-260.

(63) Hrabie, J. A., Keefer, L. K., "Chemistry of the nitric oxide-releasing diazeniumdiolate ("nitrosohydroxylamine") functional group and its oxygen-substituted derivatives." *Chem. Rev.* **2002,** *102*, 1135-1154.

(64) Davies, K. M., Wink, D. A., Saavedra, J. E., Keefer, L. K., "Chemistry of the diazeniumdiolates. 2. Kinetics and mechanism of dissociation to nitric oxide in aqueous solution." *J. Am. Chem. Soc.* **2001,** *123*, 5473-5481.

(65) Williams, D. L. H., "The chemistry of S-nitrosothiols." *Accounts Chem. Res.* **1999,** *32*, 869-876.

(66) Amadeu, T. P., Seabra, A. B., de Oliveira, M. G., Costa, A. M. A., "S-nitrosoglutathione-containing hydrogel accelerates rat cutaneous wound repair." *J. Eur. Acad. Dermatol. Venereol.* **2007,** *21*, 629-637.

(67) Amadeu, T. P., Seabra, A. B., de Oliveira, M. G., Monte-Alto-Costa, A., "Nitric oxide donor improves healing if applied on inflammatory and proliferative phase." *J. Surg. Res.* **2008,** *149*, 84-93.

(68) Coneski, P. N., Nash, J. A., Schoenfisch, M. H., "Nitric oxide-releasing electrospun polymer microfibers." *ACS Appl. Mater. Interfaces* **2011,** *3*, 426-432.

(69) Shin, J. H., Metzger, S. K., Schoenfisch, M. H., "Synthesis of nitric oxide-releasing silica nanoparticles." *J. Am. Chem. Soc.* **2007,** *129*, 4612-4619.

(70) Shin, J. H., Schoenftsch, M. H., "Inorganic/organic hybrid silica nanoparticles as a nitric oxide delivery scaffold." *Chem. Mat.* **2008,** *20*, 239-249.

(71) Riccio, D. A., Nugent, J. L., Schoenfisch, M. H., "Stober synthesis of nitric oxide-releasing S-nitrosothiol-modified silica particles." *Chem. Mat.* **2011,** *23*, 1727-1735.

(72) Riccio, D. A., Dobmeier, K. P., Hetrick, E. M., Privett, B. J., Paul, H. S., Schoenfisch, M. H., "Nitric oxide-releasing S-nitrosothiol-modified xerogels." *Biomaterials* **2009,** *30*, 4494-4502.

(73) Hetrick, E. M., Schoenfisch, M. H., "Antibacterial nitric oxide-releasing xerogels: Cell viability and parallel plate flow cell adhesion studies." *Biomaterials* **2007,** *28*, 1948-1956.

(74) Nablo, B. J., Rothrock, A. R., Schoenfisch, M. H., "Nitric oxide-releasing sol-gels as antibacterial coatings for orthopedic implants." *Biomaterials* **2005,** *26*, 917-924.

(75) Marxer, S. M., Rothrock, A. R., Nablo, B. J., Robbins, M. E., Schoenfisch, M. H., "Preparation of nitric oxide (NO)-releasing sol-gels for biomaterial applications." *Chem. Mat.* **2003,** *15*, 4193-4199.

(76) Nablo, B. J., Schoenfisch, M. H., "Antibacterial properties of nitric oxide-releasing sol-gels." *J. Biomed. Mater. Res. Part A* **2003,** *67A*, 1276-1283.

(77) Robbins, M. E., Schoenfisch, M. H., "Surface-localized release of nitric oxide via sol-gel chemistry." *J. Am. Chem. Soc.* **2003,** *125*, 6068-6069.

(78) Nablo, B. J., Chen, T. Y., Schoenfisch, M. H., "Sol-gel derived nitric-oxide releasing materials that reduce bacterial adhesion." *J. Am. Chem. Soc.* **2001,** *123*, 9712-9713.

(79) Riccio, D. A., Coneski, P. N., Nichols, S. P., Broadnax, A. D., Schoenfisch, M. H., "Photoinitiated nitric oxide-releasing tertiary S-nitrosothiol-modified xerogels." *ACS Appl. Mater. Interfaces* **2012,** *4*, 796-804.

(80) Bungay, P. M., Morrison, P. F., Dedrick, R. L., "Steady-state theory for quantitative microdialysis of solutes and water in vivo and in vitro." *Life Sci.* **1990,** *46*, 105-119.

(81) Bungay, P. M., Newton-Vinson, P., Isele, W., Garris, P. A., Justice, J. B., "Microdialysis of dopamine interpreted with quantitative model incorporating probe implantation trauma." *J. Neurochem.* **2003,** *86*, 932-946.

(82) Mou, X., Lennartz, M. R., Loegering, D. J., Stenken, J. A., "Long-term calibration considerations during subcutaneous microdialysis sampling in mobile rats." *Biomaterials* **2010,** *31*, 4530-4539.

(83) Norton, L. W., Koschwanez, H. E., Wisniewski, N. A., Klitzman, B., Reichert, W. M., "Vascular endothelial growth factor and dexamethasone release from nonfouling sensor coatings affect the foreign body response." *J. Biomed. Mater. Res. Part A* **2007,** *81A*, 858-869.

(84) Mou, X., Lennartz, M. R., Loegering, D. J., Stenken, J. A., "Modulation of the Foreign Body Reaction for Implants in the Subcutaneous Space: Microdialysis Probes as Localized Drug Delivery/Sampling Devices." *J. Diabetes Sci. Technol.* **2011,** *5*, 619-631.

(85) Hetrick, E. M., Prichard, H. L., Klitzman, B., Schoenfisch, M. H., "Reduced foreign body response at nitric oxide-releasing subcutaneous implants." *Biomaterials* **2007,** *28*, 4571-4580.

(86) Sullivan, T. P., Eaglstein, W. H., Davis, S. C., Mertz, P., "The pig as a model for human wound healing." *Wound Repair Regen.* **2001,** *9*, 66-76.

(87) Dobmeier, K. P., Schoenfisch, M. H., "Antibacterial properties of nitric oxide-releasing sol-gel microarrays." *Biomacromolecules* **2004,** *5*, 2493-2495.

(88) Rodrigues, L. R., Inhibition of Bacterial Adhesion on Medical Devices, in: Linke D, Goldman A (Eds.) Bacterial Adhesion: Chemistry, Biology and Physics, Springer-Verlag Berlin, Berlin, 2011, pp. 351-367.

(89) Nablo, B. J., Schoenfisch, M. H., "Poly(vinyl chloride)-coated sol-gels for studying the effects of nitric oxide release on bacterial adhesion." *Biomacromolecules* **2004,** *5*, 2034-2041.

(90) Charville, G. W., Hetrick, E. M., Geer, C. B., Schoenfisch, M. H., "Reduced bacterial adhesion to fibrinogen-coated substrates via nitric oxide release." *Biomaterials* **2008,** *29*, 4039-4044.

(91) Cai, W., Wu, J., Xi, C., Meyerhoff, M. E., "Diazeniumdiolate-doped poly(lactic-co-glycolic acid)-based nitric oxide releasing films as antibiofilm coatings." *Biomaterials* **2012,** *33*, 7933-7944.

(92) Nablo, B. J., Prichard, H. L., Butler, R. D., Klitzman, B., Schoenfisch, M. H., "Inhibition of implant-associated infections via nitric oxide release." *Biomaterials* **2005,** *26*, 6984-6990.

(93) Holt, J., Hertzberg, B., Weinhold, P., Storm, W., Schoenfisch, M., Dahners, L., "Decreasing bacterial colonization of external fixation pins through nitric oxide release coatings." *J. Orthop. Trauma* **2011,** *25*, 432-437.

(94) Engelsman, A. F., Krom, B. P., Busscher, H. J., van Dam, G. M., Ploeg, R. J., van der Mei, H. C., "Antimicrobial effects of an NO-releasing poly(ethylene vinylacetate) coating on soft-tissue implants in vitro and in a murine model." *Acta Biomater.* **2009,** *5*, 1905-1910.

Chapter 2:

Increased In Vivo Glucose Recovery via Nitric Oxide Release

2.1. Introduction

The development of implantable glucose sensors that function for extended durations (>1 week) remains elusive primarily due to the foreign body reaction (FBR).[1, 2] It is now well-known that the FBR is initiated upon protein adsorption to the implant and culminates with the formation of a fibrous capsule that sequesters the implant from normal tissue.[3-6] The acute inflammatory response also has a significant effect on the long-term FBR and sensor function.[7] The unfortunate isolation of implanted sensors via the FBR results in decreased analyte diffusion and analytical performance.[4, 8, 9] Achieving extended sensor lifetimes requires strategies for mitigating the FBR and improving tissue integration. Prior examples of such strategies include the use of more hydrophilic interfaces, porous coatings, and surfaces that release pro-angiogenic factors and collagen inhibitory agents.[10-12] Although some improvements in mitigating the FBR have been reported, none have fully resolved the problems that reduce the sensor lifetime in vivo.

Nitric oxide (NO) is an endogenously produced molecule that acts as a signaling mediator for cytokine production and has been used to reduce bacterial and platelet adhesion.[13-17] In vivo, active release of NO from a surface has been shown to reduce bacterial adhesion/infection and improve implant-tissue integration by reducing inflammatory cell infiltration and collagen encapsulation.[18-21] In these studies, release of NO in the first days of implantation significantly changed the short-term and long-term inflammatory response.[18] As

such, NO release has the potential to address the difficulties with the FBR associated with subcutaneous sensor platforms and improve sensor function.

The positive effects of NO release on the FBR have not been assessed with respect to analyte diffusion through the developing capsule. Our hypothesis is that a thinner capsule may result in enhanced glucose diffusion thus improving one facet of sensor performance. Microdialysis allows for direct quantification of glucose diffusion through a membrane during the FBR. Probes are calibrated by evaluating the extraction efficiency (EE, eq 2.1.) of a given analyte.[22, 23] The EE is calculated using the concentration of analyte in the perfusate, dialysate, and external solution represented by C_p, C_d, and C_e, respectively. The resistances to mass transfer through the membrane (R_m) and dialysate (R_d) are intrinsic to the individual probe and can be accounted for by *in vitro* calibration.[22] The external resistances to mass transfer of biofouling (R_{bf}), encapsulation (R_{ec}), and tissue trauma layers (R_{tr}) are dependent on the host response to the probe once implanted and may change with time.[23-26] Glucose consumption may also be increased in wounded tissue and is thus included in the tissue trauma term.[27]

As with subcutaneous sensors, microdialysis probes suffer from diminished analyte diffusion with longer implantation time.[11, 26, 28] Stenken et al. previously examined the effect of the FBR on analyte diffusion through a microdialysis membrane using magnetic resonance.[29] Others have evaluated membrane composition and the active release of vascular endothelial growth factor (VEGF) or dexamethasone to alter tissue responses.[11, 26] Neither altering membrane composition nor VEGF or dexamethasone release were found to adequately circumvent the effects that the FBR has on analyte diffusion. Herein, we evaluate

$$EE = \frac{C_d - C_p}{C_e - C_p} = 1 - \exp\left(\frac{-1}{Q_d(R_m + R_d + R_{bf} + R_{ec} + R_{tr})}\right)$$

Equation 2.1. The mathematical definition of extraction efficiency (EE). The EE of a given substance is defined as the relationship of the concentrations of the molecule in the dialysate (C_d), perfusate (C_p), and external medium (C_e). The EE can also be related to the flow rate (Q_d) and the resistances to mass transfer in the membrane (R_m), dialysate (R_d), biofouling layer (R_{bf}), collagen encapsulation (R_{ec}), and tissue trauma (R_{tr}).

the influence of NO release on glucose recovery using microdialysis probes implanted subcutaneously in a rodent model.

2.2. Materials and methods

Nitrogen, argon and nitric oxide were purchased from AirGas National Welders (Raleigh, NC). Glucose, glucose oxidase (type VII-S from *Aspergillus niger*; 168800 units/g) and horseradish peroxidase (type I, 118 units/mg) were purchased from Sigma (St. Louis, MO). CMA/20 microdialysis probes with a 10 mm polyarylethersulfone (PAES) membrane and 20-kDa molecular weight cutoff were purchased from CMA Microdialysis Inc (North Chelmsford, MA). Bioanalytical Systems (West Lafayette, IN) Baby Bee syringe pumps with 3-syringe brackets, 1 mL Bee Stinger syringes, FEP tubing, PEEK tubing and microdialysis connectors were used to perfuse microdialysis probes. O-dianisidine dihydrochloride was obtained from Alfa Aesar (Ward Hill, MA). All other reagents used were reagent grade and used as received. Phosphate buffered saline (PBS; 10 mM, pH 7.4) was prepared in-house. PBS saturated with NO (PBS-NO; 1.9 mM NO) was prepared at room temperature by purging approximately 20 mL of PBS with argon gas for 20 min to remove oxygen, followed by nitric oxide gas for 20 min. The solution was stored at 4 °C and used up to 48 h after saturation.

2.2.1. Measurement of NO release. Real-time NO release was collected using a Sievers 280 Chemiluminescent NO Analyzer (Boulder, CO). The instrument was calibrated with an atmospheric sample that had been passed through an NO zero filter and a 25.6 ppm NO gas standard (balance N_2). Nitric oxide release from the microdialysis probe was measured by immersing the probe in deoxygenated PBS at 37 °C. Solutions of PBS-NO were then perfused through the probe at rates of 0.5, 0.8, 1.0, 1.5, and 2.0 µL/min with NO carried

from the buffer to the NO Analyzer by a stream of N_2 bubbled into the solution at a flow rate of 80 mL/min.

2.2.2. In vitro glucose recovery. To determine the optimal flow rate for in vivo studies, microdialysis probes were calibrated in well-stirred solutions of 5.5 M glucose in PBS at flow rates of 0.5, 1.0, 1.5, 2.0, 2.5, 3.0, and 4.0 μL/min. Three separate dialysates were collected at each flow rate from each of three probes and stored at –20 °C until analysis.

2.2.3. Implantation and in vivo perfusion of probes. Prior to implantation, microdialysis probes were sterilized with ethylene oxide (gas treatment), outgassed for 7 days to facilitate ethylene oxide desorption, and subsequently hydrated in sterile PBS for 24 h. Probes were then calibrated in a well-stirred solution of sterile 5.5 mM glucose in PBS at a flow rate of 2.0 μL/min with PBS or PBS−NO as the perfusate. Three separate dialysates were collected from each probe and stored at −20 °C until analysis.

The animal protocol used in this study was approved by an IACUC committee at Duke University. Microdialysis probes were implanted into adult male CD rats (150−200 g) purchased from Charles River Laboratories (Raleigh, NC). Rats were anesthetized with 2−4% isoflurane (v/v in O_2). Two probes (one control and one NO-releasing) were then implanted subcutaneously in 10 rats. Probes were placed bilaterally 5−7 cm caudal to the scapulae, approximately 2 cm lateral to the spine, in the dorsal subcutis with the probe tips oriented caudally and the inflow and outflow percutaneous catheters at the base of the neck.

Polyether ether ketone (PEEK) or fluorinated ethylene propylene (FEP) tubing was used with the control probes. PEEK tubing was connected to the inlet of the NO-releasing probes because of its low permeability to NO. Rats were fitted into infusion harnesses with a spring offset attached to a dual-channel stainless steel swivel on a counter-balanced swivel

mount (Instech Laboratories, Plymouth Meeting, PA) to allow free movement while continuously perfusing probes. Immediately following implantation and for each subsequent day, probes were perfused at 2.0 μL/min for 8 h with test (NO) or control perfusate. During the last 15 min of the perfusion period, one dialysate sample was collected every 5 min and stored at −20 °C. Immediately following sample collection, a blood sample was taken via the rat tail vein to allow for blood glucose measurement using a OneTouch Ultra glucose test strip with a OneTouch Ultra Glucometer (LifeScan, Milpitas, CA).

2.2.4. Explantation and fixation of capsules. After 14 d, or after both probes failed, rats were anesthetized with 2-4% isoflurane (v/v in O_2) to allow explantation of the probes with the surrounding tissue capsule intact. Microdialysis probes were removed from the capsule if still functional and placed in PBS. The capsules were placed in 10% buffered formalin (v/v) for 24 h and then transferred to 70% ethanol for 24 h prior to their embedment into paraffin. Sections of the paraffin embedded capsule were stained with Masson's trichrome or hematoxylin and eosin (H&E) for analysis. Images of the trichrome and H&E stained samples were collected using 4x, 10x and 20x objectives on a Nikon Eclipse TE2000-U with a Nikon Digital Sight DS-2Mv Digital Camera (Nikon Inc., Melville, New York).

2.2.5. Glucose detection. All glucose samples were measured using a colorimetric glucose assay in a 96-well microtiter plate format. Phosphate buffer (58.5 μL, pH 7.0) was added to each microtiter plate followed by addition of either dialysate (3 μL) or varying volumes of a standard glucose solution (1–3 μL) for a calibration curve. In the dark, a glucose assay mix (58.5 μL, pH 7.0) containing glucose oxidase (17.2 U/mL), horseradish peroxidase (3.6 U/mL) and o-dianisidine (0.43 mM) was added to each well and incubated at 37 °C for 1 h. After incubation, 12 N sulfuric acid (80 μL) was added to end the reaction and

intensify the color. The absorbance of each well was measured using a Labsystems Multiskan RC microplate reader (Helsinki, Finland) equipped with a 540 nm filter.

2.2.6. Histological analysis. Histological analysis was performed on tissue adjacent to probes functional ≥13 d of implantation. Capsule thickness was measured from trichrome-stained tissue sample. The foreign body capsule was defined as the region of inflammatory cells at the probe surface and the dense collagen oriented parallel to the probe membrane. Two cross-sectional slides per capsule were imaged with seven measurements of the capsule thickness per image and averaged. Collagen density was calculated in four 400 x 100 μm^2 fields from each of two slides per probe using a previously developed MATLAB (The MathWorks, Natick, MA) program that determines the percent collagen.[10, 30] The inflammatory response as determined by cell density was calculated by counting the nuclei between the dense collagen and probe surface in four 50 x 100 μm^2 fields from each of two slides per probe using a MATLAB program.[30, 31]

2.3. Results and discussion

We and others have demonstrated the promising anti-infection efficacy of and wound healing properties promoted by materials that spontaneously release NO.[18, 20, 21] To date, the long-term benefits of NO on in vivo sensor or probe response have not been determined despite reduced capsule formation. Microdialysis studies allow for direct quantification of analyte diffusion to the implant surface as a function of implant time, a critical parameter for developing biocompatible in vivo sensors. In contrast to standard tissue histology, daily monitoring is feasible as the tissue is not disrupted for analysis, thus requiring fewer animals for a complete study. To evaluate the effect of NO release during the early stages of the wound healing process, an appropriate method for delivering NO was determined.

An initial approach for achieving controlled NO release from a microdialysis probe focused on perfusing small molecule NO donors. First attempts to realize successful and consistent NO release was through utilization of the *N*-diazeniumdiolated form of the amino acid L-proline, PROLI/NO. This small molecule NO donor has a very short half life in physiological media (~1 min). Therefore, to deliver PROLI/NO in vivo, the NO donor was dissolved into a basic solution of 0.01 M NaOH, which preserved the majority of NO release capabilities (~90% of NO payload still available after 1 h). In vivo tests in rat subcutaneous tissue utilized 1 h perfusion periods over 7 d. While the NO release from PROLI/NO did appear to improve the glucose diffusion to the probes (n = 2), the use of 0.01 M NaOH solutions were found to decrease glucose diffusion compared to PBS. Therefore benefits gained by NO release would be, at least in part, masked by the use of the basic solutions.

Other small molecules were tested while only using physiological solutions, but the high instability of small molecule NO donors led to the formation of bubbles in the syringe, resulting in inconsistent flow rates, a major detriment in microdialysis studies. Therefore polymeric systems were implemented. Silica-based nanoparticles were explored due to their extended NO release, but resulted in significantly large probe failure rates. The failures were attributed to blocking of the probe and/or tubing by particles. A smaller polymer system was implemented instead to avoid this clogging issue. A *N*-diazeniumdiolated polyethyleneimine compound was synthesized as previously described.[32] Due to the large amine content on the polymers, the compounds were capable of inducing pH changes in 10 mM PBS. To counteract this problem, a dual-syringe setup was utilized, with one syringe containing the PEI-NO in PBS and the other containing a low pH PBS. When the two streams combined, the pH dropped to ~7.4 resulting in continuous NO release from a polymer system in a

physiological solution. When implemented in vivo, the PEI-NO system actually resulted in decreases in glucose EE. This was hypothesized to be a result of incomplete mixing of the two streams prior to reaching the membrane and/or a increased salt content from the acid/base reaction. Specifically, a large salt content would induce diffusion of water into the probe, resulting in diminished glucose recovery.

As an alternative to perfusing NO donors through the microdialysis probe, a coating could be directly applied to the exterior of the probe. Norton et al. previously coated hydrogels onto microdialysis probes with only modest decreases in EE. Unfortunately, coating of NO-releasing polyurethane directly onto the membrane significantly diminished glucose recovery (EE < 30%), preventing usefulness in vivo. We thus determined that using saturated NO solutions provided steady, controlled NO release without compromising the probe prior to implantation.

2.3.1. In vitro glucose extraction efficiency. To determine EE%, EE (from equation 2.1) was multiplied by 100. An optimal microdialysis flow rate would provide a sufficiently large EE of glucose (0.7) to more easily detect differences in vivo. Flow rates from 0.5 to 2.0 μL/min provided EEs of glucose from 0.7 to 0.95 while flow rates from 2.5 to 4.0 μL/min could only recover 0.35 to 0.55 of glucose in vitro (Figure 2.1). Therefore, only flow rate ≤2 μL/min were investigated in NO studies.

2.3.2. Nitric oxide release from microdialysis probes. Flow rates of 0.5, 0.8, 1.0, 1.5, and 2.0 μL/min were investigated for their steady-state NO release when perfused with PBS-NO solutions (Figure 2.2). As expected, the fastest flow rate (2.0 μL/min) provided the greatest NO flux. However, the measured NO flux was significantly less than expected from

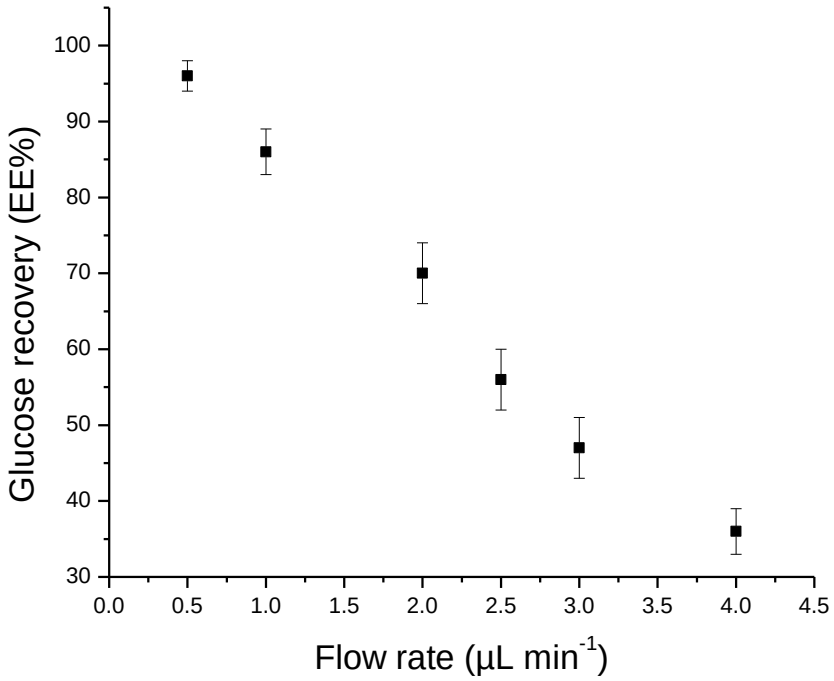

Figure 2.1. Flow rate-dependent recovery of glucose in vitro to PAES microdilaysis probes. Data are mean ± standard deviation.

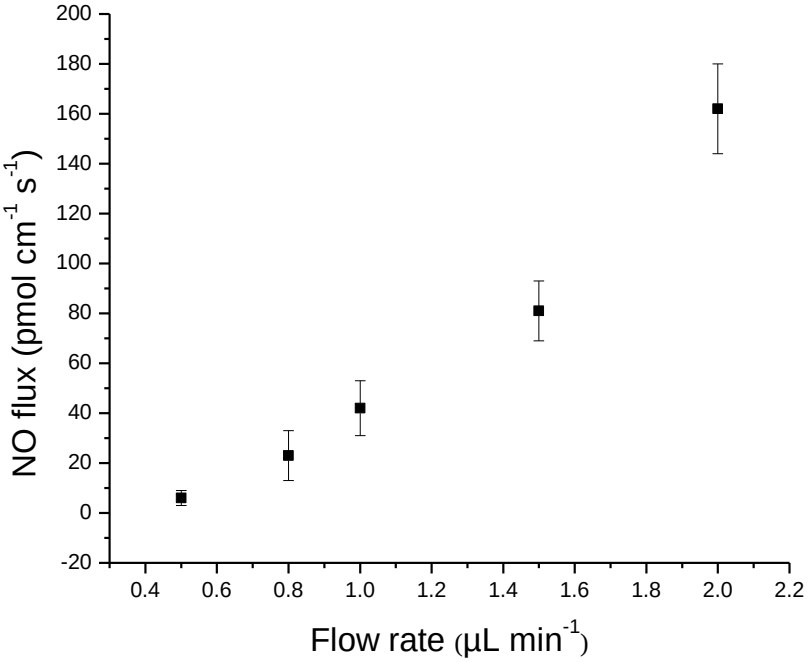

Figure 2.2. Flow rate-dependent NO flux from microdialysis probes. The relationship is not linear due to incomplete diffusion through the probe membrane and leakage through polyurethane microdialysis tubing. Data are mean ± standard deviation.

the saturated NO solution (theoretical flux = 420 pmol cm^{-2} s^{-1}). Furthermore, the relationship of NO flux and flow rate was not linear as might be expected. For example, reducing the flow rate from 2.0 to 1.0 does not lead to a 50% decrease in NO flux, but instead resulted in a ~75% decrease in flux. While a portion of the decreased NO flux may be attributed to incomplete diffusion of the NO through the probe membrane, in vitro experiments replacing the polyurethane probe tubing with a gas impermeable PEEK tubing confirmed that NO diffused out of the tubing. To reduce NO loss, we attempted to replace the inlet tubing with gas-impermeable PEEK tubing. Unfortunately, the stiffness of the PEEK tubing led to a greater rate of probe failure due to undesirable mechanical stress. Although the polyurethane tubing resulted in lower (~60%) NO flux, its use was necessary for enabling a robust set up, with levels of NO similar to previous NO-releasing xerogel materials that reduced the capsule formation in vivo.

The perfusion of PBS-NO solution through the microdialysis probe at 2.0 μL/min provided a constant NO flux during the perfusion period (Figure 2.3.). An 8 h perfusion window allowed time for the probes to be disconnected, reducing mechanical stress on the percutaneous implants (mechanical stress has been shown to affect wound healing in vivo).[10] In PBS, we measure an average NO flux of 162 ± 18 pmol cm^{-2} s^{-1}, corresponding to a total release of 4.6 ± 0.5 μmol cm^{-2} per day over 14 d of implantation. By releasing NO from the perfusate, we were able to compare the control and NO-releasing probes directly as the membrane material contacting the surrounding tissue remained identical. While constant noise in the NO flux originating from the syringe pump noise was noted, the observed signal was always >3σ greater in magnitude (Figure 2.3).

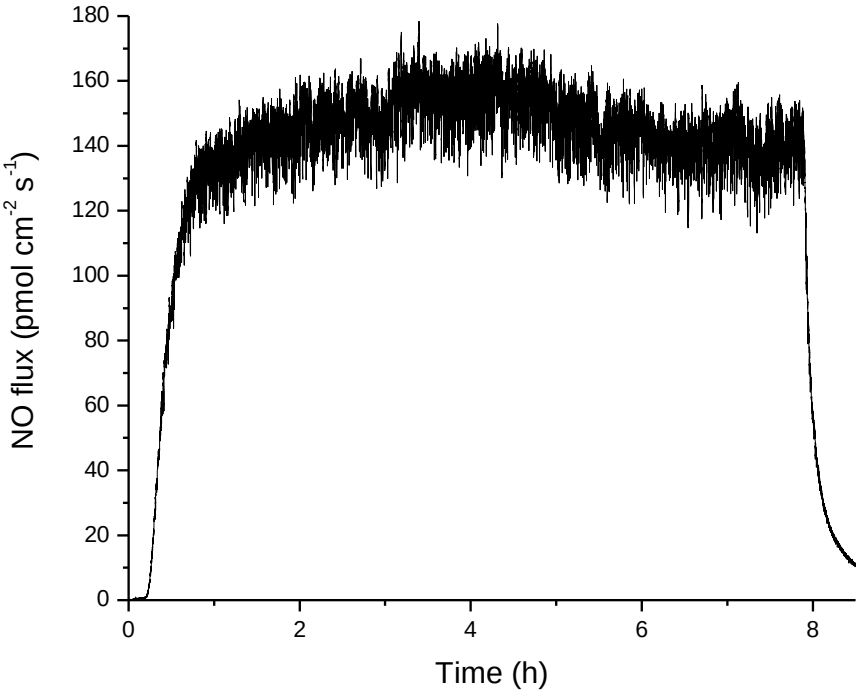

Figure 2.3. Representative daily NO release from a microdialysis probe over 8 h while flowing PBS-NO at 2.0 µL/min.

2.3.3. In vivo glucose recovery. Either the glucose concentration in the external solution (bench studies) or the blood glucose concentration (in vivo) were used with the dialysate concentrations to calculate the EE using Equation 2.1 and multiplied by 100 to obtain EE%. Blood glucose levels were used to estimate the glucose concentration in subcutaneous tissue (C_e).[33] The EE% for glucose of probes in well-stirred in vitro solutions using PBS and PBS−NO was 70 ± 5 and 71 ± 5%, respectively. The observed difference was not statistically significant and allowed for direct comparison between the control and experimental microdialysis probes in vivo. While the in vivo microdialysis flow rate employed (2.0 μL/min) may deplete local glucose more rapidly than an implanted electrochemical sensor,[34] the steady-state equilibrium established in vivo at such a flow rate was necessary to quantify the wound healing response. As shown in Figure 2.4, the EE% of NO-releasing probes remained constant over the 2 week implantation while control probes suffered from diminished analyte diffusion after 7 days of perfusion. As much prior work has noted that fibrous encapsulation diminishes diffusion of small analytes to implant surfaces, our results may indicate a reduced capsule thickness and ultimately improve sensor performance.[35] Indeed, others have indicated that the lag in sensor response time originates from greater resistance to mass transfer.[36] Equally problematic, lowered analyte diffusion through a highly resistive fibrous capsule may interfere with glucose and oxygen levels at the sensor−tissue interface, thereby negatively affecting sensor performance.[37] On the basis of the EE%, we predict that NO-releasing glucose sensor membranes would facilitate enhanced glucose diffusion over long implantation periods compared to controls and improve sensor performance. Such studies are currently underway in our laboratory.

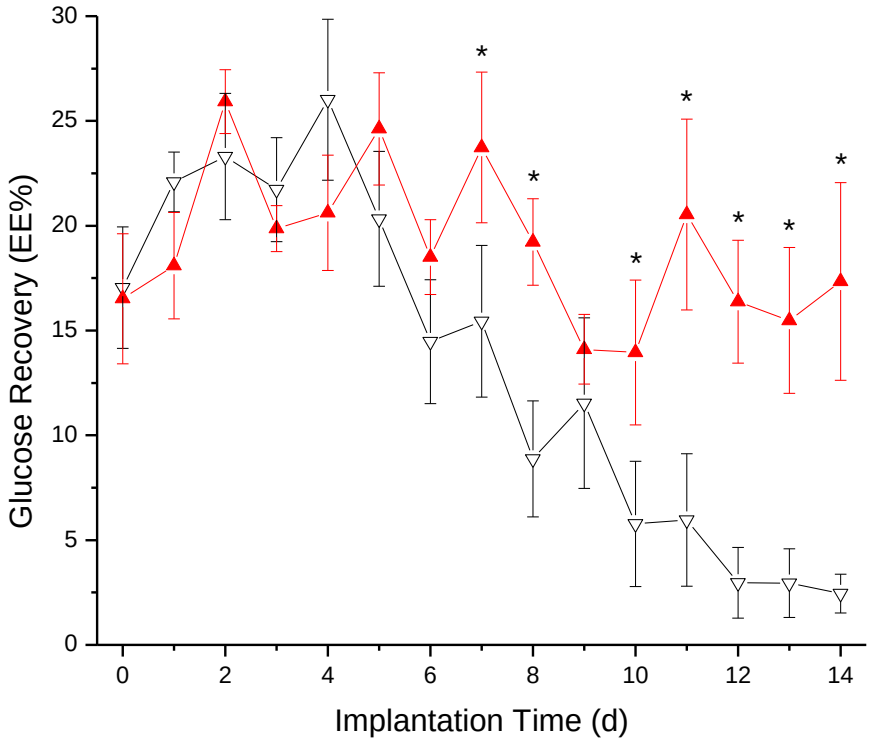

Figure 2.4. Glucose recovery at various times of implantation for the NO-releasing (filled, red) and control (empty, black) microdialysis probes. Data are mean ± standard error of the mean. Significant differences (*) are $p<0.05$.

2.3.4. Histological analysis. Wang et al. previously reported the encapsulation of their microdialysis probes in a rat model after ~7 days.[25] We thus hypothesize that the EE% difference between NO and the control probes is the result of decreased microdialysis probe encapsulation from NO release. Histological analysis of the capsules surrounding NO-releasing and control probes is shown in Figure 2.5. As expected, the thickness of the fibrous capsule surrounding the Masson's trichrome-stained cross sections of control probes (Table 2.1) was greater than that measured for the NO-releasing probes. The cross sections stained with H&E (Figure 2.5) also revealed decreased inflammatory cell densities at the NO-releasing probe membranes relative to controls, indicative of a mitigated FBR. Unexpectedly, the collagen density adjacent to NO-releasing was greater than that adjacent to control probes.

The cause for increased collagen density is presently unknown. While we previously reported a decrease in collagen density for NO-releasing xerogel membranes, others have reported that NO at high concentrations increases collagen deposition in wound healing.[18, 38-40] Of note, the xerogel system resulted in a burst of NO initially followed by significantly less (~95%) NO release for ~3 days. In contrast, the NO release levels used in this study were equivalent to daily NO bursts for 8 h. Although improving glucose recovery and reducing the initial FBR, our data indicates that intermittent NO bursts at large NO flux may negatively impact long-term wound reconstruction. Koschwanez et al. have also reported that percutaneous and subcutaneous implants behave differently, possibly due to mechanical stresses.[10] As well, significant migration of the percutaneously implanted probes was observed during our study, likely caused by animal movement and resulting stress from the

Table 2.1. Results of histological analysis from both hematoxylin and eosin and Masson's trichrome stained slides. Data are mean ± standard deviation.

Probe type	Cell density (nuclei / 50 x 100 μm^2)	Capsule thickness (μm)	Collagen density (%)
Control (n=5)	60 ± 9*	690 ± 60†	62 ± 6*
NO-releasing (n=4)	38 ± 7	600 ± 70	72 ± 4

*Significantly different at $p<0.05$

†Significantly different at $p<0.10$

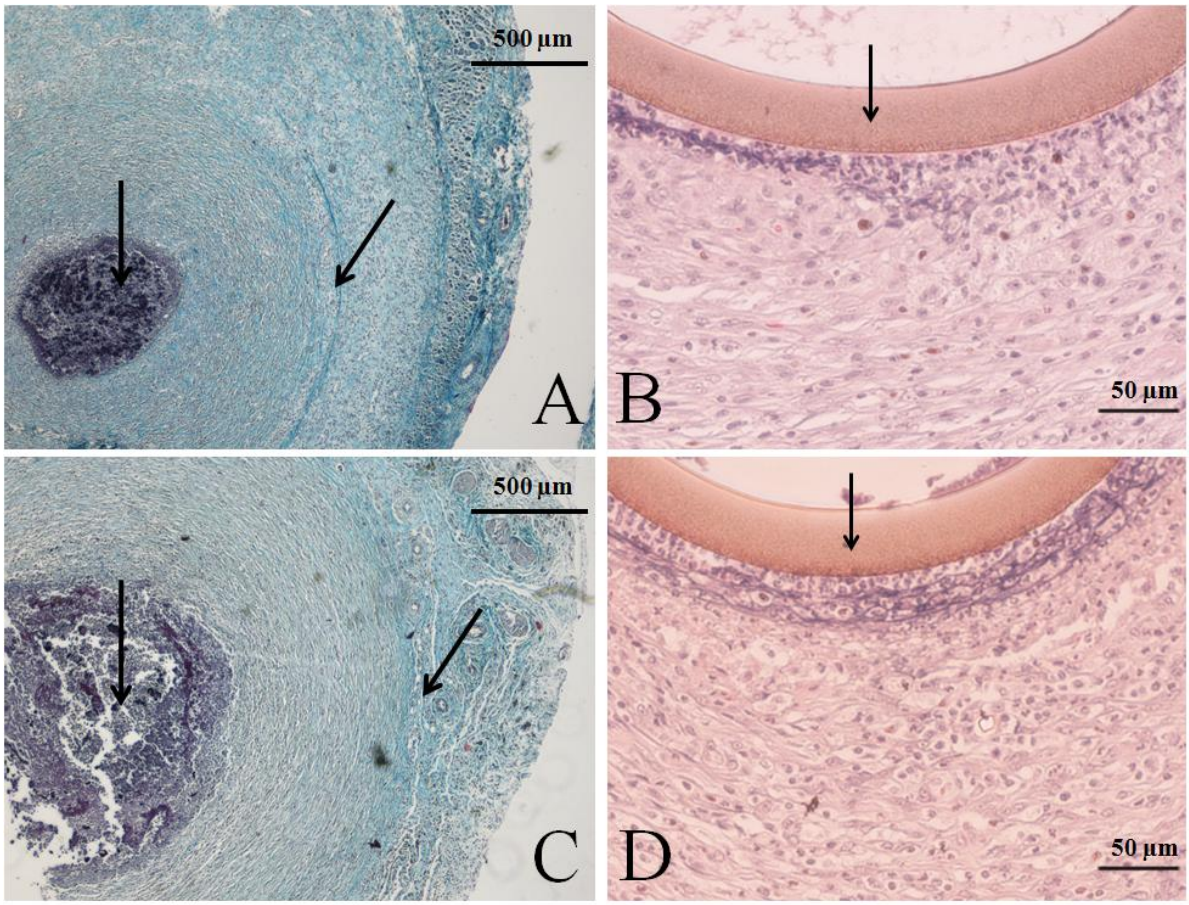

Figure 2.5. Representative histology slides of cross sections stained with Masson's trichrome (A and C) or hematoxylin and eosin (B and D) of NO-releasing (A and B) and control (C and D) probes explanted at 14 d. Arrows in the hematoxylin and eosin stained pictures indicate the probe membrane. Arrows in the Masson's trichrome stained pictures indicate the implant site, surrounded by dark stained inflammatory cells and the collagen capsule. An increased capsule size and inflammatory response at the membrane surface are observed at control probes.

microdialysis tubing. Such stress would augment the FBR to the implanted material. Future studies should examine the effect of NO as a function of implant type (i.e., subcutaneous or percutaneous). Furthermore, NO is a potent vasodilator,[38] and the effect of blood flow changes on glucose recovery using microdialysis probes is controversial.[39-41] However, the glucose recovery in our model was not affected in the acute phase (<7 days) as a function of NO release (Figure 2.4.), indicating no effects due to NO-induced vasodilation. While microdialysis allowed for daily NO release and subsequent analysis of the FBR, probe failure remained a limitation. For example, total microdialysis probe failure rates were ~30 and 65% over 8 and 14 days, respectively (Fig. 2.6.). With the use of these methods, studies lasting ≥14 days would likely suffer similarly high failure rates, regardless of NO release.

2.4. Conclusions

We demonstrated the benefits of *in vivo* NO release using microdialysis with respect to glucose recovery and the FBR. The observed difference in EE% obtained from glucose recovery data suggested improved tissue integration of the microdialysis probe. Histological analysis indicated that the release of NO reduced both the capsule thickness and inflammatory cell density at the surface. While the kinetics and total release of NO employed are not yet achievable through conventional NO storage/release chemistries (e.g., NO donors), our results support the conclusion that NO release is a viable strategy for mitigating the FBR and improving analyte diffusion to a sensor. Future work may determine the optimal NO release flux and durations and the concomitant effects of NO on long-term tissue viability. With the glucose diffusion to a subcutaneous implanted sensor maintained, both the

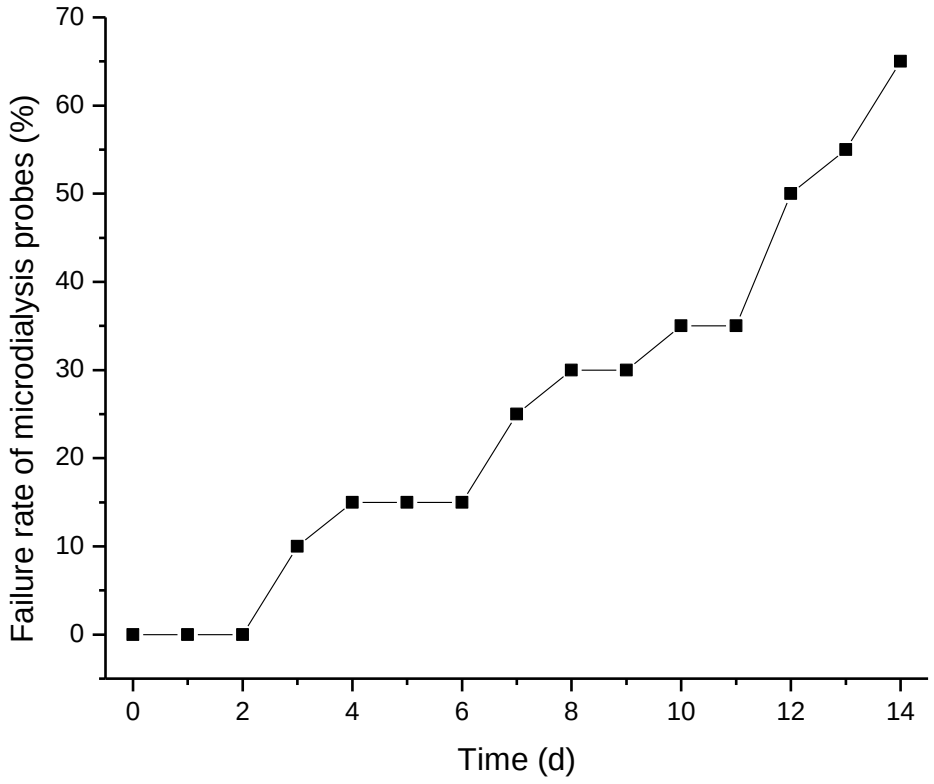

Figure 2.6. In vivo failure rate of microdialysis probes. All probes remained functional for 2 d post-implant, but began to fail thereafter. Over the time course of the study (i.e. 14 d), only 35% of probes were still functional.

sensitivity and response time may be enhanced circumventing previous FBR-mediated limitations. Studies evaluating the effects of NO release on the analytical performance of *in vivo* glucose sensors are currently underway.

2.5. References

(1) Frost, M. C., Meyerhoff, M. E., "Implantable chemical sensors for real-time clinical monitoring: progress and challenges." *Curr. Opin. Chem. Biol.* **2002,** *6*, 633-641.

(2) Wilson, G. S., Gifford, R., "Biosensors for real-time in vivo measurements." *Biosens. Bioelectron.* **2005,** *20*, 2388-2403.

(3) Coleman, D. L., King, R. N., Andrade, J. D., "Foreign body reaction - Chronic inflammatory response." *J. Biomed. Mater. Res.* **1974,** *8*, 199-211.

(4) Gifford, R., Kehoe, J. J., Barnes, S. L., Kornilayev, B. A., Alterman, M. A., Wilson, G. S., "Protein interactions with subcutaneously implanted biosensors." *Biomaterials* **2006,** *27*, 2587-2598.

(5) Ratner, B. D., "Reducing capsular thickness and enhancing angiogenesis around implant drug release systems." *J. Control. Release* **2002,** *78*, 211-218.

(6) Ratner, B. D., Bryant, S. J., "Biomaterials: Where we have been and where we are going." *Annu. Rev. Biomed. Eng.* **2004,** *6*, 41-75.

(7) Wisniewski, N., Reichert, M., "Methods for reducing biosensor membrane biofouling." *Colloid. Surface. B* **2000,** *18*, 197-219.

(8) Dungel, P., Long, N., Yu, B., Moussy, Y., Moussy, F., "Study of the effects of tissue reactions on the function of implanted glucose sensors." *J. Biomed. Mater. Res. Part A* **2008,** *85A*, 699-706.

(9) Koschwanez, H. E., Reichert, W. M., "In vitro, in vivo and post explantation testing of glucose-detecting biosensors: Current methods and recommendations." *Biomaterials* **2007,** *28*, 3687-3703.

(10) Koschwanez, H. E., Yap, F. Y., Klitzman, B., Reichert, W. M., "In vitro and in vivo characterization of porous poly-L-lactic acid coatings for subcutaneously implanted glucose sensors." *J. Biomed. Mater. Res. Part A* **2008,** *87A*, 792-807.

(11) Norton, L. W., Koschwanez, H. E., Wisniewski, N. A., Klitzman, B., Reichert, W. M., "Vascular endothelial growth factor and dexamethasone release from nonfouling sensor coatings affect the foreign body response." *J. Biomed. Mater. Res. Part A* **2007,** *81A*, 858-869.

(12) Ward, W. K., Wood, M. D., Casey, H. M., Quinn, M. J., Federiuk, I. F., "The effect of local subcutaneous delivery of vascular endothelial growth factor on the function of a chronically implanted amperometric glucose sensor." *Diabetes Technol. Ther.* **2004,** *6*, 137-45.

(13) Hetrick, E. M., Schoenfisch, M. H., "Antibacterial nitric oxide-releasing xerogels: Cell viability and parallel plate flow cell adhesion studies." *Biomaterials* **2007,** *28*, 1948-1956.

(14) Mowery, K. A., Schoenfisch, M. H., Saavedra, J. E., Keefer, L. K., Meyerhoff, M. E., "Preparation and characterization of hydrophobic polymeric films that are thromboresistant via nitric oxide release." *Biomaterials* **2000,** *21*, 9-21.

(15) Schoenfisch, M. H., Mowery, K. A., Rader, M. V., Baliga, N., Wahr, J. A., Meyerhoff, M. E., "Improving the thromboresistivity of chemical sensors via nitric oxide release: Fabrication and in vivo evaluation of NO-releasing oxygen-sensing catheters." *Anal. Chem.* **2000,** *72*, 1119-1126.

(16) Schwentker, A., Vodovotz, Y., Weller, R., Billiar, T. R., "Nitric oxide and wound repair: role of cytokines?" *Nitric Oxide-Biol. Chem.* **2002,** *7*, 1-10.

(17) Bogdan, C., "Nitric oxide and the immune response." *Nat. Immunol.* **2001,** *2*, 907-916.

(18) Hetrick, E. M., Prichard, H. L., Klitzman, B., Schoenfisch, M. H., "Reduced foreign body response at nitric oxide-releasing subcutaneous implants." *Biomaterials* **2007,** *28*, 4571-4580.

(19) Amadeu, T. P., Seabra, A. B., de Oliveira, M. G., Costa, A. M. A., "S-nitrosoglutathione-containing hydrogel accelerates rat cutaneous wound repair." *J. Eur. Acad. Dermatol. Venereol.* **2007,** *21*, 629-637.

(20) Gifford, R., Batchelor, M. M., Lee, Y., Gokulrangan, G., Meyerhoff, M. E., Wilson, G. S., "Mediation of in vivo glucose sensor inflammatory response via nitric oxide release." *J. Biomed. Mater. Res. Part A* **2005,** *75A*, 755-766.

(21) Nablo, B. J., Prichard, H. L., Butler, R. D., Klitzman, B., Schoenfisch, M. H., "Inhibition of implant-associated infections via nitric oxide release." *Biomaterials* **2005,** *26*, 6984-6990.

(22) Bungay, P. M., Morrison, P. F., Dedrick, R. L., "Steady-state theory for quantitative microdialysis of solutes and water in vivo and in vitro." *Life Sci.* **1990,** *46*, 105-119.

(23) Bungay, P. M., Newton-Vinson, P., Isele, W., Garris, P. A., Justice, J. B., "Microdialysis of dopamine interpreted with quantitative model incorporating probe implantation trauma." *J. Neurochem.* **2003,** *86*, 932-946.

(24) Stenken, J. A., "Methods and issues in microdialysis calibration." *Anal. Chim. Acta* **1999,** *379*, 337-358.

(25) Wang, X., Lennartz, M. R., Loegering, D. J., Stenken, J. A., "Interleukin-6 collection through long-term implanted microdialysis sampling probes in rat subcutaneous space." *Anal. Chem.* **2007,** *79*, 1816-1824.

(26) Wisniewski, N., Klitzman, B., Miller, B., Reichert, W. M., "Decreased analyte transport through implanted membranes: Differentiation of biofouling from tissue effects." *J. Biomed. Mater. Res.* **2001,** *57*, 513-521.

(27) Forster, J., Morris, A. S., Shearer, J. D., Mastrofrancesco, B., Inman, K. C., Lawler, R. G., Bowen, W., Caldwell, M. D., "Glucose uptake and flux through phosphofructokinase in wounded rat skeletal muscle." *Am. J. Physiol.* **1989,** *256*, E788-E797.

(28) Mou, X., Lennartz, M. R., Loegering, D. J., Stenken, J. A., "Long-term calibration considerations during subcutaneous microdialysis sampling in mobile rats." *Biomaterials* **2010,** *31*, 4530-4539.

(29) Stenken, J. A., Reichert, W. M., Klitzman, B., "Magnetic resonance imaging of a tissue/implanted device biointerface using in vivo microdialysis sampling." *Anal. Chem.* **2002,** *74*, 4849-4854.

(30) Bancroft, J., Gamble, M., Theory and practice of histological techniques, 6 ed., Churchill Livingstone, London 2007.

(31) Badie, N., Satterwhite, L., Bursac, N., "A method to replicate the microstructure of heart tissue in vitro using DTMRI-based cell micropatterning." *Ann. Biomed. Eng.* **2009,** *37*, 2510-2521.

(32) Zhou, Z., Annich, G. M., Wu, Y., Meyerhoff, M. E., "Water-soluble oly(ethylenimine)-based nitric oxide donors: Preparation, characterization, and potential application in hemodialysis." *Biomacromolecules* **2006,** *7*, 2565-2574.

(33) Fischer, U., Ertle, R., Abel, P., Rebrin, K., Brunstein, E., Vondorsche, H. H., Freyse, E. J., "Assessment of subcutaneous glucose-concentration - Validation of the wick technique as a reference for implanted electrochemical sensors in normal and diabetic dogs." *Diabetologia* **1987,** *30*, 940-945.

(34) Lowry, J. P., O'Neill, R. D., Boutelle, M. G., Fillenz, M., "Continuous monitoring of extracellular glucose concentrations in the striatum of freely moving rats with an implanted glucose biosensor." *J. Neurochem.* **1998,** *70*, 391-396.

(35) Sharkawy, A. A., Klitzman, B., Truskey, G. A., Reichert, W. M., "Engineering the tissue which encapsulates subcutaneous implants. I. Diffusion properties." *J. Biomed. Mater. Res.* **1997,** *37*, 401-412.

(36) Jablecki, M., Gough, D. A., "Simulations of the frequency response of implantable glucose sensors." *Anal. Chem.* **2000,** *72*, 1853-1859.

(37) Wilson, G. S., Hu, Y. B., "Enzyme based biosensors for in vivo measurements." *Chem. Rev.* **2000,** *100*, 2693-2704.

(38) Lloyd-Jones, M. D., Donald M., Bloch, M. D., Kenneth D., "The vascular biology of nitric oxide and its role in Atherogenesis." *Annu. Rev. Med.* **1996,** *47*, 365-375.

(39) Kurosawa, M., Hallstrom, A., Ungerstedt, U., "Changes in cerebral blood-flow do not directly affect in vivo recovery of extracellular lactate through microdialysis probe." *Neurosci. Lett.* **1991,** *126*, 123-126.

(40) Rosdahl, H., Lind, L., Millgard, J., Lithell, H., Ungerstedt, U., Henriksson, J., "Effect of physiological hyperinsulinemia on blood flow and interstitial glucose concentration in human skeletal muscle and adipose tissue studied by microdialysis." *Diabetes* **1998,** *47*, 1296-1301.

(41) Stenken, J. A., Lunte, C. E., Southard, M. Z., Stahle, L., "Factors that influence microdialysis recovery. Comparison of experimental and theoretical microdialysis recoveries in rat liver." *J. Pharm. Sci.* **1997,** *86*, 958-966.

Chapter 3:

The Effect of Nitric Oxide Surface Flux on the Foreign Body Response to Subcutaneous Implants

3.1. Introduction

The foreign body response (FBR) is a major impediment toward the development and long-term functionality of most implanted biomedical devices. Implantation disrupts the native tissue, initiating the FBR with the adhesion of proteins and other biomolecules to the device surface.[1, 2] This process continues with the infiltration of inflammatory cells that attempt to phagocytose the foreign object.[1, 2] Within a few weeks, the cells create a relatively avascular collagen-rich encapsulation, effectively sequestering the implant from the surrounding tissue.[3] Macrophages undergo cell fusion to form multi-nucleated foreign body giant cells (FBGCs) that remain at the implant surface and enhance its degradation, often leading to device failure or performance mitigation.[4, 5] In the case of implanted glucose sensors, this isolation blocks the diffusion of glucose from surrounding tissue, inhibiting accurate measurements.

Efforts to improve the fate of subcutaneous implants have largely focused on developing materials with chemical and physical properties that mitigate the FBR and allow better tissue integration. The use of natural materials (e.g., collagen)[6, 7] and synthetic polymers[8, 9] to alter the tissue-sensor interface has slightly improved tissue integration of such devices. However, complete avoidance of the FBR has yet to be achieved and the field

of biomaterials has evolved to include the design of coatings that actively release FBR mediators.[10] For glucose sensors, the focus has been on materials that release anti-inflammatory (i.e., dexamethasone) and/or pro-angiogenic (i.e., vascular endothelial growth factor (VEGF)) mediators.[11-14] Unfortunately, reports on the combined use of dexamethasone and VEGF have been controversial, possibly due to the molecules acting in an antagonistic manner.[13-16]

Other work has focused on the design of interfaces that release nitric oxide (NO) and endogenous signaling molecule that plays multiple roles in the immune response including an initiator of cytokine production,[17, 18] collagen deposition,[19-22] angiogenesis,[23] and anti-microbial activity.[24] Hetrick et al. examined the subcutaneous in vivo response to NO-releasing *N*-diazeniumdiolated xerogels coated onto rectangular silicone rubber substrates.[25] These coatings released ~1.35 μmol/cm^2 of NO over 72 hours with 50% of the NO payload exhausted within 5 h. A >50% decrease in collagen capsule thickness was observed after 3 weeks of implantation.[25] Furthermore, NO release reduced the chronic inflammation at 3 and 6 weeks while enhancing angiogenesis adjacent to the implant after only 1 week of implantation.[25] As found in Chapter 2, mitigation of the FBR with NO release was found to improve glucose diffusion to NO-releasing microdialysis probes after 7 days of implantation in rat subcutaneous tissue which would effectively decrease implantable glucose sensor lag time.[26] In this case, 4.6 μmol NO/cm^2 was released each day by perfusing saturated NO solutions for 8 h over 14 d of implantation.[26] Histological analysis at 14 d revealed a thinner collagen capsule and reduced inflammatory response for the NO-releasing probes.[26] Gifford et al. prepared subcutaneous glucose sensors capable of releasing NO for 18 h by doping the NO donor (Z)-1-[*N*-methyl-*N*-[6-(*N*-butylammoniohexyl)amino]]-diazen-1-ium-1,2-diolate

(DBHD/N_2O_2) into a polymer matrix.[27] The in vivo inflammatory response was significantly reduced in response to the NO-releasing materials after implantation of 24 h but not at 48 h.[27] The authors noted that the reduction in the inflammatory response correlated well with the NO release duration, supporting a need for long-term NO release.[27] Decreased collagen encapsulation and inflammation with increased angiogenesis have been identified previously as key factors that enhance glucose sensor function.[28] Taken together, these reports support the promise of improved tissue integration and subcutaneous sensor functionality using materials that release NO.

While the positive effects of NO are well known, the optimal rate and amounts of NO release are unclear. Previously, Koh et al. reported the ability to dope NO-releasing nanoparticles of various compositions into polyurethane (PU) matrices and control the NO release kinetics based on the properties of the PU and/or NO-releasing scaffold.[29] The NO-releasing properties from these materials suggest that they are idea for systematically studying the effect of NO on the FBR from chemically identical interfaces. To better mimic the human FBR and wound healing, this study is carried out in a porcine subcutaneous implant model.[30]

3.2. Materials and methods

Tetramethoxysilane (TMOS) and L-proline were purchased from Sigma Aldrich (St. Louis, MO). 3-Mercaptopropyltrimethoxysilane (MPTMS), *N*-(2-aminoethyl)-3-aminopropyltrimethoxysilane (AEAP3), and tetraethoxysilane (TEOS) were purchased from Gelest (Tullytown, PA). Diethylenetriamine pentaacetic acid (DTPA) was purchased from Fluka (Buchs, Switzerland). Ethanol (EtOH), methanol (MeOH), tetrahydrofuran (THF), and ammonia solution (NH_4OH, 30 wt % in water) were purchased from Fisher Scientific (Fair

Lawn, NJ). Stainless steel wire (316L, 381 μm diameter) was purchased from McMaster-Carr (Atlanta, GA). Tecoplast TP-470-000 (TP-470), Tecophillic HP-93A-100 (HP 93A) and Tecoflex SG-80A (TPU) were gifts from Thermedics (Woburn, MA). Hydrothane AL 25-80A (HPU) was a gift from AdvanSource Biomaterials Corporation (Wilmington, MA). Nitric oxide was purchased from Praxair (Danbury, CT). Nitric oxide calibration gas (26.39 ppm; balance nitrogen), nitrogen, and argon were purchased from National Welders (Raleigh, NC). Distilled water was purified to 18.2 MΩ/cm with a Millipore Milli-Q Gradient A-10 water purification system (Bedford, MA). All other reagents were reagent grade and used as received.

3.2.1. Preparation of NO-releasing scaffolds. 1-[2-(carboxylato)pyrrolidin-1-yl]diazen-1-ium-1,2-diolate (PROLI/NO) was prepared by converting the secondary amine in L-proline to an *N*-diazeniumdiolate following a previously described procedure.[31] Nitric oxide-releasing silica particles were synthesized based on the sol–gel process via the co-condensation of AEAP3 (70 mol% balance TMOS) or MPTMS (75 mol% balance TEOS).[32, 33] Subsequent *N*-diazeniumdiolation of the amine- containing particles was performed under high pressure of NO for 3 d in the presence of sodium methoxide in methanol at room temperature.[32] Nitrosation of the thiol-containing nanoparticles was carried out by reaction with acidified nitrite in the dark at 0 °C.[33] The details of the NO-releasing characteristics for each system are provided in Table 3.1.

3.2.2. Preparation of polyurethane-coated wire substrates. Stainless steel wires were cut to ~5 cm and cleaned by sonicating sequentially in EtOH, water, and EtOH again for 30 min each and sterilized by autoclaving. To create the NO-releasing coating, the NO-releasing vehicle (i.e., PROLI/NO, AEAP3 nanoparticles or MPTMS nanoparticles) was dispersed into

Table 3.1. Nitric oxide release properties of silica nanoparticles at pH 7.4 and 37 °C. Data are mean ± standard deviation.

Nanoparticle system	Max flux (pmol mg^{-1})	t_{max} (min)	$t_{1/2}$ (min)	total NO (μmol mg^{-1})
AEAP3	145 ± 28	1.13 ± 0.27	185 ± 35	2.05 ± 0.06
MPTMS	241 ± 35	1.87 ± 0.31	213 ± 20	2.95 ± 0.25

cold EtOH (2.5 mL) at concentrations of 36 or 72 mg/mL. This solution was then mixed with an equal volume of 50:50 wt% HPU/TPU (160 mg/mL total PU) dissolved in THF (2.5 mL) for a resulting concentration of 18 or 36 mg/mL scaffold and 80 mg/mL PU in 50:50 v/v EtOH/THF. In a sterile laminar flow hood, wires were then dip-coated four times in the scaffold-containing PU solution with brief ambient drying between dips. A polyurethane topcoat (TP-470, TPU, HPU/TPU, HPU or HP 93A; 40 mg/mL dissolved in THF) was then applied and allowed to dry. The PU-coated wire was then cut to 3 cm, and the freshly cut end was coated with the same PU topcoat. The PU-modified wires were placed into individual, sterile, microcentrifuge tubes and kept vacuum sealed in the dark at -20 °C until use. Control (non-NO-releasing) wires were made using the same protocol but with no scaffold in the PU solutions.

3.2.3. Characterization of polyurethane-coated wires. Scanning electron microscopy was used to evaluate the macroscopic surface roughness of the coated wires using a Quanta 200 (FEI, Hillsboro, OR) in high vacuum mode before and after the topcoating process. Release of NO was measured continuously using a Sievers 280i Chemiluminescence Nitric Oxide Analyzer (NOA) (Boulder, CO).[34] Calibration of the NOA was performed with both air passed through a Sievers NO zero filter and 26.39 ppm NO gas (balance N_2). For analysis, NO-releasing wire substrates were immersed in 25 mL of deoxygenated phosphate buffered saline (PBS; 10 mM, pH 7.4). Released NO was carried to the analyzer in a nitrogen stream (200 mL min^{-1}). Temperature control was maintained using a water bath at 37 °C. Nitric oxide release from nitrosothiol nanoparticle-doped coatings were studied by shielding the sample flask from light and using PBS with 500 μM DTPA to chelate trace copper. The thickness of the wire coatings was estimated by optical microscopy.

3.2.4. Silicon elemental analysis. To characterize particle stability (via leaching) in the various polyurethane polymers, substrates were incubated at 37 °C in PBS (1 mL) for 1, 3 and 6 weeks. Samples were then further prepared for Si elemental analysis by adding aqua regia (2.5 mL), hydrofluoric acid (1 mL), and 40% triethanolamine (3.575 mL) to dissolve the particles, and then diluted to 50 mL with water. To determine the mass of silica nanoparticles contained in the PU films, the coatings were dissolved in piranha solution (1 mL), exposed to hydrofluoric acid (1 mL) and 40% triethanolamine (3.575 mL), then diluted to 50 mL with water. (CAUTION: hydrofluoric acid and piranha are extremely corrosive and require special handling). The silicon concentration in the solutions was subsequently measured using inductively coupled plasma-optical emission spectroscopy (ICP-OES; Prodigy, Teledyne Leeman Labs, Hudson, NH).

3.2.5. Implantation and explantation of wire substrates. The animal protocol used in this study was reviewed and approved by the IACUC at Duke University. Coated wire substrates were implanted into seventeen mixed breed Yorkshire-type piglets weighing approximately 5–7 kg. Pigs were initially anesthetized with ketamine:xylazine (20 mg/kg and 2 mg/kg, respectively) and maintained on 2–4% isoflurane (v/v in O_2) during implantation. The dorsal skin was prepared by clipping of the hair and triplicate scrubbing with chlorhexidine and alcohol. Four 1 cm incisions were created 4 cm lateral to the dorsal midline and 8 cm and 18 cm caudal to the scapulae using a scalpel. Five or six wires were then inserted radially ("clock hour" pattern) in the 2, 4, 6, 8, 10, and 12 o'clock positions, extending 2 cm out from the incision. The 6 o'clock position was eliminated in two caudal implant sites, resulting in 22 wires implanted per pig.

After 3, 7, 21 or 42 d, pigs were anesthetized and the tissue surrounding the wire implants was explanted and placed into 10% buffered formalin (v/v) for 24 h, then transferred to 70% EtOH (v/v in H_2O) for at least 24 h prior to embedding into paraffin. Sections of the paraffin embedded tissue were stained with Masson's trichrome or hematoxylin and eosin (H&E). Micrographs of the trichrome and H&E stained samples were collected using 4, 10, and 20X objectives on a Nikon Eclipse TE2000-U with a Nikon Digital Sight DS-2Mv digital camera (Nikon Inc., Melville, NY).

3.2.6. Histological analysis. Histological analysis was performed on all explanted tissue samples. Capsule thickness was measured from Masson's trichrome-stained tissue sections. The foreign body capsule was defined as beginning at the edge of the implant and consisting of the region of dense collagen oriented parallel to the implant. The end of the capsule thickness was determined to be where collagen was no longer the primary tissue constituent (indicated by a decrease in the density of blue-green stain) nor oriented parallel to the surface. Eight capsule thickness measurements, taken radially at 45° intervals, were averaged for each image. Three images of the collagen capsule were processed using a previously developed MATLAB (The MathWorks, Natick, MA) program that quantifies the percent collagen.[35, 36] The program defines collagen from trichrome-stained images by the characteristic blue-green color, divides the number of collagen positive pixels by the total pixels in the image, and multiplies this ratio by 100 to obtain the percent collagen. Hematoxylin and eosin-stained tissue sections were used to measure the inflammatory response. The inflammatory response, as determined by cell density, was determined by counting all cell nuclei within 50 μm of the implant surface from three 50 x 100 μm^2 fields from each slide. Cell nuclei were defined as the purple-stained, spherical features in the

H&E-stained tissue sections. Histology data are expressed as mean ± standard error of the mean and tested for significance (i.e., $p < 0.05$) using a non-parametric Wilcoxon rank-sum test.

3.3. Results and discussion

3.3.1. Characterization of polyurethane coatings. Wire substrates were successfully coated with particle-doped polyurethanes (PUs) capable of releasing NO via dip-coating. The use of wire substrates was pursued to mimic the shape and size of an electrochemical glucose sensor. Both size and shape have been shown to affect the FBR.[37, 38] The thickness of the PU coatings remained constant even with the incorporation of a range of NO-releasing scaffold and concentrations. For example, control PU and 36 mg/mL MPTMS nanoparticle-doped PU coatings were 46 ± 4 and 49 ± 4 μm, respectively. Prior to topcoating, the particle-doped films exhibited significantly greater surface roughness than controls as evaluated using SEM (Fig. 3.1.A). As previous in vivo studies have reported that surface roughness may significantly alter the FBR,[39, 40] a PU topcoat was added (Fig. 3.1.B) to ensure that the tissue response observed in vivo was a result of NO release and not physical properties.

Although silica is generally considered non-toxic,[41] leaching of nanoparticles was quantified to address concerns of unexpected effects in vivo. To determine the percentage of silica particles leached, the mass of nanoparticles within the films was measured by dissolving the PU coatings and quantifying via ICP-OES. Wires dipcoated in 36 mg/mL AEAP3 nanoparticle-doped PU and 36 mg/mL MPTMS nanoparticle-doped PU contained 1.1 ± 0.2 mg and 1.2 ± 0.1 mg of silica nanoparticles, respectively. Over 6 weeks, AEAP3 nanoparticles leached 4.2 ± 0.7% of the total loaded scaffold, with the majority of the leaching (>90%) occurring during the first 3 weeks (Fig. 3.2). The MPTMS soak

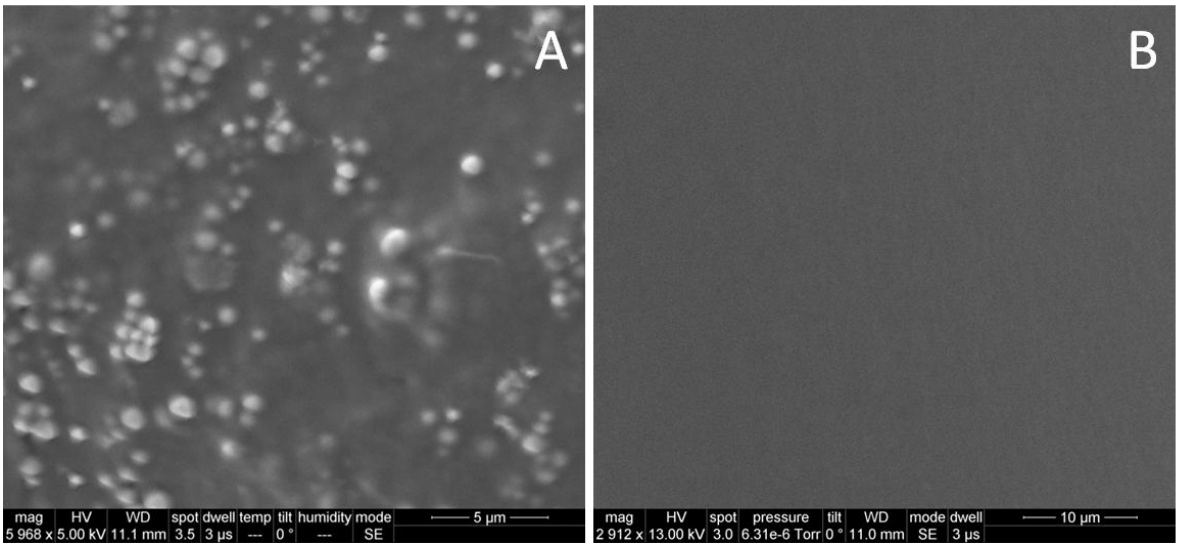

Figure 3.1. Scanning electron microscope images of polyurethane-coated wire substrates A) dipcoated four times in 36 mg/mL MPTMS nanoparticles in 80 mg/mL HPU/TPU before topcoating, and B) after topcoating with a 40 mg/mL HPU/TPU solution. Nanoparticle-induced surface roughness is masked after topcoating.

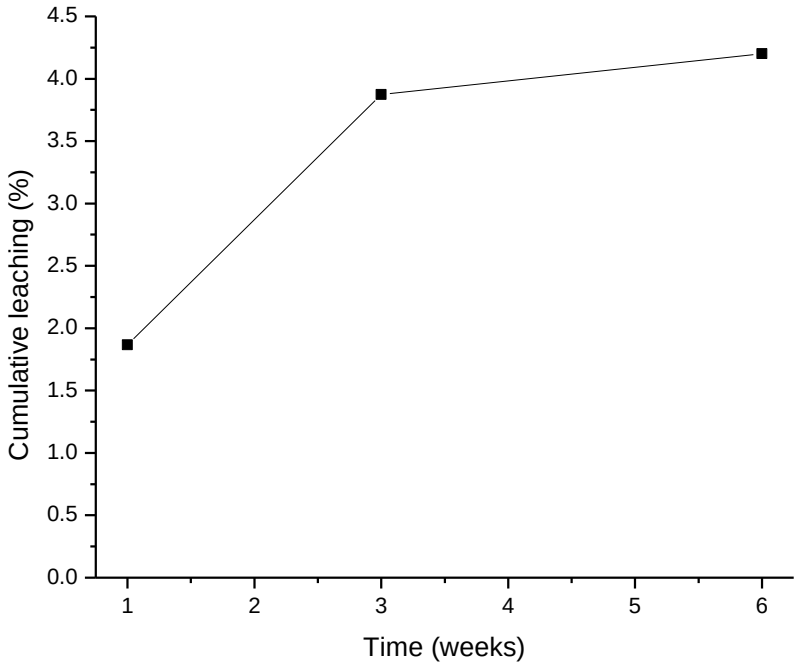

Figure 3.2. Cumulative leaching from HPU/TPU topcoated 36 mg/mL AEAP3 nanoparticle system over 6 weeks as quantified by ICP-OES. More than 90% of the total leaching occurs over the first 3 weeks. Over the maximum length of the in vivo study (i.e., 6 weeks), 4.2% of the AEAP3 nanoparticles may leach from the polyurethane.

solutions had no detectable leaching, likely due to the larger particle size of the MPTMS (~750-900 nm) compared to the AEAP3 (~110-150 nm) nanoparticles.

3.3.2. Nitric oxide release from polyurethane films. To evaluate the effect of NO release kinetics on the FBR, several NO-releasing scaffolds were employed including PROLI/NO, AEAP3, and MPTMS. The low molecular weight (LMW) *N*-diazeniumdiolate PROLI/NO provided the fastest NO release with >90% of NO storage liberated after 6 min. Longer durations of NO release from *N*-diazeniumdiolate donors was achieved using a hybrid silica nanoparticle scaffold containing AEAP3 with a NO release half-life of 185 min. By varying the water uptake by selection of the PU topcoat, NO release kinetics were further tuned for *N*-diazeniumdiolate systems whereby NO donor composition is proton initiated.[42, 43] As shown in Table 3.2, the four PUs used in the study were chosen in part due to their water uptake.[29]

The release of NO from *N*-diazeniumdiolate and *S*-nitrosothiol NO donors follows pseudo first-order kinetics. Although doping the NO donors into polyurethane matrices may slow NO donor breakdown (and thus NO release), the materials still follow approximate first-order kinetics, with an initial maximum and exponential decay in NO flux. Due to rapid NO donor breakdown, LMW PROLI/NO-doped PUs released NO rapidly (~24 h) and with the greatest NO fluxes (1400 to 3100 pmol cm^{-2} s^{-1}) depending on the polyurethane matrix (Table 3.3). The prominent burst of NO may impact the FBR. For example, exogenous NO has been shown to inhibit platelet adhesion and aggregation, and thus elevated NO may slow early healing.[44, 45] Compared to the PROLI/NO-doped polymers, the NO release from AEAP3 nanoparticle-doped PUs (Tables 3.4 and 3.5) was significantly longer in duration (up to 72 h) compared to the PROLI/NO-doped polymers due to the longer half-life of the

Table 3.2. Water uptake of polyurethane topcoats.[29] Data are mean ± standard deviation.

Polyurethane	Water Uptake (mg H_2O/mg PU)
Tecophillic HP-93A-100 (HP 93A)	2.6 ± 0.3
Hydrothane AL 25-80A (HPU)	0.63 ± 0.3
Tecoflex SG-80A (TPU)	0.20 ± 0.2
Tecoplast TP-470-000 (TP-470)	0.04 ± 0.05

Table 3.3. Nitric oxide release from coatings doped at 18 mg/mL PROLI/NO as a function of polyurethane topcoat. Data are mean ± standard deviation.

NO release properties	Type of polyurethane topcoat				
	HP 93A	HPU	HPU/TPU	TPU	TP-470
$[NO]_{max}$ (pmol cm^{-2} s^{-1})	3100 ± 700	2900 ± 400	2600 ± 400	1500 ± 200	1400 ± 300
t_{max} (min)	8.4 ± 0.8	8.4 ± 0.6	9.1 ± 0.5	18 ± 1	17 ± 3
$[NO]_{6\ h}$ (pmol cm^{-2} s^{-1})	5 ± 2	7 ± 2	23 ± 4	28 ± 4	27 ± 4
$[NO]_{12\ h}$ (pmol cm^{-2} s^{-1})	0	1.9 ± 0.2	2.5 ± 0.4	5.7 ± 0.7	7.0 ± 0.8
$[NO]_{24\ h}$ (pmol cm^{-2} s^{-1})	0	0	0.9 ± 0.3	1.7 ± 0.3	2.0 ± 0.3
Total NO (μmol cm^{-2})	3.9 ± 0.4	3.8 ± 0.5	4.1 ± 0.5	4.2 ± 0.5	4.1 ± 0.4

Table 3.4. Nitric oxide release from coatings doped at 18 mg/mL AEAP3 nanoparticles as a function of polyurethane topcoat. Data are mean ± standard deviation.

NO release properties	Type of polyurethane topcoat				
	HP 93A	HPU	HPU/TPU	TPU	TP-470
$[NO]_{max}$ (pmol cm^{-2} s^{-1})	110 ± 20	100 ± 20	100 ± 20	80 ± 20	42 ± 9
t_{max} (min)	9 ± 1	7 ± 1	19 ± 3	70 ± 20	80 ± 20
$[NO]_{6\ h}$ (pmol cm^{-2} s^{-1})	28 ± 4	50 ± 5	45 ± 5	43 ± 6	38 ± 8
$[NO]_{12\ h}$ (pmol cm^{-2} s^{-1})	11 ± 2	19 ± 3	21 ± 2	19 ± 1	22 ± 4
$[NO]_{24\ h}$ (pmol cm^{-2} s^{-1})	1.0 ± 0.3	1.9 ± 0.2	2.3 ± 0.3	5.6 ± 0.9	11 ± 2
$[NO]_{48\ h}$ (pmol cm^{-2} s^{-1})	0	0.98 ± 0.04	1.13 ± 0.08	1.37 ± 0.09	1.7 ± 0.2
Total NO (μmol cm^{-2})	2.7 ± 0.3	3.0 ± 0.3	3.0 ± 0.4	2.8 ± 0.3	2.7 ± 0.3

Table 3.5. Nitric oxide release from coatings doped at 36 mg/mL AEAP3 nanoparticles as a function of polyurethane topcoat. Data are mean ± standard deviation.

NO release properties	Type of polyurethane topcoat				
	HP 93A	HPU	HPU/TPU	TPU	TP-470
$[NO]_{max}$ (pmol cm^{-2} s^{-1})	350 ± 90	320 ± 70	320 ± 70	189.2 ± 51.4	123.4 ± 36.1
t_{max} (min)	7.2 ± 0.9	6.6 ± 0.8	18 ± 3	72 ± 19	96 ± 21
$[NO]_{6\ h}$ (pmol cm^{-2} s^{-1})	90 ± 10	93 ± 9	110 ± 10	68 ± 7	87 ± 7
$[NO]_{12\ h}$ (pmol cm^{-2} s^{-1})	30 ± 4	36 ± 3	39 ± 3	42 ± 4	52 ± 6
$[NO]_{24\ h}$ (pmol cm^{-2} s^{-1})	2.8 ± 0.7	3.6 ± 0.4	5 ± 1	10 ± 2	11 ± 1
$[NO]_{48\ h}$ (pmol cm^{-2} s^{-1})	1.0 ± 0.2	1.12 ± 0.06	1.4 ± 0.3	2.6 ± 0.6	2.8 ± 0.4
$[NO]_{72\ h}$ (pmol cm^{-2} s^{-1})	0	0.92 ± 0.04	1.2 ± 0.2	1.28 ± 0.08	1.6 ± 0.2
Total NO (μmol cm^{-2})	6.1 ± 0.6	6.1 ± 0.5	6.0 ± 0.5	5.9 ± 0.6	5.8 ± 0.5

AEAP3 nanoparticles. As expected for each of the PROLI/NO and AEAP3 systems, the total NO payload for any given scaffold and concentration was the same regardless of topcoat. In contrast to the *N*-diazeniumdiolate-based scaffolds, *S*-nitrosothiols decompose when exposed to heat, light, or Cu^{+} to form 1 mol of NO per mol of thiol.[46] Furthermore, the decomposition of *S*-nitrosothiols is not affected by water uptake and therefore only the HPU/TPU polyurethane topcoat was utilized for MPTMS nanoparticle-doped PUs. While the MPTMS nanoparticles have similar initial release kinetics as the *N*-diazeniumdiolate systems, the *S*-nitrosothiol nanoparticles release lower levels of NO over long periods through thermal release mechanisms. As expected, the MPTMS nanoparticle-doped PUs released NO for the longest duration, with NO still detectable at 14 d (Table 3.6). Of note, previously implanted NO release studies are based on materials capable of uninterrupted NO release for up to 3 d.[25, 27] The 36 mg/mL MPTMS nanoparticle-doped PUs produced the greatest NO payload (9.3 μmol cm^{-2}) in this study, ~7 times more NO than previous subcutaneous NO-releasing xerogels.[25] Based on the nanoparticle concentrations measured via the ICP-OES leaching study, the predicted total NO release for the 36 mg/mL AEAP3 and MPTMS nanoparticle-doped PUs are 6.3 and 10.1 μmol cm^{-2}, respectively. The slight loss in NO likely occurs during the wire dipcoating process. Moisture, light, and heat that are unavoidable under ambient conditions may initiate NO release from both *N*-diazeniumdiolate- and *S*-nitrosothiol-based scaffolds. The range of NO release kinetics utilized in this study allowed for the investigation of the effects of NO release flux (initial burst versus sustained delivery) to be compared.

3.3.3. Collagen deposition. A characteristic event of the FBR is collagen encapsulation that begins to form 1–2 weeks after implantation. The capsule persists for the

Table 3.6. Nitric oxide release from coatings doped at 18 mg/mL or 36 mg/mL MPTMS nanoparticles with a HPU/TPU polyurethane topcoat. Data are mean ± standard deviation.

NO release properties	Nanoparticle concentration doped into polyurethane	
	18 mg/mL	36 mg/mL
$[NO]_{max}$ (pmol cm^{-2} s^{-1})	290 ± 20	380 ± 30
t_{max} (min)	9 ± 2	9 ± 2
$[NO]_{6\ h}$ (pmol cm^{-2} s^{-1})	32 ± 2	74 ± 7
$[NO]_{12\ h}$ (pmol cm^{-2} s^{-1})	14 ± 2	31 ± 3
$[NO]_{24\ h}$ (pmol cm^{-2} s^{-1})	6.8 ± 0.6	13 ± 1
$[NO]_{72\ h}$ (pmol cm^{-2} s^{-1})	2.7 ± 0.3	5.2 ± 0.4
$[NO]_{7\ d}$ (pmol cm^{-2} s^{-1})	1.6 ± 0.1	1.7 ± 0.1
$[NO]_{14\ d}$ (pmol cm^{-2} s^{-1})	1.1 ± 0.1	1.3 ± 0.1
Total NO (μmol cm^{-2})	5.1 ± 0.4	9.3 ± 0.6

life of the device has low microvessel density,[3, 47] impeding diffusion of analytes from the surrounding native tissue and blood capillaries.[48] For glucose sensors, the collagen capsule results in reduced sensitivity and increased lag time.[49-52] Capsule thickness and collagen density via Masson's trichrome-stained histology was thus evaluated as a function of NO release kinetics and doses.

As expected, collagen capsule formation surrounding PU-coated wire substrates was not observed until 3 weeks following implantation. The collagen capsule thickness for all wire substrates after 3 and 6 weeks of implantation are provided in Fig. 3.3. At 3 weeks (Fig. 3.3.A), PROLI/NO-doped PUs showed no significant reduction in the collagen capsule thickness relative to control ($p < 0.05$). In contrast, both the TPU and TP-470 PU topcoats significantly reduced collagen capsule formation for both the 18 mg/mL and 36 mg/mL AEAP3 nanoparticle-doped PUs versus controls. Both TPU and TP-470 are characterized by low water uptake and thus enabled the longest NO release for the *N*-diazeniumdiolate particle-doped PU systems. The data from the AEAP3 nanoparticle-doped PUs suggest that longer NO-releasing substrates with similar NO payloads are more successfully mitigate the FBR. Furthermore, the data suggests that the total NO payload may be less important than the NO release kinetics for reducing collagen encapsulation at 3 weeks. For example, the TP-470 topcoated 18 mg/mL AEAP3 nanoparticle-doped PU has a lower total NO payload but a greater NO flux at 48 h than HP 93A, HPU or HPU/TPU topcoated 36 mg/mL AEAP3 nanoparticle-doped PUs (Tables 3.4 and 3.5). These slow NO release kinetics correlate well with the mitigated FBR. The even longer (in duration) NO-releasing PUs (i.e., MPTMS nanoparticle-doped) reduced the collagen capsule at both dopant concentrations of 18 and 36

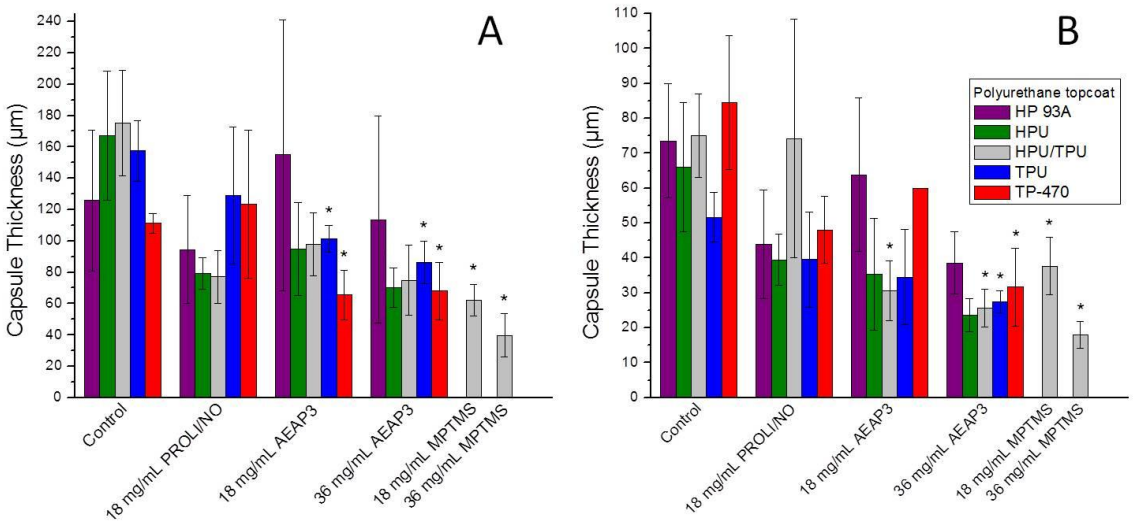

Figure 3.3. Collagen capsule thickness surrounding polyurethane-coated wire substrates at A) 3 and B) 6 weeks. Significant differences between NO-releasing and relative controls are indicated at $p < 0.05$ (*).At 6 weeks, the TP-470 topcoated 18 mg/mL AEAP3 nanoparticle system was not tested due to low sample size (n = 2). Data are mean ± standard error of the mean.

mg/mL by ~64 and ~77%, respectively. Indeed, the MPTMS nanoparticle-doped PU systems represented the two largest decreases in collagen capsule thickness at 3 weeks.

At 6 weeks, the average collagen capsule thickness adjacent to all implanted materials was reduced compared to 3 weeks. While not anticipated, a decrease in collagen encapsulation surrounding subcutaneous materials has been observed over time for non-NO-releasing materials [53]. As was also observed at 3 weeks, PROLI/NO-doped PUs did not appreciably reduce the collagen capsule thickness (Fig. 3.2.B). Of the 18 mg/mL AEAP3 nanoparticle-doped PUs, only the HPU/TPU topcoated system displayed a significant reduction in capsule thickness (~59% reduction vs. control). It is currently unknown why this composition would best mitigate the FBR. The other 18 mg/mL AEAP3 nanoparticle-doped PU systems with slightly longer or shorter NO durations proved inadequate in altering the resulting capsule thickness. Although speculative at this stage, we believe that the NO release from the HPU/TPU topcoat provided both a sufficiently high maximum and NO release duration. Other PU topcoats resulted in either insufficient maximum NO flux or duration negatively impacting the FBR mitigation. Clearly other relevant parameters are likely since materials with a greater maximum flux and similar NO flux at 48 h (e.g., HPU topcoated 36 mg/mL AEAP3 nanoparticle-doped PUs) did not result in similar reductions in capsule thickness.

In contrast to the 18 mg/mL AEAP3 nanoparticle-doped PUs, the three longest NO-releasing PU topcoats (i.e., HPU/TPU, TPU, and TP-470) applied to the 36 mg/mL AEAP3 nanoparticle-doped PU systems were capable of significant reductions in the capsule thickness at 6 weeks. The higher incidence of significant capsule thickness reductions with the 36 versus the 18 mg/mL AEAP3 nanoparticle system indicates a possible advantage to

materials releasing a greater NO payload. The NO release originating from low water uptake PU topcoats (i.e., HPU/TPU, TPU, and TP-470) provided the longest NO release duration for the 36 mg/mL AEAP3 nanoparticle system albeit with identical NO payloads to the statistically insignificant PU topcoats (i.e., HP 93A and HPU). The data from the 36 mg/mL AEAP3 nanoparticle systems further indicates that NO release kinetics of implanted materials greatly impact the FBR. Both concentrations of the MPTMS nanoparticle-doped polyurethanes significantly reduced the capsule size with the 18 and 36 mg/mL MPTMS nanoparticle systems achieving a ~50 and ~76% reduction in capsule thickness, respectively. Since the long-term NO release fluxes (i.e., 7 to 14 d) for both the 18 and 36 mg/mL MPTMS nanoparticle systems were similar (Table 3.6), the difference in the initial 7 d of NO release is attributed to the enhanced FBR mitigation. The combination of significant NO levels initially and sustained, low NO release over 14 d may improve tissue integration by altering the initial inflammatory response.[25] The 36 mg/mL MPTMS nanoparticle-doped systems reduced the collagen encapsulation to the greatest level at both 3 and 6 weeks of implantation, indicating the advantage of a large initial NO payload and sustained NO release for decreasing capsule thickness.

The density of the collagen within the encapsulation is another factor that may affect the sequestering of the foreign body. A previously developed and implemented MATLAB program was thus used to quantify collagen density in captured micrographs of the collagen capsule.[54] The program measures the number of pixels attributed to collagen when stained with Masson's trichrome, divides this number by the total pixels in the image, and multiplies by 100 to give a collagen density index (CDI) ranging from 0 to 100, with a CDI value of 100 indicating every pixel represents collagen. At 3 weeks, the capsules surrounding the HP

93A, HPU, and TPU topcoated PROLI/NO systems exhibited significantly increased CDI compared to controls (Fig. 3.4.A) with no other NO-releasing substrates exhibiting a significant change. Of note, the maximum NO flux from PROLI/NO-doped PUs was an order of magnitude greater (1400 to 3100 pmol cm^{-2} s^{-1}) than that from any previously implanted NO-releasing materials. Though the NO payload (~4 μmol/cm^2) from the PROLI/NO systems falls between that of the two concentrations of AEAP3 nanoparticle systems, neither concentration of AEAP3 nanoparticle systems exhibited an increase in CDI at 3 weeks. As such, the CDI enhancement is most likely the result of the large NO bolus from the PROLI/NO systems. The inability to significantly reduce capsule thickness while simultaneously causing an increase in the collagen density indicates long-term disadvantages of bolus NO release from implant surfaces.

At 6 weeks, the capsules surrounding the TP-470 topcoated 36 mg/mL AEAP3 and HPU/TPU topcoated 36 mg/mL MPTMS nanoparticle systems showed significantly increased CDI versus controls (Fig. 3.4.B). This enhancement of collagen density at 6 weeks may also be the result of too much NO. Previously reported microdialysis implants with high NO payloads (4.6 μmol cm^{-2} each day) also increased collagen density,[26] perhaps not unexpected since NO has been shown to enhance collagen deposition from fibroblasts.[20-22] Nevertheless, the NO-releasing microdialysis probes resulted in superior glucose recovery compared to control probes despite an enhanced CDI.[26] While the TP-470 topcoated 36 mg/mL AEAP3 and the HPU/TPU topcoated 36 mg/mL MPTMS nanoparticle systems were characterized by increased CDI, both of these materials significantly reduced the thickness of the collagen encapsulation. Therefore, the materials may still be advantageous for certain subcutaneous device applications (e.g., glucose sensors).

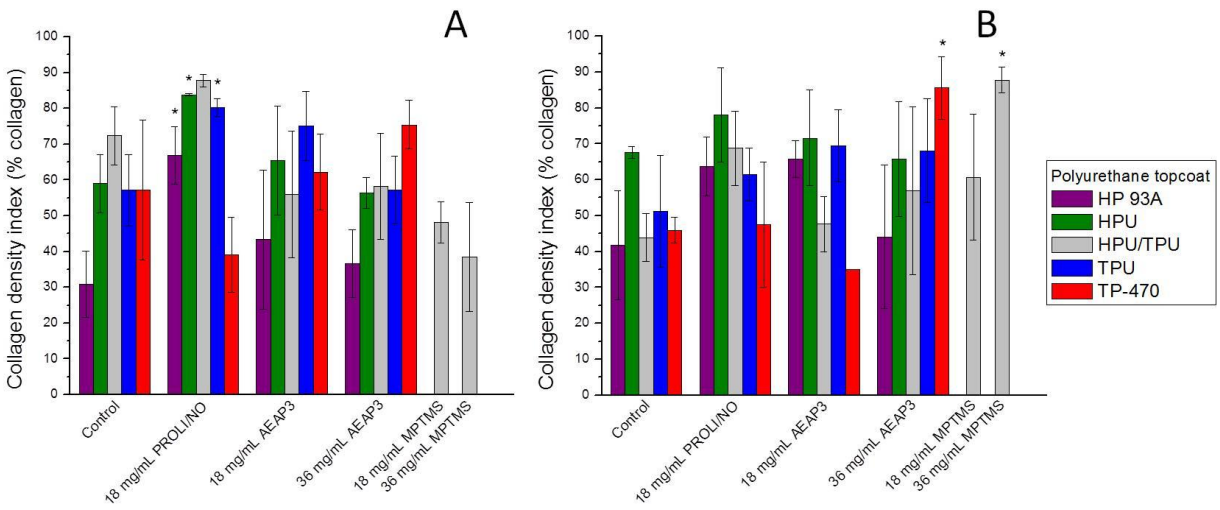

Figure 3.4. Collagen density index (CDI) of collagen capsules surrounding polyurethane-coated wire substrates at A) 3 and B) 6 weeks. Significant differences between NO-releasing and relative controls are indicated at $p < 0.05$ (*). At 6 weeks, the TP-470 topcoated 18 mg/mL AEAP3 nanoparticle system was not tested due to low sample size ($n = 2$). Data are mean ± standard error of the mean.

*3.3.4. Inflammatory response.*The localization of inflammatory cells may contribute to erratic device performance (e.g., sensor) and ultimate failure.[55] Inflammatory cells adjacent to the implant become activated while attempting to phagocytose the foreign body. This activation decreases local pH and produces superoxide and peroxide. Several studies have linked these factors to poor sensor performance.[55-57] As the FBR progresses, the formation of foreign body giant cells (FBGCs) enhances implant degradation, also diminishing the sensor lifetime.[4, 5] To quantify the inflammatory response, the number of cell nuclei localized within 50 μm of the implant surface was measured in hematoxylin and eosin-stained histology sections. For these reasons, the inflammatory response to the NO-releasing substrates was examined histologically at both acute (3 and 7 d) and chronic (3 and 6 week) stages.

During the acute phase, the NO release led to a significant reduction in the inflammatory response (Fig. 3.5.A and 3.5.B). The inflammatory response was most significantly impacted by substrates with large and long NO release (e.g., 36 mg/mL AEAP3 and MPTMS nanoparticle systems). The PROLI/NO and 18 mg/mL AEAP3 nanoparticle systems, only releasing NO up to 48 h, did not decrease the inflammatory response. Likewise, Gifford et al. reported that the inflammatory response only seemed to be influenced (reduced) while NO was actively released.[27] However, the HPU/TPU topcoated 18 mg/mL AEAP3 nanoparticle system was also observed to decrease the inflammatory response, likely due to the achievement of release kinetics and duration via the HPU/TPU topcoat. Of the 36 mg/mL AEAP3 nanoparticle systems, the three topcoats with the slowest NO release kinetics (i.e., HPU/TPU, TPU, and TP-470) also significantly reduced the inflammatory cell density adjacent to the implant. The difference in inflammation with

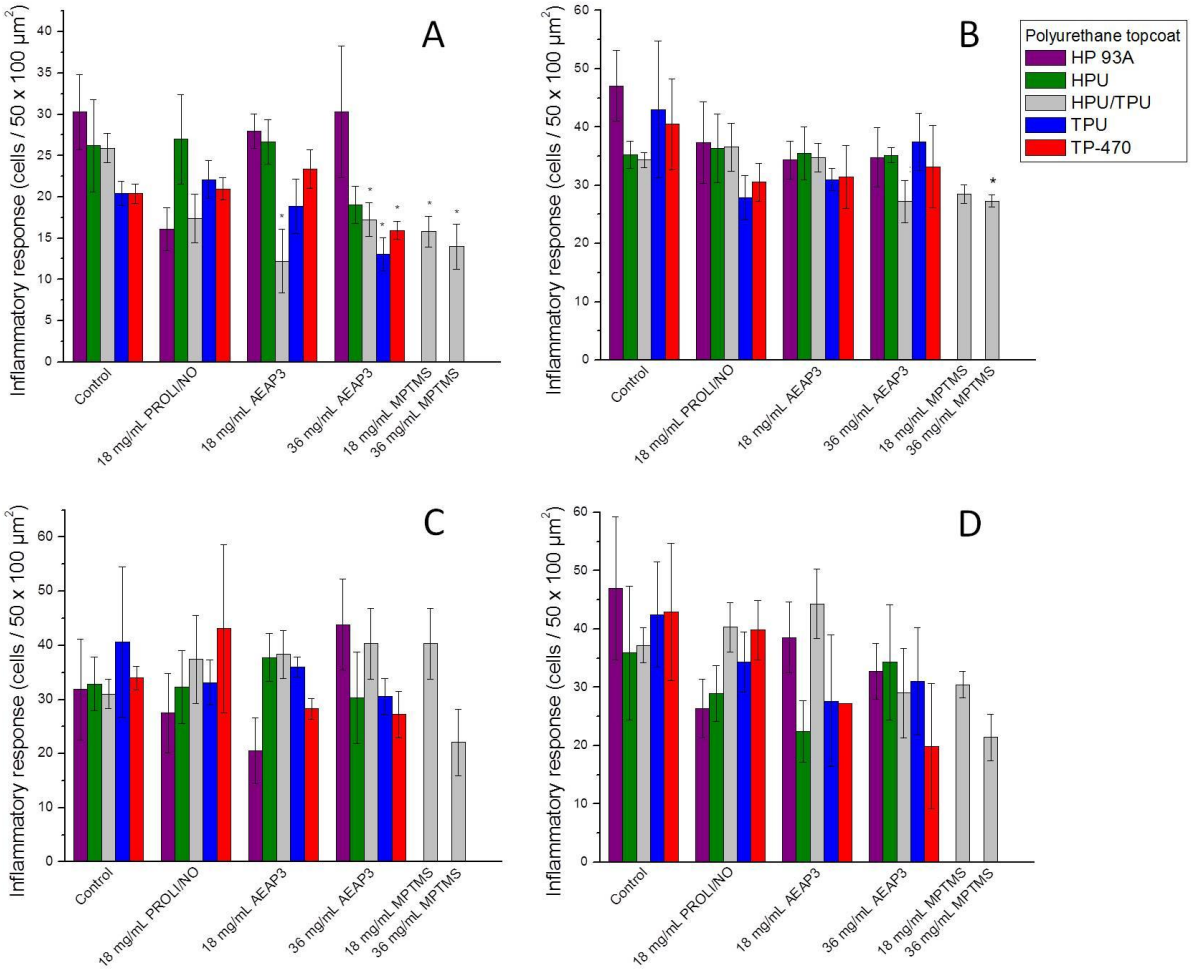

Figure 3.5. Inflammatory response to polyurethane-coated wire substrates at A) 3 d and B) 1, C) 3, and D) 6 weeks. Significant differences between NO-releasing and relative controls are indicated at $p < 0.05$ (*).At 6 weeks, the TP-470 topcoated 18 mg/mL AEAP3 nanoparticle system was not tested due to low sample size (n = 2). Data are mean ± standard error of the mean.

identical NO payloads further stresses the need to extend NO release to achieve the most desirable FBR. At 1 week, only the 36 mg/mL MPTMS nanoparticle system, releasing the greatest NO flux over this length of time, showed a statistically significant reduction in the inflammatory response, further supporting Gifford's observations.

In contrast, the chronic inflammatory response was largely unaffected by NO release in this study as no NO-releasing substrate was capable of mitigating the inflammatory response at 3 or 6 weeks of implantation (Fig. 3.5.C and 3.5.D). At 6 weeks, the 36 mg/mL MPTMS nanoparticle system resulted in an apparent 22% reduction in the inflammatory response ($0.05 < p < 0.10$). Such results are contradictory to a previously reported short-term (72 h) NO-releasing xerogel system that improved the chronic inflammatory response,[25] but are in good agreement with the Gifford et al. study where the inflammatory response was mitigated only during active NO release from the implant.[27] It is important to note previous experiments by Gifford et al. and Hetrick et al. were performed in rodent models that may not be as quantitatively relevant to humans as porcine models.[25, 27, 30]

3.4. Conclusions

These results stress the need to examine NO release kinetics in the development of implantable materials. Furthermore, there is a need to create materials with NO release durations exceeding two weeks, specifically in relation to mitigating the inflammatory response. Approaches for enhancing NO release durations include increasing the hydrophobicity of the polymer matrix or making use of longer releasing *S*-nitrosothiol NO donors (e.g., tertiary *S*-nitrosothiols). Of course, such changes may affect glucose sensor response/performance. Although the mitigation of the FBR observed in our study may prove beneficial for indwelling glucose sensors, the effects of NO release should also be evaluated

for percutaneous implants to confirm if the same degree of tissue integration is achieved. Studies evaluating the effects of NO release on the performance of percutaneous implants are currently underway in our lab.

3.5. References

(1) Anderson, J. M., Rodriguez, A., Chang, D. T., "Foreign body reaction to biomaterials." *Semin. Immunol.* **2008,** *20*, 86-100.

(2) Coleman, D. L., King, R. N., Andrade, J. D., "The foreign body reaction: A chronic inflammatory response." *J Biomed Mater Res* **1974,** *8*, 199-211.

(3) Ratner, B. D., Bryant, S. J., "Biomaterials: Where we have been and where we are going." *Annu Rev Biomed Eng* **2004,** *6*, 41-75.

(4) Klueh, U., Kaur, M., Qiao, Y., Kreutzer, D. L., "Critical role of tissue mast cells in controlling long-term glucose sensor function in vivo." *Biomaterials* **2010,** *31*, 4540-4551.

(5) Anderson, J. M., Defife, K., McNally, A., Collier, T., Jenney, C., "Monocyte, macrophage and foreign body giant cell interactions with molecularly engineered surfaces." *J. Mater. Sci.-Mater. Med.* **1999,** *10*, 579-588.

(6) Ju, Y. M., Yu, B. Z., Koob, T. J., Moussy, Y., Moussy, F., "A novel porous collagen scaffold around an implantable biosensor for improving biocompatibility. I. In vitro/in vivo stability of the scaffold and in vitro sensitivity of the glucose sensor with scaffold." *J. Biomed. Mater. Res. Part A* **2008,** *87A*, 136-146.

(7) Ju, Y. M., Yu, B. Z., West, L., Moussy, Y., Moussy, F., "A novel porous collagen scaffold around an implantable biosensor for improving biocompatibility. II. Long-term in vitro/in vivo sensitivity characteristics of sensors with NDGA- or GA-crosslinked collagen scaffolds." *J. Biomed. Mater. Res. Part A* **2010,** *92A*, 650-658.

(8) Wang, C., Yu, B., Knudsen, B., Harmon, J., Moussy, F., Moussy, Y., "Synthesis and performance of novel hydrogels coatings for implantable glucose sensors." *Biomacromolecules* **2008,** *9*, 561-567.

(9) Yu, B. Z., Wang, C. Y., Ju, Y. M., West, L., Harmon, J., Moussy, Y., Moussy, F., "Use of hydrogel coating to improve the performance of implanted glucose sensors." *Biosens. Bioelectron.* **2008,** *23*, 1278-1284.

(10) Koh, A., Nichols, S. P., Schoenfisch, M. H., "Glucose sensor membranes for mitigating the foreign body response." *J. Diabetes Sci. Technol.* **2011,** *5*, 1052-9.

(11) Ju, Y. M., Yu, B. Z., West, L., Moussy, Y., Moussy, F., "A dexamethasone-loaded PLGA micirospheres/collagen scaffold composite for implantable glucose sensors." *J. Biomed. Mater. Res. Part A* **2010,** *93A*, 200-210.

(12) Ward, W. K., Wood, M. D., Casey, H. M., Quinn, M. J., Federiuk, I. F., "The effect of local subcutaneous delivery of vascular endothelial growth factor on the function of a chronically implanted amperometric glucose sensor." *Diabetes Technol. Ther.* **2004,** *19*, 155-163.

(13) Patil, S. D., Papadmitrakopoulos, F., Burgess, D. J., "Concurrent delivery of dexamethasone and VEGF for localized inflammation control and angiogenesis." *J. Control. Release* **2007,** *117*, 68-79.

(14) Norton, L. W., Koschwanez, H. E., Wisniewski, N. A., Klitzman, B., Reichert, W. M., "Vascular endothelial growth factor and dexamethasone release from nonfouling sensor coatings affect the foreign body response." *J. Biomed. Mater. Res. Part A* **2007,** *81A*, 858-869.

(15) Edelman, J. L., Lutz, D., Castro, M. R., "Corticosteroids inhibit VEGF-induced vascular leakage in a rabbit model of blood-retinal and blood-aqueous barrier breakdown." *Exp. Eye Res.* **2005,** *80*, 249-258.

(16) Machein, M. R., Kullmer, J., Ronicke, V., Machein, U., Krieg, M., Damert, A., Breier, G., Risau, W., Plate, K. H., "Differential downregulation of vascular endothelial growth factor by dexamethasone in normoxic and hypoxic rat glioma cells." *Neuropathol. Appl. Neurobiol.* **1999,** *25*, 104-112.

(17) Thomassen, M. J., Buhrow, L. T., Connors, M. J., Kaneko, F. T., Erzurum, S. C., Kavuru, M. S., "Nitric oxide inhibits inflammatory cytokine production by human alveolar macrophages." *Am. J. Respir. Cell Mol. Biol.* **1997,** *17*, 279-283.

(18) Schwentker, A., Vodovotz, Y., Weller, R., Billiar, T. R., "Nitric oxide and wound repair: role of cytokines?" *Nitric Oxide-Biol. Chem.* **2002,** *7*, 1-10.

(19) Shukla, A., Rasik, A. M., Shankar, R., "Nitric oxide inhibits wound collagen synthesis." *Mol. Cell. Biochem.* **1999,** *200*, 27-33.

(20) Schäffer, M. R., Efron, P. A., Thornton, F. J., Klingel, K., Gross, S. S., Barbul, A., "Nitric oxide, an autocrine regulator of wound fibroblast synthetic function." *J. Immunol.* **1997,** *158*, 2375-2381.

(21) Schäffer, M. R., Tantry, U., Gross, S. S., Wasserkrug, H. L., Barbul, A., "Nitric oxide regulates wound healing." *J. Surg. Res.* **1996,** *63*, 237-240.

(22) Thornton, F. J., Schäffer, M. R., Witte, M. B., Moldawer, L. L., MacKay, S. L. D., Abouhamze, A., Tannahill, C. L., Barbul, A., "Enhanced collagen accumulation following direct transfection of the inducible nitric oxide synthase gene in cutaneous wounds." *Biochem. Biophys. Res. Commun.* **1998,** *246*, 654-659.

(23) Cooke, J. P., "NO and angiogenesis." *Atheroscler. Suppl.* **2003,** *4*, 53-60.

(24) Hetrick, E. M., Schoenfisch, M. H., "Antibacterial nitric oxide-releasing xerogels: Cell viability and parallel plate flow cell adhesion studies." *Biomaterials* **2007,** *28*, 1948-1956.

(25) Hetrick, E. M., Prichard, H. L., Klitzman, B., Schoenfisch, M. H., "Reduced foreign body response at nitric oxide-releasing subcutaneous implants." *Biomaterials* **2007,** *28*, 4571-4580.

(26) Nichols, S. P., Le, N. N., Klitzman, B., Schoenfisch, M. H., "Increased in vivo glucose recovery via nitric oxide release." *Anal. Chem.* **2011,** *83*, 1180-1184.

(27) Gifford, R., Batchelor, M. M., Lee, Y., Gokulrangan, G., Meyerhoff, M. E., Wilson, G. S., "Mediation of in vivo glucose sensor inflammatory response via nitric oxide release." *J Biomed Mater Res Part A* **2005,** *75A*, 755-766.

(28) Novak, M. T., Yuan, F., Reichert, W. M., "Modeling the relative impact of capsular tissue effects on implanted glucose sensor time lag and signal attenuation." *Anal. Bioanal. Chem.* **2010,** *398*, 1695-1705.

(29) Koh, A., Riccio, D. A., Sun, B., Carpenter, A. W., Nichols, S. P., Schoenfisch, M. H., "Fabrication of nitric oxide-releasing polyurethane glucose sensor membranes." *Biosens. Bioelectron.* **2011,** *28*, 17-24.

(30) Sullivan, T. P., Eaglstein, W. H., Davis, S. C., Mertz, P., "The pig as a model for human wound healing." *Wound Repair Regen.* **2001,** *9*, 66-76.

(31) Saavedra, J. E., Southan, G. J., Davies, K. M., Lundell, A., Markou, C., Hanson, S. R., Adrie, C., Hurford, W. E., Zapol, W. M., Keefer, L. K., "Localizing antithrombotic and vasodilatory activity with a novel, ultrafast nitric oxide donor." *J. Med. Chem.* **1996,** *39*, 4361-4365.

(32) Shin, J. H., Metzger, S. K., Schoenfisch, M. H., "Synthesis of nitric oxide-releasing silica nanoparticles." *J. Am. Chem. Soc.* **2007,** *129*, 4612-4619.

(33) Riccio, D. A., Nugent, J. L., Schoenfisch, M. H., "Stober synthesis of nitric oxide-releasing S-nitrosothiol-modified silica particles." *Chem. Mat.* **2011,** *23*, 1727-1735.

(34) Coneski, P. N., Schoenfisch, M. H., "Nitric oxide release: Part III. Measurement and reporting." *Chem. Soc. Rev.* **2012,** *41*, 3753-3758.

(35) Bancroft, J., Gamble, M., Theory and practice of histological techniques, 6 ed., Churchill Livingstone, London 2007.

(36) Koschwanez, H. E., Yap, F. Y., Klitzman, B., Reichert, W. M., "In vitro and in vivo characterization of porous poly-L-lactic acid coatings for subcutaneously implanted glucose sensors." *J. Biomed. Mater. Res. Part A* **2008,** *87A*, 792-807.

(37) Davila, J. C., Lautsch, E. V., Palmer, T. E., "Some physical factors affecting the acceptance of synthetic materials as tissue implants." *Ann. N.Y. Acad. Sci.* **1968,** *146*, 138-147.

(38) Ward, W. K., Slobodzian, E. P., Tiekotter, K. L., Wood, M. D., "The effect of microgeometry, implant thickness and polyurethane chemistry on the foreign body response to subcutaneous implants." *Biomaterials* **2002,** *23*, 4185-4192.

(39) Bota, P. C. S., Collie, A. M. B., Puolakkainen, P., Vernon, R. B., Sage, E. H., Ratner, B. D., Stayton, P. S., "Biomaterial topography alters healing in vivo and monocyte/macrophage activation in vitro." *J. Biomed. Mater. Res. Part A* **2010,** *95A*, 649-657.

(40) Cao, H. Q., McHugh, K., Chew, S. Y., Anderson, J. M., "The topographical effect of electrospun nanofibrous scaffolds on the in vivo and in vitro foreign body reaction." *J. Biomed. Mater. Res. Part A* **2010,** *93A*, 1151-1159.

(41) Barbe, C., Bartlett, J., Kong, L. G., Finnie, K., Lin, H. Q., Larkin, M., Calleja, S., Bush, A., Calleja, G., "Silica particles: A novel drug-delivery system." *Adv. Mater.* **2004,** *16*, 1959-1966.

(42) Hrabie, J. A., Keefer, L. K., "Chemistry of the nitric oxide-releasing diazeniumdiolate ("nitrosohydroxylamine") functional group and its oxygen-substituted derivatives." *Chem. Rev.* **2002,** *102*, 1135-1154.

(43) Davies, K. M., Wink, D. A., Saavedra, J. E., Keefer, L. K., "Chemistry of the diazeniumdiolates. 2. Kinetics and mechanism of dissociation to nitric oxide in aqueous solution." *J. Am. Chem. Soc.* **2001,** *123*, 5473-5481.

(44) Degraaf, J. C., Banga, J. D., Moncada, S., Palmer, R. M. J., Degroot, P. G., Sixma, J. J., "Nitric oxide functions as an inhibitor of platelet adhesion under flow conditions." *Circulation* **1992,** *85*, 2284-2290.

(45) Forstermann, U., "Nitric oxide and oxidative stress in vascular disease." *Pflugers Arch.* **2010,** *459*, 923-939.

(46) Williams, D. L. H., "The chemistry of S-nitrosothiols." *Accounts Chem. Res.* **1999,** *32*, 869-876.

(47) Sieminski, A. L., Gooch, K. J., "Biomaterial-microvasculature interactions." *Biomaterials* **2000,** *21*, 2233-2241.

(48) Wisniewski, N., Klitzman, B., Miller, B., Reichert, W. M., "Decreased analyte transport through implanted membranes: Differentiation of biofouling from tissue effects." *J. Biomed. Mater. Res.* **2001,** *57*, 513-521.

(49) Wilson, G. S., Gifford, R., "Biosensors for real-time in vivo measurements." *Biosens. Bioelectron.* **2005,** *20*, 2388-2403.

(50) Jablecki, M., Gough, D. A., "Simulations of the frequency response of implantable glucose sensors." *Anal. Chem.* **2000,** *72*, 1853-1859.

(51) Sharkawy, A. A., Klitzman, B., Truskey, G. A., Reichert, W. M., "Engineering the tissue which encapsulates subcutaneous implants. 1. Diffusion properties." *J. Biomed. Mater. Res.* **1997,** *37*, 401-412.

(52) Wisniewski, N., Reichert, M., "Methods for reducing biosensor membrane biofouling." *Colloid. Surface. B* **2000,** *18*, 197-219.

(53) Gangjee, T., Colaizzo, R., Vonrecum, A. F., "Species-related differences in percutaneous wound-healing." *Ann. Biomed. Eng.* **1985,** *13*, 451-467.

(54) Koschwanez, H. E., Yap, F. Y., Klitzman, B., Reichert, W. M., "In vitro and in vivo characterization of porous poly-L-lactic acid coatings for subcutaneously implanted glucose sensors." *J Biomed Mater Res Part A* **2008,** *87A*, 792-807.

(55) Wilson, G. S., Hu, Y. B., "Enzyme based biosensors for in vivo measurements." *Chem. Rev.* **2000,** *100*, 2693-2704.

(56) Forster, J., Morris, A. S., Shearer, J. D., Mastrofrancesco, B., Inman, K. C., Lawler, R. G., Bowen, W., Caldwell, M. D., "Glucose-uptake and flux through phosphofructokinase in wounded rat skeletal-muscle." *Am. J. Physiol.* **1989,** *256*, E788-E797.

(57) Zhao, Q. H., McNally, A. K., Rubin, K. R., Renier, M., Wu, Y., Rosecaprara, V., Anderson, J. M., Hiltner, A., Urbanski, P., Stokes, K., "Human plasma alpha-2-macroglobulin promotes in vitro oxidative stress cracking of pellethane-2363-80A - In vivo and in vitro correlations." *J. Biomed. Mater. Res.* **1993,** *27*, 379-389.

Chapter 4:

Nitric oxide-flux dependent adhesion and viability of bacteria to fibrinogen-adsorbed surfaces

4.1. Introduction

Implanted medical devices and materials are increasingly used in hospitals to treat and/or monitor a multitude of health problems. While some devices are implanted for days (e.g., catheters), others may reside in a patient's body for years (e.g., orthopedic implants). Regardless of time implanted, device-associated infections are a problem for many of these medical implants.[1] For example, central venous catheters (CVCs) result in ~80,000 bloodstream infections annually, extending the patient's hospital stay while requiring rigorous and expensive treatment.[2, 3]

Bacterial adhesion is an important factor for mitigating implant-associated infection as bacteria readily adhere to and colonize on medical device surfaces, often leading to infection.[4] Protein adsorption influences subsequent bacterial adhesion.[5] Once protein adsorbs, bacteria adhere to the protein-coated interface, colonizing within 6 h post-implantation.[6] Subsequently, bacteria proliferate, eventually depositing an extracellular matrix to protect the community of cells, resulting in a biofilm.[7] Eradication of biofilm bacteria requires greater concentrations (up to 1000x) of antibiotics than simple planktonic bacteria killing with ineffective treatments resulting in device removal.[8, 9] Both killing of adhered bacteria and prevention of bacterial adhesion have been shown to decrease implant-associated infections.[4]

To date, many clinically approved materials do not sufficiently prevent bacterial adhesion and biofilm formation.[10] Development of anti-adhesive and antibacterial surfaces is thus important for next generation devices. Two approaches are most common: 1) the development of surface coatings that promote passivation (by either reducing protein or bacterial adhesion); and/or, 2) biomaterials that actively release an antimicrobial agent.[1] Passive materials (e.g., quaternary ammonium-modified interfaces)[11-13] have a limited sphere of influence as they are only able to affect bacteria in direct contact with the biomaterial. Often, the efficacy of passive coatings us reduced upon protein adsorption. Materials that actively release antimicrobial agents impact bacteria both in contact with and in the vicinity of the implant, providing a more robust response to bacteria challenge, particularly if the agent is biocidal. Indeed, the release of molecules that inhibit or kill adhered bacteria allow for improved device performance and/or longevity. Antimicrobial agents that have been effectively loaded into polymeric biomaterials include antibiotics,[14, 15] antibodies,[16] silver ions,[17] and nitric oxide (NO),[18, 19] with each significantly impacting bacterial adhesion and adhered bacteria viability. Of these, NO is particularly advantageous due to its central role in the immune response to pathogens, localized action/reactivity, and broad-spectrum efficacy. Nitric oxide is in fact produced by macrophages to fight bacteria.[20, 21]

Materials capable of storing and releasing NO are being developed as coatings to limit bacterial adhesion and subsequent infection.[22, 23] Release of NO from an implanted material has been demonstrated to decrease the incidence of bacterial colonization versus control materials.[24, 25] Nablo and Schoenfisch reported that NO fluxes $\geq$32 pmol cm^{-2} s^{-1} inhibited *Pseudomonas aeruginosa* adhesion by 85%.[19] Charville et al. subsequently examined the NO flux-induced reduction of bacterial adhesion in the presence of adsorbed

fibrinogen (Fg) to better mimic in vivo conditions.[18] Adsorbed fibrinogen actually enhanced bacterial adhesion to substrates though NO release still decreased adhesion in a flux-dependent manner.

Along with a reduction in initial bacterial adhesion, NO has the potential to kill adhered bacteria since it is a biocidal agent. Nitric oxide release from small molecule and macromolecular NO donors has proved efficacious in the eradication of planktonic bacteria.[26-29] The increased killing activity of macromolecular scaffolds was attributed to the direct association of such materials with the bacteria, effectively concentrating the NO delivery.[26, 29] Surfaces capable of NO release would deliver a similar concentrated payload to adhered bacteria. Hetrick and Schoenfisch previously reported the killing efficacy of NO for *P. aeruginosa*, and demonstrated dose-dependent bactericidal action.[30] Herein, we investigated the NO fluxes necessary to inhibit bacterial adhesion and reduce the viability of adhered bacteria as a function of bacteria species.

4.2. Materials and Methods

3-mercaptopropyltrimethoxysilane (MPTMS) was purchased from Gelest (Morrisville, PA). Methyltrimethoxysilane (MTMOS), poly(vinyl chloride) (PVC), and diethylenetriamine pentaacetic acid (DTPA) were purchased from Fluka (Buchs, Switzerland). Human fibrinogen (Fg) was obtained from Enzyme Research Laboratories (Southbend, IN). Fibrinogen was stored at -80 °C, thawed at 37 °C for 10 min, and maintained at ambient temperature. *Staphylococcus aureus* (ATCC #29213), methicillin-resistant *Staphylococcus aureus* (MRSA; ATCC #33591), *Staphylococcus epidermidis* (ATCC #35983), *Enterococcus faecalis* (ATCC #29212), *Pseudomonas aeruginosa* (ATCC #19143), and *Escherichia coli* (ATCC #53323) were obtained from American Type Culture

Collection (Manassas, VA). Nitric oxide was purchased from Praxair (Danbury, CT). Nitric oxide calibration gas (26.39 ppm; balance nitrogen), nitrogen, and argon were purchased from National Welders (Raleigh, NC).

4.2.1. Xerogel synthesis. Xerogels (40% (v/v) MPTMS/MTMOS) were prepared on glass slides as previously described by mixing 800 µL ethanol (EtOH), 480 µL MTMOS, 320 µL MPTMS, and 25 µL hydrochloric acid (HCl; 0.5 M).[31] The solution was vortexed for 1 h, and allowed to age for 4 h at room temperature. Glass microscope slides (9 x 25 mm^2) were sonicated in EtOH for 30 min and dried under a stream of nitrogen. A 30 µL aliquot of the xerogel mixture was cast onto each glass slide and dried overnight under ambient conditions, then cured in a 70 °C oven for 2 d. The resulting xerogels were stored at room temperature until further use.

4.2.2. Nitrosation of xerogels. Subsequently, xerogels were nitrosated via incubation in 0.5 M HCl containing a 10x molar excess of nitrite (versus moles of thiol) and 100 µM DTPA for 3 h.[31] Of note, xerogels were kept on ice and shielded from light during nitrosation to prevent decomposition. Slides were then washed with 100 µM DTPA and stored at -20 °C in the dark until further use. Non-nitrosated xerogels were used as control non-NO-releasing interfaces.

4.2.3. Poly(vinyl chloride) coating. Poly(vinyl chloride) (1.0 g) was dissolved in tetrahydrofuran (THF; 10 mL). Approximately 300 µL of the PVC/THF solution was spin-coated onto control and NO-releasing xerogels using a CHEMAT Technology KW-4A Precision Spin-Coater (Northridge, CA) set to spin at 3.0 krpm. The PVC-coated xerogels were also stored at -20 °C until further use.

4.2.4. Bacterial adhesion. Bacteria were cultured in tryptic soy broth (TSB) at 37 °C, pelleted by centrifugation, rinsed with sterile water, resuspended in a solution of phosphate buffered saline (PBS; 10 mM, pH 7.4) with 15% (v/v) glycerol, and stored at -80 °C. Secondary cultures were grown from an aliquot of the frozen stock in TSB overnight. A 1 mL portion of the overnight bacteria was inoculated into 100 mL of TSB and grown to ~10^8 colony-forming units (CFU) per mL as measured by optical density. The resulting culture was collected by centrifugation (4500 g, 5 min) and resuspended in PBS.

To reach the desired NO flux, the PVC-coated NO-releasing xerogels were incubated at 37 °C for varying lengths of time from 0.5–96 h. Next, Fg was adsorbed to the PVC-coated NO-releasing and control xerogel surfaces by incubating the slides in 4 mL of a 20 μg/mL solution of Fg in PBS (pH 7.4) for 90 min at 37 °C (gentle shaking). The PVC-coated xerogels were then removed from the Fg solution and immediately immersed in 4 mL of a bacterial suspension (10^8 CFU/mL) at 37 °C for 60 min.

4.2.5. Optical microscopy for imaging of adhered bacteria. Following incubation in the bacterial suspension, the xerogels were removed, dipped in H_2O to remove loosely adhered bacteria, and then dried with a stream of air. Adhered bacteria were imaged via phase contrast optical microscopy using a Zeiss Axiovert 200 Inverted Microscope equipped with a Zeiss Axiocam at 20x magnification. Three different PVC-coated xerogel slides were imaged for each NO flux. Five randomly selected regions on each slide were used to calculate an average bacterial surface coverage. The images were digitally processed by thresholding to make dark cells contrast sharply with the light background. Percent surface coverage was translated from the number of black pixels in the thresholded image and normalized relative to controls (i.e., non-NO-releasing) which were scored as 100%.

4.2.6. Adhered bacterial viability. Following adhesion of bacteria to Fg-adsorbed PVC-coated xerogels, slides were dipped in sterile H_2O to remove any loosely adhered bacteria, and then transferred to 4 mL of PBS for incubation for 0, 6, 12, or 24 h. For *S. aureus*, MRSA, *S. epidermidis*, and *E. coli*, PBS was supplemented with 0.5% (v/v) TSB to ensure viability for 24 h. After incubation, the slides were gently rinsed in sterile H_2O. The PVC layer was then carefully removed, placed into 1 mL of PBS, and then sonicated for 15 min at 40 kHz to remove all adhered bacteria.[16, 30] Removal of bacteria cells via sonication was confirmed by optical microscopy of the PVC layer. After sonication, the solution was serially diluted and plated onto tryptic soy agar (TSA) nutrient plates. The plates were incubated at 37 °C and the bacterial viability was determined by counting the colonies on the plates using an IUL Flash & Go (Neutec Group, Farmingdale, NY). The plate counting method used herein has an inherent limit of detection of 2.5×10^3 CFU/mL.[32]

4.2.7. Contact angle measurements. Static water contact angle measurements of fibrinogen-adsorbed PVC-coated, PVC-coated, and bare control and NO-releasing xerogels were acquired with a KSV Instruments Cam 200 Optical Contact Angle Meter (Helsinki, Finland).

4.2.8. Nitric oxide release measurements. Nitric oxide release was measured continuously using a Sievers 280i Chemiluminescence Nitric Oxide Analyzer (NOA) (Boulder, CO).[33] Calibration of the NOA was performed by passing ambient air through a Sievers NO zero filter and using a 26.39 ppm NO gas (balance N_2). For analysis, NO-releasing xerogels were immersed in 30 mL of deoxygenated PBS shielded from light and released NO was carried to the analyzer in a nitrogen stream (200 mL min^{-1}). Temperature control was maintained using a water bath at 37 °C.

4.3. Results and Discussion

4.3.1. Material characterization. *S*-Nitrosothiol NO-donor-modified xerogels[31] were chosen for study to enable investigation of a large range of NO surface fluxes. Indeed, *S*-nitrosothiols provide longer NO-release kinetics compared to *N*-diazeniumdiolate NO donors when incorporated into xerogel films.[19, 31, 34, 35] The desired NO release flux was achieved by pre-incubating the xerogels at 37 °C for varying lengths of time. To control for deviations in the contact angles of the non-nitrosated and nitrosated xerogels (70 ± 1 and 54 ± 3°, respectively), and potentially varied bacterial adhesion,[31] a PVC topcoat was applied on top of the xerogels. The contact angles for controls and NO-releasing xerogels were the same (~89 ± 4°) after PVC-modification, as expected. Neither delamination nor degradation of the PVC or xerogel layers was observed for the PVC-coated xerogels.

Initial experiments revealed that several species (e.g., *S. aureus*, MRSA, and *E. coli*) did not readily adhere to control PVC-coated substrates (<10% surface coverage). Low absolute adhesion for these strains would make accurate measurements of the relative adhesion to NO-releasing substrates difficult due to the error inherent with optical microscopy evaluation. To enhance bacterial adhesion as well as better mimic in vivo biofouling, PVC-coated slides were incubated in fibrinogen (Fg) prior to bacteria exposure. Contact angles of the Fg-adsorbed PVC-coated control and NO-releasing xerogels were both 55 ± 5° (decreased from 89°), confirming Fg adsorption to the PVC-coating altered the surface characteristics. Charville et al. previously reported that Fg adsorbs equally to NO-releasing and control PVC-coated xerogels.[18] Soaking the Fg-adsorbed surfaces in PBS for 24 h had no effect on the contact angle.

The NO-release properties of the bare and PVC-coated *S*-nitrosothiol xerogels are provided in Table 4.1. As expected, the PVC topcoat did not significantly alter the NO-release properties of the xerogels since the NO release is thermally triggered. The xerogels released NO up to 14 d at low NO fluxes (e.g., 0.16 pmol cm^{-2} s^{-1} at 14 d). Average NO fluxes used in the bacteria studies ranged from 0.5–50 pmol cm^{-2} s^{-1}, with 50 pmol cm^{-2} s^{-1} selected as the largest flux due to natural loss of NO during the pre-incubation of the xerogels in Fg prior to bacteria exposure. Before incubation, the PVC-coated NO-releasing xerogels reached a maximum NO flux of 260 pmol cm^{-2} s^{-1} (Table 4.1). The NO flux changes by a large degree initially due to the pseudo first-order NO-release kinetics commonly observed for *S*-nitrosothiol-modified xerogels,[31] so significant NO is lost even during this relatively short incubation period.

4.3.2. Bacterial adhesion. The degree of bacterial adhesion to PVC-coated control and NO-releasing xerogels was examined at large bacteria concentrations (~10^8 CFU/mL). Although such concentrations are not biologically relevant for most implants, a starting concentration of ~10^8 CFU/mL of bacteria allowed for larger absolute surface coverage for all bacterial strains, a requirement for observing differences in bacterial adhesion via optical microscopy. Using the NO-release data provided in Table 4.1, nitrosothiol xerogels were pre-incubated at 37 °C for periods between 30 min and 4 d to achieve a wide-range of average NO fluxes over a subsequent 1 h bacteria assay (0.50 ± 0.08, 1.0 ± 0.1, 2.5 ± 0.4, 5.0 ± 0.8, 10 ± 2, 20 ± 4, 35 ± 5, and 50 ± 10 pmol cm^{-2} s^{-1}). The resulting NO fluxes allowed for careful investigation of NO's anti- bacterial adhesion properties. Increased error was noted for the larger NO fluxes due to the pseudo first-order NO-release kinetics that rapidly change at early time points (e.g., NO flux is reduced by >50% between 1 and 5 h).

Table 4.1. Nitric oxide-release properties of bare and PVC-coated 40% MPTMS/MTMOS xerogels. Data are mean ± standard deviation.

NO-release properties	40% MPTMS/MTMOS xerogel	PVC-coated 40% MPTMS/MTMOS xerogel
t_{max} (min)	1.1 ± 0.2	1.2 ± 0.2
$[NO]_{max}$ (pmol cm^{-2} s^{-1})	290 ± 70	260 ± 60
$[NO]_{1\,h}$ (pmol cm^{-2} s^{-1})	64 ± 10	58 ± 8
$[NO]_{5\,h}$ (pmol cm^{-2} s^{-1})	26 ± 5	22 ± 4
$[NO]_{12\,h}$ (pmol cm^{-2} s^{-1})	9 ± 1	8 ± 1
$[NO]_{24\,h}$ (pmol cm^{-2} s^{-1})	3.4 ± 0.5	3.2 ± 0.5
$[NO]_{48\,h}$ (pmol cm^{-2} s^{-1})	1.2 ± 0.1	1.1 ± 0.1
$[NO]_{96\,h}$ (pmol cm^{-2} s^{-1})	0.5 ± 0.1	0.5 ± 0.1
Total NO (μmol cm^{-2})	2.6 ± 0.4	2.5 ± 0.3

Prior to investigating the anti-adhesion properties of NO, we hypothesized a negative correlation between adhesion and NO flux would be observed for all strains of bacteria. Indeed, a NO flux-dependent decrease in bacterial adhesion was observed for all six bacterial strains investigated (Figure 4.1). Of note, the bacterial adhesion is relative to controls with 100% indicating identical amounts to the control substrates. Four of the strains (*S. aureus*, MRSA, *E. faecalis*, and *E. coli*) showed a large susceptibility to NO from 0–20 pmol cm^{-2} s^{-1} with little to no additional reduction in bacterial surface coverage at increased NO fluxes. This maximum plateau in reduced adhesion corroborates a previous study by Nablo and Schoenfisch where NO release resulted in a large initial reduction in bacterial adhesion but was followed by little additional effect beyond some threshold.[19] In contrast, inhibition of *P. aeruginosa* and *S. epidermidis* by 50% (20 and 35 pmol cm^{-2} s^{-1}, respectively) and 80% (35 and 50 pmol cm^{-2} s^{-1}, respectively) required larger NO fluxes than other strains. While greater NO fluxes were necessary to reduce adhesion for these particular strains, the NO release still decreased adhesion by >80%, analogous to the relative inhibition for other strains (Table 4.2).

Linear regressions of the relative bacteria surface coverage as a function of NO flux were performed from 0–20 pmol cm^{-2} s^{-1} to compare the relative susceptibility of each bacterial strain to NO (Table 4.2). This range was chosen as all of the bacteria strains showed good linearity (r^2 = 0.91–0.98), allowing for direct comparison between strains. Five of the strains had similar linear regression slopes, ranging from -3.6 to -4.3. Slight variations in slope were independent of the class of bacteria (Gram-positive or Gram-negative) and are likely an attribute of the broad-spectrum activity of NO arising from multiple mechanisms of biocidal action (e.g., nitrosative and oxidative stress).[36] One exception was *S. epidermidis*,

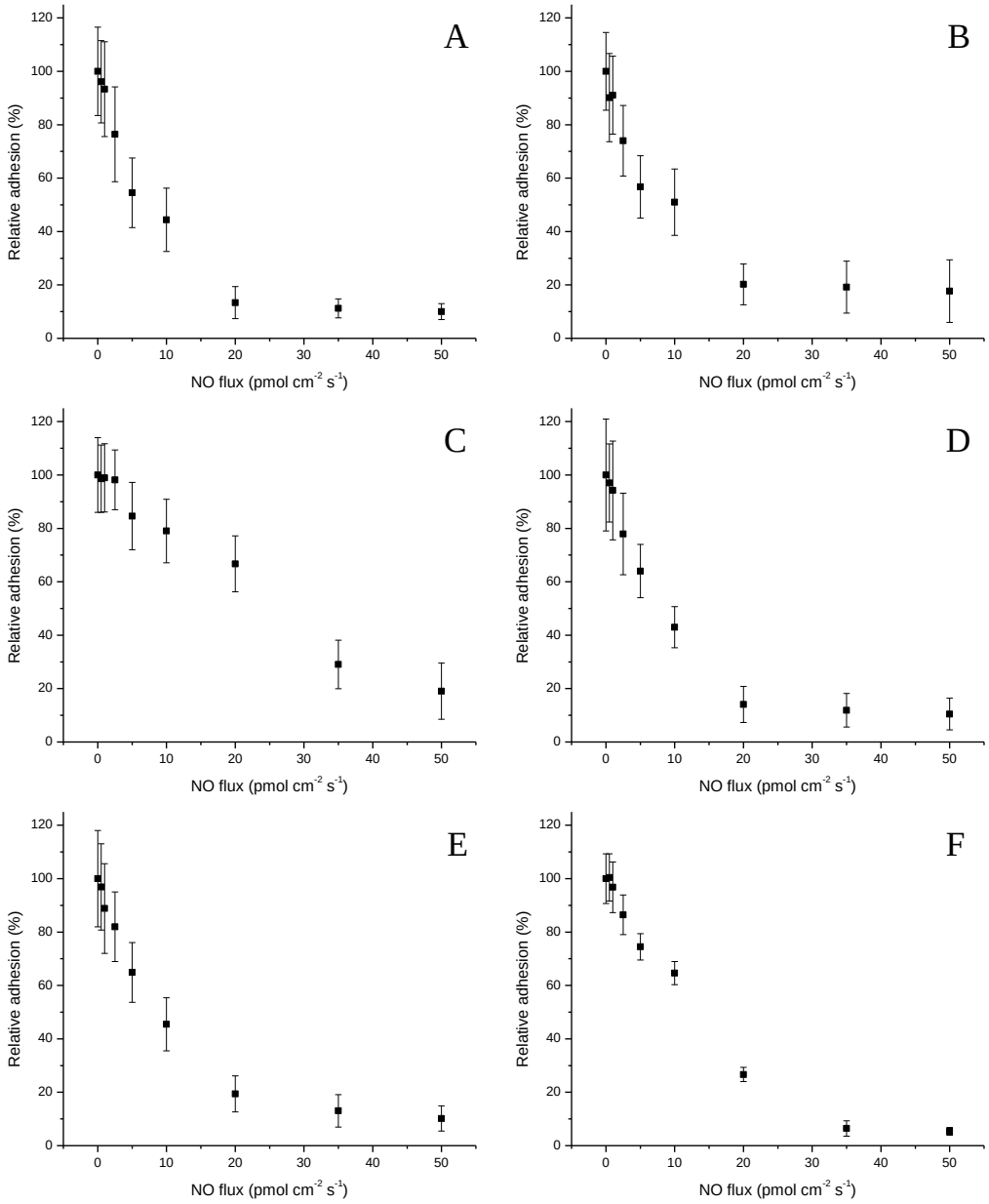

Figure 4.1. The NO flux-dependent relative adhesion of A) *S. aureus*, B) MRSA, C) *S. epidermidis*, D) *E. faecalis*, E) *E. coli*, and F) *P. aeruginosa* to Fg-adsorbed PVC-coated xerogels. A relative adhesion of 100% represents the adhesion of the strain to control (i.e., non-NO-releasing) substrates. Data are mean ± standard deviation.

Table 4.2. Linear regression analysis and NO flux required to inhibit adhesion of each bacteria strain by 50 and 80% relative to control (i.e., non-NO-releasing) surfaces. Data are mean ± standard deviation.

Bacteria strain	Gram class	Linear regression slope[a]	r^2	NO flux required to reduce adhesion by 50% (pmol cm^{-2} s^{-1})	NO flux required to reduce adhesion by 80% (pmol cm^{-2} s^{-1})
S. aureus	+	-4.3 ± 0.5	0.922	10	20
MRSA	+	-3.7 ± 0.5	0.914	10	20
S. epidermidis	+	-1.7 ± 0.2	0.939	35	50
E. faecalis	+	-4.3 ± 0.4	0.954	10	20
E. coli	-	-4.0 ± 0.4	0.953	10	20
P. aeruginosa	-	-3.6 ± 0.3	0.984	20	35

[a]Slopes calculated from NO fluxes between 0–20 pmol cm^{-2} s^{-1}

the only bacterium with a relatively low susceptibility to NO with respect to bacterial adhesion (slope of ~1.7). Charville et al. observed a similar phenomenon while investigating the role of Fg and NO release on bacterial adhesion.[18] *S. epidermidis* is unique in that it has Fg-binding proteins, such as serine-aspartate repeat G (SdrG), present on its surface.[37] While *S. aureus* strains also have Fg-binding proteins (e.g., Clumping Factor A),[38] the dissociation constant (K_D) of SdrG is two orders of magnitude lower than Clumping Factor A, indicating a significantly increased binding strength.[39] The large affinity of SdrG to Fg likely decreases the susceptibility of *S. epidermidis* to the anti-adhesive effects of surface-derived NO. Despite the relatively low efficacy of NO in preventing adhesion of *S. epidermidis*, exposure to fluxes >20 pmol cm^{-2} s^{-1} further diminished bacterial surface coverage with an 81% reduction in adhesion compared to control surfaces for a flux of 50 pmol cm^{-2} s^{-1}. Greater NO fluxes may further inhibit *S. epidermidis* adhesion, however, over the 1 h period the maximum average NO flux achieved was limited to 50 pmol cm^{-2} s^{-1} using the *S*-nitrosothiol-modified xerogels.

4.3.3. Bacteria surface viability. Reduction of bacterial adhesion is an important initial step in the design of antibacterial interfaces that prevent colonization on implanted materials. However, the most effective antibacterial surfaces should not only reduce bacterial adhesion, but also eradicate adhered bacteria to minimize bacteria proliferation and biofilm formation.[40] Previous work with *P. aeruginosa* demonstrated reduced viability of adhered bacteria on a NO-releasing interface in a dose-dependent manner.[30] However, the previous study was limited to *P. aeruginosa*, and thus the effect of NO release on the viability of adhered bacteria was not systematically investigated with respect to bacterial strains. Based

on prior literature, we hypothesized that many bacteria species will exhibit reduced viability in a NO dose-dependent manner since NO's actions are broad spectrum. The effect of total NO payload (i.e., cumulative NO release) over time was thus investigated against six strains of bacteria adhered to Fg-adsorbed PVC-coated xerogels to evaluate the potential for surface-derived NO to kill biomedically-relevant adhered bacteria. After the 1 h bacterial adhesion assay, substrates were incubated in PBS (*E. faecalis* and *P. aeruginosa*) or 0.5% TSB in PBS (*S. aureus*, MRSA, *S. epidermidis*, and *E. coli*) to provide bacteriostatic conditions for 0, 6, 12, and 24 h. As not all bacteria survived in PBS for 24 h due to lack of nutrients, 0.5% TSB was added to *S. aureus*, MRSA, *S. epidermidis*, and *E. coli* solutions to preserve their viability. The time-dependent NO payloads of the various initial average NO fluxes are provided in Table 4.3. The initial average NO fluxes from 0.5–50 pmol cm^{-2} s^{-1} provided NO payloads ranging from 38–1700 nmol cm^{-2} over 24 h of incubation. The NO release follows pseudo first-order kinetics and therefore substrates with an initial average NO flux of 20, 35, and 50 pmol cm^{-2} s^{-1} delivered 48, 53, and 77% of their 24 h NO payload in the first 6 h, respectively (Table 4.3). In contrast, substrates with lower initial average NO fluxes (0.5 and 1.0 pmol cm^{-2} s^{-1}) from the PVC-coated *S*-nitrosothiol xerogels delivered their NO payloads at a constant rate throughout the 24 h experiment, with only ~25% of the 24 h NO payload delivered during the first 6 h.

Adhered bacteria were removed from PVC-coated xerogel substrates via sonication, plated onto TSA plates, and the resulting colonies were enumerated to quantify viable bacteria.[30] Optical microscopy confirmed that this process (sonication) removed 93–100% of bacteria from the Fg-adsorbed PVC-coated substrates, allowing for further determination of bacterial viability. To ensure study of only the bacteria adhered to the PVC-coated xerogel

Table 4.3. Nitric oxide payloads (nmol cm^{-2}) at 6, 12, and 24 h after the 1 h adhesion assay for the eight initial average NO fluxes examined. Data are mean ± standard deviation.

	NO payload (nmol cm^{-2})		
Initial NO flux (pmol cm^{-2} s)	6 h	12 h	24 h
0.5	9.5 ± 0.8	19 ± 2	38 ± 2
1.0	17 ± 2	33 ± 3	66 ± 4
2.5	40 ± 3	72 ± 5	105 ± 9
5.0	90 ± 9	140 ± 10	240 ± 20
10	150 ± 20	250 ± 20	370 ± 20
20	270 ± 20	410 ± 30	550 ± 50
35	390 ± 50	560 ± 50	740 ± 60
50	1300 ± 200	1500 ± 200	1700 ± 200

and not to the sides or back of the glass substrates, the outer PVC layer was physically removed from the glass slide and sonicated. The relative adhered bacterial viability was calculated at each time point (t = 6, 12, or 24 h) by dividing the observed viable bacteria concentration by the concentration observed for the same NO-releasing material at t = 0 for a given bacteria strain and then multiplying by 100 (Equation 4.1). A viability of 100% would thus indicate an identical concentration of live bacteria at a given time point relative to that NO-releasing material at t = 0. Of note, bacteria adhered to control substrates exhibited minimal death or desorption during the 24 h incubation.

We aimed to evaluate the time-dependent killing of bacteria to NO-releasing substrates. Bacterial viability and surface coverage were comparable at t = 0 for each NO flux versus control materials. For example, *S. aureus* viability at t = 0 for substrates with an initial average flux of 50 pmol cm^{-2} s^{-1} was ~15% that of control substrates, which matches closely with the ~10% relative adhesion over 1 h (Figure 4.1). The positive agreement between surface coverage and viable bacteria counts immediately following the adhesion assay indicates that NO release did not result in significant killing of adhered bacteria during the 1 h adhesion assay.

The time-dependent viability of bacteria adhered to the NO-releasing surfaces is provided in Tables 4.4, 4.5, and 4.6. The reduction in viability of all bacteria exhibited a dose dependence to NO. At 6 h, NO-releasing substrates notably reduced viability of adhered bacteria of five strains of bacteria (MRSA, *S. epidermidis*, *E. faecalis*, *E. coli*, and *P. aeruginosa*). However, the viability of adhered *S. aureus* cells experienced minimal reductions prior to the 24 h time point (Table 4.6). The delay in reduction of S. *aureus* viability may be due to a minimal NO concentration threshold necessary to induce killing for

$$\text{Relative viability}_{t=x,\,[NO]} = \frac{[\text{viable adhered bacteria}]_{t=x,\,[NO]}}{[\text{viable adhered bacteria}]_{t=0,\,[NO]}} \times 100\%$$

Equation 4.1. Calculation for relative viability of bacteria adhered at t = x (x = 6, 12 or 24 h) to a given NO-releasing material ([NO] = 0.5, 1.0, 2.5, 5.0, 10, 20, 35, or 50 pmol cm^{-2} s^{-1}).

Table 4.4. Relative viability (%) of bacteria adhered to NO-releasing surfaces after 6 h incubation in bacteriostatic conditions. A relative viability of 100% represents the viability of bacteria adhered at the initial average NO flux at t = 0. Data are mean ± standard error of the mean.

	Initial average NO flux (pmol cm^{-2} s^{-1})							
Bacteria strain	0.5	1.0	2.5	5.0	10	20	35	50
S. aureus	105 ± 19	106 ± 19	85 ± 17	69 ± 28	61 ± 23	84 ± 31	86 ± 21	87 ± 23
MRSA	93 ± 28	93 ± 30	46 ± 17	39 ± 12	42 ± 16	46 ± 15	45 ± 18	32 ± 12
S. epidermidis	118 ± 30	84 ± 21	75 ± 22	101 ± 30	41 ± 18	28 ± 13	25 ± 10	24 ± 8
E. faecalis	96 ± 3	94 ± 2	42 ± 5	24 ± 7	22 ± 6	27 ± 10	33 ± 10	29 ± 9
E. coli	116 ± 10	116 ± 15	51 ± 17	21 ± 10	22 ± 8	27 ± 8	17 ± 5	16 ± 4
P. aeruginosa	92 ± 6	110 ± 15	41 ± 18	20 ± 7	18 ± 6	20 ± 8	6 ± 2	5 ± 0.9

Table 4.5. Relative viability (%) of bacteria adhered to NO-releasing surfaces after 12 h incubation in bacteriostatic conditions. A relative viability of 100% represents the viability of bacteria adhered at the initial average NO flux at t = 0. Data are mean ± standard error of the mean.

	Initial average NO flux (pmol cm^{-2} s^{-1})							
Bacteria strain	0.5	1.0	2.5	5.0	10	20	35	50
S. aureus	69 ± 6	61 ± 25	65 ± 9	39 ± 9	54 ± 13	56 ± 16	60 ± 15	49 ± 6
MRSA	75 ± 18	82 ± 26	34 ± 13	34 ± 14	23 ± 8	54 ± 13	28 ± 10	21 ± 6
S. epidermidis	72 ± 20	75 ± 22	40 ± 15	57 ± 17	34 ± 11	24 ± 9	20 ± 8	20 ± 8
E. faecalis	91 ± 4	61 ± 10	34 ± 11	20 ± 8	21 ± 7	21 ± 6	16 ± 5	11 ± 3
E. coli	95 ± 22	73 ± 22	38 ± 13	16 ± 4	14 ± 5	7 ± 2	10 ± 3	8 ± 2
P. aeruginosa	57 ± 2	46 ± 10	33 ± 5	25 ± 12	16 ± 6	8 ± 2	5 ± 2	4 ± 1

Table 4.6. Relative viability (%) of bacteria adhered to NO-releasing surfaces after 24 h incubation in bacteriostatic conditions. A relative viability of 100% represents the viability of bacteria adhered at the initial average NO flux at t = 0. Data are mean ± standard error of the mean.

	Initial average NO flux (pmol cm^{-2} s^{-1})							
Bacteria strain	0.5	1.0	2.5	5.0	10	20	35	50
S. aureus	67 ± 17	66 ± 19	69 ± 23	43 ± 16	25 ± 12	38 ± 12	22 ± 7	15 ± 6
MRSA	66 ± 13	72 ± 18	27 ± 11	25 ± 9	21 ± 6	18 ± 6	19 ± 7	15 ± 4
S. epidermidis	80 ± 12	80 ± 19	38 ± 12	45 ± 16	34 ± 13	20 ± 8	15 ± 5	14 ± 4
E. faecalis	83 ± 7	50 ± 20	34 ± 2	21 ± 3	23 ± 2	22 ± 4	13 ± 5	9 ± 3
E. coli	76 ± 11	36 ± 7	36 ± 8	14 ± 5	11 ± 4	8 ± 3	9 ± 3	5 ± 1
P. aeruginosa	66 ± 3	34 ± 4	29 ± 11	13 ± 4	14 ± 4	4 ± 1	4 ± 1	2 ± 0.4

this strain. *S. aureus* is known to resist NO via metabolic activities and therefore killing may require greater NO concentrations.[41] The rate of the total NO delivery appears to affect the decrease in bacteria viability. For example, the cumulative NO payloads of xerogels with initial NO fluxes of 2.5 and 0.5 pmol cm^{-2} s^{-1} are approximately equivalent at 6 and 24 h, respectively (38–40 nmol cm^{-2}, Table 4.3). However, the viability of *E. faecalis* at 6 h to surfaces with an initial NO flux of 2.5 pmol cm^{-2} s^{-1} (42 ± 5%) is significantly lower than the viability at 24 h to surfaces with an initial NO flux of 0.5 pmol cm^{-2} s^{-1} (83 ± 7%).

The NO payloads necessary to decrease the viability of adhered bacteria by 50% and 80% after 24 h are provided in Table 4.7. Cumulative NO release of 66–240 and 240–1700 nmol cm^{-2} reduced viability of adhered bacteria by 50 and 80%, respectively (Table 4.7). The lowest 24 h NO payload investigated (38 nmol cm^{-2}) eradicated 17–34% of adhered bacteria for all strains. The maximum reductions in adhered bacteria viability for *S. aureus*, MRSA, *S. epidermidis*, *E. faecalis*, *E. coli*, and *P. aeruginosa* at 24 h exposure to substrates with an initial NO flux of 50 pmol cm^{-2} s^{-1} were 85, 85, 86, 92, 95, and 98%, respectively (Table 4.6). Therefore, substrates with an initial NO flux of 50 pmol cm^{-2} s^{-1} delivering a payload of 1.7 μmol cm^{-2} over 24 h inhibited adhesion of all strains by >80% and eradicated ≥85% of the adhered bacteria.

While the NO payloads employed in the current study were bactericidal to many strains, to be used successfully in vivo the materials must avoid cytotoxic effects. Previous work by Nablo and Schoenfisch found that materials with an initial NO flux of ~50 pmol cm^{-2} s^{-1} were only slightly cytotoxic to L929 fiborblasts after 24 h incubation.[42] Furthermore, even greater NO payloads were determined to be only mildly cytotoxic. A study using the same MPTMS/MTMOS xerogels capable of delivering larger NO payloads than the current study

Table 4.7. The necessary surface-derived total NO release to decrease adhered bacteria viability by 50% and 80% after 24 h incubation.

	NO payload necessary to reduce adhered bacteria viability by 50% after 24 h (nmol cm^{-2})	NO payload necessary to reduce adhered bacteria viability by 80% after 24 h (nmol cm^{-2})
S. aureus	240 ± 20	1700 ± 200
MRSA	105 ± 9	550 ± 50
S. epidermidis	105 ± 9	550 ± 50
E. faecalis	66 ± 4	740 ± 60
E. coli	66 ± 4	240 ± 20
P. aeruginosa	66 ± 4	240 ± 20

revealed that NO release reduced adhered L929 fibroblast viability by ~30% over 24 h compared to control xerogels.[31] These previous results reveal that NO fluxes capable of greatly reducing bacterial adhesion and viability avoid cytotoxic effects against mammalian cells.

4.4. Conclusion

The adhesion and viability of six bacteria species (*S. aureus*, MRSA, *S. epidermidis*, *E. faecalis*, *E. coli*, and *P. aeruginosa*) in the presence of adsorbed Fg was reduced at NO-releasing surfaces. An average NO flux from 20–50 pmol cm^{-2} s^{-1} decreased bacterial adhesion by >80% for all bacteria over a 1 h exposure. With the exception of *S. epidermidis*, the adhesion of Gram-positive and Gram-negative bacteria were equally affected by surface-derived NO release. *S. epidermidis* required significantly greater NO fluxes to inhibit adhesion by >80%, that we hypothesize is due to the affinity of the Fg-binding proteins on the cell surface to the adsorbed Fg. In addition to NO influencing general adhesion, it was also shown to decrease bacteria viability. Indeed, the number of viable bacteria adhered to NO-releasing substrates was decreased after 24 h in a dose-dependent manner by up to 98% compared to bacteria viable immediately following adhesion. Future experiments should optimize the NO concentrations and NO release kinetics to maximize the effects of NO on bacterial adhesion and killing.

4.5. References

(1) Hetrick, E. M., Schoenfisch, M. H., "Reducing implant-related infections: active release strategies." *Chem. Soc. Rev.* **2006,** *35*, 780-789.

(2) Mermel, L. A., "Prevention of intravascular catheter-related infections." *Ann. Intern. Med.* **2000,** *132*, 391-402.

(3) Walz, J. M., Memtsoudis, S. G., Heard, S. O., "Analytic Reviews: Prevention of Central Venous Catheter Bloodstream Infections." *J. Intensive Care Med.* **2010,** *25*, 131-138.

(4) Rodrigues, L. R., Inhibition of Bacterial Adhesion on Medical Devices, in: Linke D, Goldman A (Eds.) Bacterial Adhesion: Chemistry, Biology and Physics, Springer-Verlag Berlin, Berlin, 2011, pp. 351-367.

(5) Pascual, A., "Pathogenesis of catheter-related infections: lessons for new designs." *Clin. Microbiol. and Infec* **2002,** *8*, 256-264.

(6) Emmerson, M., "A microbiologist's view of factors contributing to infection." *New Horiz.-Sci. Pract. Acute Med.* **1998,** *6*, S3-S10.

(7) Katsikogianni, M., Missirlis, Y. F., "Concise review of mechanisms of bacterial adhesion to biomaterials and of techniques used in estimating bacteria-material interactions." *Eur. Cell. Mater.* **2004,** *8*, 37-57.

(8) Ceri, H., Olson, M. E., Stremick, C., Read, R. R., Morck, D., Buret, A., "The Calgary Biofilm Device: New technology for rapid determination of antibiotic susceptibilities of bacterial biofilms." *J. Clin. Microbiol.* **1999,** *37*, 1771-1776.

(9) Williams, I., Venables, W. A., Lloyd, D., Paul, F., Critchley, I., "The effects of adherence to silicone surfaces on antibiotic susceptibility in Staphylococcus aureus." *Microbiology-(UK)* **1997,** *143*, 2407-2413.

(10) Estivill, D., Arias, A., Torres-Lana, A., Carrillo-Munoz, A. J., Arevalo, M. P., "Biofilm formation by five species of Candida on three clinical materials." *J. Microbiol. Methods* **2011,** *86*, 238-242.

(11) Yao, C., Li, X. S., Neoh, K. G., Shi, Z. L., Kang, E. T., "Surface modification and antibacterial activity of electrospun polyurethane fibrous membranes with quaternary ammonium moieties." *J. Membr. Sci.* **2008,** *320*, 259-267.

(12) Thebault, P., de Givenchy, E. T., Geribaldi, S., Levy, R., Vandenberghe, Y., Guittard, F., "Surface and antimicrobial properties of semi-fluorinated quaternary ammonium thiol surfactants potentially usable for Self-Assembled Monolayers." *J. Fluor. Chem.* **2010,** *131*, 592-596.

(13) Carpenter, A. W., Worley, B. V., Slomberg, D. L., Schoenfisch, M. H., "Dual Action Antimicrobials: Nitric Oxide Release from Quaternary Ammonium-Functionalized Silica Nanoparticles." *Biomacromolecules* **2012,** *13*, 3334-3342.

(14) Anderson, E. M., Noble, M. L., Garty, S., Ma, H. Y., Bryers, J. D., Shen, T. T., Ratner, B. D., "Sustained release of antibiotic from poly(2-hydroxyethyl methacrylate) to prevent blinding infections after cataract surgery." *Biomaterials* **2009,** *30*, 5675-5681.

(15) Schierholz, J. M., Steinhauser, H., Rump, A. F. E., Berkels, R., Pulverer, G., "Controlled release of antibiotics from biomedical polyurethanes: morphological and structural features." *Biomaterials* **1997,** *18*, 839-844.

(16) Rojas, I. A., Slunt, J. B., Grainger, D. W., "Polyurethane coatings release bioactive antibodies to reduce bacterial adhesion." *J. Control. Release* **2000,** *63*, 175-189.

(17) Monteiro, D. R., Gorup, L. F., Takamiya, A. S., Ruvollo-Filho, A. C., Camargo, E. R. d., Barbosa, D. B., "The growing importance of materials that prevent microbial adhesion: antimicrobial effect of medical devices containing silver." *Int. J. Antimicro. Ag.* **2009,** *34*, 103-110.

(18) Charville, G. W., Hetrick, E. M., Geer, C. B., Schoenfisch, M. H., "Reduced bacterial adhesion to fibrinogen-coated substrates via nitric oxide release." *Biomaterials* **2008,** *29*, 4039-4044.

(19) Nablo, B. J., Schoenfisch, M. H., "Poly(vinyl chloride)-coated sol-gels for studying the effects of nitric oxide release on bacterial adhesion." *Biomacromolecules* **2004,** *5*, 2034-2041.

(20) Mannick, J. B., "Immunoregulatory and antimicrobial effects of nitrogen oxides." *Proc. Am. Thorac. Soc.* **2006,** *3*, 161-165.

(21) Wink, D. A., Mitchell, J. B., "Chemical biology of nitric oxide: Insights into regulatory, cytotoxic, and cytoprotective mechanisms of nitric oxide." *Free Radic. Biol. Med.* **1998,** *25*, 434-456.

(22) Riccio, D. A., Schoenfisch, M. H., "Nitric oxide release: Part I. Macromolecular scaffolds." *Chem. Soc. Rev.* **2012,** *41*, 3731-3741.

(23) Carpenter, A. W., Schoenfisch, M. H., "Nitric oxide release: Part II. Therapeutic applications." *Chem. Soc. Rev.* **2012,** *41*, 3742-3752.

(24) Nablo, B. J., Prichard, H. L., Butler, R. D., Klitzman, B., Schoenfisch, M. H., "Inhibition of implant-associated infections via nitric oxide release." *Biomaterials* **2005,** *26*, 6984-6990.

(25) Holt, J., Hertzberg, B., Weinhold, P., Storm, W., Schoenfisch, M., Dahners, L., "Decreasing bacterial colonization of external fixation pins through nitric oxide release coatings." *J. Orthop. Trauma* **2011,** *25*, 432-437.

(26) Hetrick, E. M., Shin, J. H., Stasko, N. A., Johnson, C. B., Wespe, D. A., Holmuhamedov, E., Schoenfisch, M. H., "Bactericidal efficacy of nitric oxide-releasing silica nanoparticles." *ACS Nano* **2008,** *2*, 235-246.

(27) Privett, B. J., Deupree, S. M., Backlund, C. J., Rao, K. S., Johnson, C. B., Coneski, P. N., Schoenfisch, M. H., "Synergy of Nitric Oxide and Silver Sulfadiazine against Gram-Negative, Gram-Positive, and Antibiotic-Resistant Pathogens." *Mol. Pharm.* **2010,** *7*, 2289-2296.

(28) Carpenter, A. W., Slomberg, D. L., Rao, K. S., Schoenfisch, M. H., "Influence of Scaffold Size on Bactericidal Activity of Nitric Oxide-Releasing Silica Nanoparticles." *ACS Nano* **2011,** *5*, 7235-7244.

(29) Sun, B., Slomberg, D. L., Chudasama, S. L., Lu, Y., Schoenfisch, M. H., "Nitric Oxide-Releasing Dendrimers as Antibacterial Agents." *Biomacromolecules* **2012,** *13*, 3343-3354.

(30) Hetrick, E. M., Schoenfisch, M. H., "Antibacterial nitric oxide-releasing xerogels: Cell viability and parallel plate flow cell adhesion studies." *Biomaterials* **2007,** *28*, 1948-1956.

(31) Riccio, D. A., Dobmeier, K. P., Hetrick, E. M., Privett, B. J., Paul, H. S., Schoenfisch, M. H., "Nitric oxide-releasing S-nitrosothiol-modified xerogels." *Biomaterials* **2009,** *30*, 4494-4502.

(32) Breed, R. S., Dotterrer, W. D., "The Number of Colonies Allowable on Satisfactory Agar Plates." *J. Bacteriol.* **1916,** *1*, 321-331.

(33) Coneski, P. N., Schoenfisch, M. H., "Nitric oxide release: Part III. Measurement and reporting." *Chem. Soc. Rev.* **2012,** *41*, 3753-3758.

(34) Marxer, S. M., Chen, T. Y., Schoenfisch, M. H., "Nitric oxide releasing sol-gel materials: Toward improved subcutaneous sensors." *Abstr. Pap. Am. Chem. Soc.* **2001,** *222*, U95-U95.

(35) Marxer, S. M., Rothrock, A. R., Nablo, B. J., Robbins, M. E., Schoenfisch, M. H., "Preparation of nitric oxide (NO)-releasing sol-gels for biomaterial applications." *Chem. Mat.* **2003,** *15*, 4193-4199.

(36) Fang, F. C., "Mechanisms of nitric oxide-related antimicrobial activity." *J. Clin. Invest.* **1997,** *99*, 2818-2825.

(37) Nilsson, M., Frykberg, L., Flock, J. I., Pei, L., Lindberg, M., Guss, B., "A fibrinogen-binding protein of Staphylococcus epidermidis." *Infect. Immun.* **1998,** *66*, 2666-2673.

(38) McDevitt, D., Nanavaty, T., HousePompeo, K., Bell, E., Turner, N., McIntire, L., Foster, T., Hook, M., "Characterization of the interaction between the Staphylococcus aureus clumping factor (ClfA) and fibrinogen." *Eur. J. Biochem.* **1997,** *247*, 416-424.

(39) Davis, S. L., Gurusiddappa, S., McCrea, K. W., Perkins, S., Hook, M., "SdrG, a fibrinogen-binding bacterial adhesin of the microbial surface components recognizing adhesive matrix molecules subfamily from Staphylococcus epidermidis, targets the thrombin cleavage site in the B beta chain." *J. Biol. Chem.* **2001,** *276*, 27799-27805.

(40) Hendricks, S. K., Kwok, C., Shen, M. C., Horbett, T. A., Ratner, B. D., Bryers, J. D., "Plasma-deposited membranes for controlled release of antibiotic to prevent bacterial adhesion and biofilm formation." *J. Biomed. Mater. Res.* **2000,** *50*, 160-170.

(41) Richardson, A. R., Libby, S. J., Fang, F. C., "A nitric oxide-inducible lactate dehydrogenase enables Staphylococcus aureus to resist innate immunity." *Science* **2008,** *319*, 1672-1676.

(42) Nablo, B. J., Schoenfisch, M. H., "In vitro cytotoxicity of nitric oxide-releasing sol–gel derived materials." *Biomaterials* **2005,** *26*, 4405-4415.

Chapter 5:

Summary and Future Directions

5.1. Summary

Nitric oxide was shown to directly influence bacterial adhesion and viability as well as subcutaneous tissue integration of materials. In Chapter 2, the tissue integration of NO-releasing materials was quantified temporally through microdialysis. The technique quantifies the resistances to mass transfer due to the FBR when using a non-equilibrium, steady-state flow rate. Nitric oxide release was imparted to microdialysis probes through the use of saturated NO solutions to achieve a constant NO flux of 162 ± 18 pmol cm^{-2} s^{-1}. When implanted into rat subcutaneous tissue, probes were perfused daily for 8 h, delivering 4.6 ± 5 μmol cm^{-2} of NO. Recovery of glucose by NO-releasing microdialysis probes was significantly greater than control probes at 7 d post-implantation. The recovery of glucose by NO-releasing probes was constant over the 14 d implantation period. Histological analysis of the adjacent tissue revealed a decreased collagen capsule thickness and reduced inflammation. These observations may account for the significant improvement in glucose recovery and further support the effect of NO in improving tissue integration.

In Chapter 3, investigations on the roles of both NO release kinetics and payloads on the tissue integration of materials with dimensions similar to implantable glucose sensors were detailed. Stainless steel wires were coated with NO donor-doped polyurethane. Nitric oxide donors were used to achieve varying NO release kinetics including small molecules (i.e., PROLI/NO), *N*-diazeniumdiolate nanoparticles (i.e., AEAP3/TMOS), and *S*-nitrosothiol

nanoparticles (i.e., MPTMS/TEOS). To further alter NO release kinetics, polyurethanes of varying hydrophobicity were coated onto the NO donor-doped polyurethane. The hydrophobic polymer topcoats were confirmed to slow the NO release from *N*-diazeniumdiolate NO donors. Collectively, these strategies allowed us to vary the total NO payloads from ~2.7–9.3 μmol cm^{-2}, the maximum NO fluxes from 41.8–3128 pmol cm^{-2} s^{-1}, and the NO release durations from 6 h–14 d. Histological analysis revealed that extended NO release kinetics correlated with reduced capsule thickness. Substrates with the longest NO release duration (i.e., 14 d) and greatest NO payload (i.e., 9.3 μmol cm^{-2}) resulted in the largest reduction in capsule thickness (i.e., ~75%) at both 3 and 6 weeks of implantation. Though these substrates most significantly impacted collagen capsule thickness, they also increased collagen density in the capsule that may act to impede glucose diffusion. Inflammatory cell counts were only affected while substrates were still releasing NO. Therefore, differences were only observed at 3 and 7 d as none of the substrates were releasing NO after 2 weeks. These results illustrate the necessity for large NO payloads and long release kinetics to maximally enhance the tissue integration of subcutaneous implants.

While the focus of Chapters 2 and 3 was to evaluate the effects of NO on the FBR, NO's influence on bacterial colonization, and specifically its ability to prevent adhesion and viability, were described in Chapter 4. *S*-nitrosothiol xerogels were utilized for these studies due to their ability to produce long and constant NO release, a necessity for complete evaluation of the effect of flux on bacterial adhesion. To provide reproducible interfaces for the bacteria to adhere to and eliminate any differences based on contact angle, a PVC layer was spin-coated onto the xerogels. Furthermore, substrates were incubated with fibrinogen prior to adhesion thus enhancing bacterial affinity for the substrates to better simulate the in

vivo environment and enhance bacterial adhesion. These experiments revealed that fluxes of 20–50 pmol cm^{-2} s^{-1} resulted in >80% reduction in adhesion for bacterial strains tested. To evaluate the effect of NO on adhered bacteria, the viability was quantified at 0, 6, 12, and 24 h post-adhesion. The adhered bacterial viability showed NO dose-dependent behavior, with large NO payloads (1.7 μmol cm^{-2}) eradicating ≥85% of adhered bacteria after 24 h incubation in bacteriostatic conditions.

5.2. Future Directions

While a direct effect of NO on the FBR was observed, the ability of NO release to enhance sensor performance in subcutaneous tissue remains uncertain. A thinner collagen capsule and decreased inflammatory response should decrease lag time and sensor attenuation,[1] but only in vivo experiments will confirm this. The NO donor-doped polyurethanes could be employed as glucose sensor membranes to achieve variable NO-release kinetics and payloads, and careful investigation of NO-releasing glucose sensors in vivo should be conducted to evaluate any benefit of the observed tissue integration on sensor performance. It is also important to note that the FBR may be different for percutaneous compared implants (versus subcutaneous) due to external forces.[2, 3] Though histological differences and increased glucose recovery were achieved with percutaneous NO-releasing microdialysis probes, these probes may have benefited from large NO fluxes from daily perfusion of saturated NO solutions. Studies examining the differential tissue integration of substrates implanted percutaneously versus purely subcutaneously with identical NO-release properties should be investigated next.

While NO release was shown to enhance tissue integration (Chapter 3), the molecular mechanisms responsible remain poorly understood. In vitro cell culture is one method for

investigating the cellular responses to NO-releasing materials. In this way, materials could be exposed to NO-releasing small molecules, dendrimers, nanoparticles, or surfaces and their cytokine expression (e.g., vascular endothelial growth factor) studied as a function of NO flux and duration. Similar to experiments in Chapter 4, the NO flux-dependent adhesion/behavior of mammalian cells to NO-releasing surfaces should be studied. Nablo et al. previously examined the adhesion and morphology of L929 fibroblasts to AHAP/BTMOS-based NO-releasing xerogels.[4] Future studies should examine the effects of NO release on cell expression of fibroblasts and other inflammatory cells (e.g., macrophages). Furthermore, it is known that the development of foreign body giant cells (FBGCs) can negatively impact the performance and stability of implanted devices.[5] The development of FBGCs has been previously examined in vitro over time upon exposure to cytokines (e.g., interleukin 4).[6, 7] In this manner, the effect of NO-releasing surfaces on the development of FBGCs could also be studied.

While in vitro cell culture is generally a cost-effective and simple way to test materials, the FBR is not fully represented in vitro. Investigations of the molecular response in vivo has been studied using a cage implant system, first described by Marchant and coworkers.[8] This in vivo method allows for testing of tissue response to biomaterials through either the quantification and characterization of inflammatory cells and/or by evaluation of cytokines present in the exudates.[9] This method also provides temporal information without premature sacrifice of the animal. Upon explantation of the cage, the extent of foreign body giant cell formation may be quantified. These giant cells contribute reactive oxygen species that at times degrade polymer membranes.[5] In this manner, the mechanisms in which NO

release enhances tissue integration can be more thoroughly understood when exposed under vivo conditions.

Investigations on the biocompatibility of glucose sensors are often tested in healthy animals, though the sensors are designed for diabetic patients. It is well known that diabetics suffer from diminished wound-healing capabilities.[10] Measurements of nitrite and nitrate by Schaeffer et al. indicate, at least indirectly, that wound NO concentrations in diabetic animals are significantly depressed compared to controls.[11, 12] Even when hyperglycemia is controlled to normoglycemic concentrations, these concentrations are significantly depressed.[12] The lack of NO produced in the wound environment may contribute to the diminished healing capacity in diabetic patients. Indeed, investigations found that the administration of NO to diabetic wounds in mice was more effective in enhancing wound healing compared to controls.[13] For these reasons, testing of tissue compatibility for NO-releasing materials in diabetic animals is essential. It is possible that the enhancements in tissue integration via NO release will be more pronounced in diabetic animals, while other potential strategies (e.g., porosity, VEGF) may not provide as drastic results.

Lastly, the effects of NO-mediated bacterial adhesion and viability were investigated in Chapter 4. While the data were promising with respect to indentifying an optimal NO flux, the ability to prevent adhesion and viability in vivo will provide better insight into the ability of NO to affect bacterial colonization. For example, while silver treatments are capable of reducing bacterial viability in vitro, in vivo tests often do not achieve such results.[14] Our lab has previously examined the ability of AHAP3/BTMOS-based NO-releasing xerogels to reduce bacterial colonization to orthopedic implants in rats.[15] This study only examined the antibacterial performance of one NO flux (to impede bacterial colonization), and may not

represent the optimal NO release. Future studies should examine in vivo antibacterial behavior as a function of NO flux and duration. As previously noted, the primary focus of this work is to develop more compatible glucose sensors for diabetic patients, which suffer from diminished healing.[10] Therefore, materials found to be suitable for decreasing bacterial adhesion and viability should be examined in diabetic models as these are more susceptible to infection compared to healthy (i.e., non-diabetic) subjects. It may be that the apparent lack of NO in diabetic animals will greatly benefit from NO release and therefore inhibit bacterial colonization at the implant site.

5.3. References

(1) Novak, M. T., Yuan, F., Reichert, W. M., "Modeling the relative impact of capsular tissue effects on implanted glucose sensor time lag and signal attenuation." *Anal. Bioanal. Chem.* **2010,** *398*, 1695-1705.

(2) Koschwanez, H. E., Reichert, W. M., Klitzman, B., "Intravital microscopy evaluation of angiogenesis and its effects on glucose sensor performance." *J. Biomed. Mater. Res. Part A* **2010,** *93A*, 1348-1357.

(3) Koschwanez, H. E., Yap, F. Y., Klitzman, B., Reichert, W. M., "In vitro and in vivo characterization of porous poly-L-lactic acid coatings for subcutaneously implanted glucose sensors." *J. Biomed. Mater. Res. Part A* **2008,** *87A*, 792-807.

(4) Nablo, B. J., Schoenfisch, M. H., "In vitro cytotoxicity of nitric oxide-releasing sol-gel derived materials." *Biomaterials* **2005,** *26*, 4405-4415.

(5) Zhao, Q., Topham, N., Anderson, J. M., Hiltner, A., Lodoen, G., Payet, C. R., "Foreign-body giant cells and polyurethane biostability: In vivo correlation of cell adhesion and surface cracking." *J. Biomed. Mater. Res.* **1991,** *25*, 177-183.

(6) Jenney, C. R., Anderson, J. M., "Effects of surface-coupled polyethylene oxide on human macrophage adhesion and foreign body giant cell formation in vitro." *J. Biomed. Mater. Res.* **1999,** *44*, 206-216.

(7) Jenney, C. R., DeFife, K. M., Colton, E., Anderson, J. M., "Human monocyte/macrophage adhesion, macrophage motility, and IL-4-induced foreign body giant cell formation on silane-modified surfaces in vitro." *J. Biomed. Mater. Res.* **1998,** *41*, 171-184.

(8) Marchant, R., Hiltner, A., Hamlin, C., Rabinovitch, A., Slobodkin, R., Anderson, J. M., "In vivo biocompatibility studies. I. The cage implant system and a biodegradable hydrogel." *J. Biomed. Mater. Res.* **1983,** *17*, 301-325.

(9) Schutte, R. J., Xie, L., Klitzman, B., Reichert, W. M., "In vivo cytokine-associated responses to biomaterials." *Biomaterials* **2009,** *30*, 160-168.

(10) Le, N. N., Rose, M. B., Levinson, H., Klitzman, B., "Implant healing in experimental animal models of diabetes." *J. Diabetes Sci. Technol.* **2011,** *5*, 605-618.

(11) Schaffer, M. R., Tantry, U., Efron, P. A., Ahrendt, G. M., Thornton, F. J., Barbul, A., "Diabetes-impaired healing and reduced wound nitric oxide synthesis: A possible pathophysiologic correlation." *Surgery* **1997,** *121*, 513-519.

(12) Schaffer, M., Bongartz, M., Fischer, S., Proksch, B., Viebahn, R., "Nitric oxide restores impaired healing in normoglycaemic diabetic rats." *J. Wound Care* **2007,** *16*, 311-6.

(13) Weller, R., Finnen, M. J., "The effects of topical treatment with acidified nitrite on wound healing in normal and diabetic mice." *Nitric Oxide-Biol. Chem.* **2006,** *15*, 395-399.

(14) Hetrick, E. M., Schoenfisch, M. H., "Reducing implant-related infections: active release strategies." *Chem. Soc. Rev.* **2006,** *35*, 780-789.

(15) Nablo, B. J., Prichard, H. L., Butler, R. D., Klitzman, B., Schoenfisch, M. H., "Inhibition of implant-associated infections via nitric oxide release." *Biomaterials* **2005,** *26*, 6984-6990.